

Geologic and geochronologic update of the Turtle Lake area, NTS 104M/16, northwest British Columbia



Mitchell G. Mihalynuk^{1, a}, Alexandre Zagorevski², Dejan Milidragovic¹, Maria Tsekhmistrenko³, Richard M. Friedman⁴, Nancy Joyce², Alfredo Camacho⁵, and Martyn Golding⁶

¹ British Columbia Geological Survey, Ministry of Energy, Mines and Petroleum Resources, Victoria, BC, V8W 9N3

² Geological Survey of Canada, Ottawa, ON, K1A 0E8

³ Department of Earth Sciences, University of Oxford, Oxford, OX1 3AN, UK

⁴ Pacific Centre for Isotopic and Geochemical Research, The University of British Columbia, Vancouver, BC, V6T 1Z4

⁵ Department of Mechanical Engineering, University of Victoria, Victoria, BC, V8P 5C2

⁶ Geological Survey of Canada, Vancouver, BC, V6B 5J3

^a corresponding author: Mitch.Mihalynuk@gov.bc.ca

Recommended citation: Mihalynuk, M.G., Zagorevski, A., Milidragovic, D., Tsekhmistrenko, M., Friedman, R.M., Joyce, N., Camacho, A., and Golding, M., 2018. Geologic and geochronologic update of the Turtle Lake area, NTS 104M/16, northwest British Columbia. In: Geological Fieldwork 2017, British Columbia Ministry of Energy, Mines and Petroleum Resources, British Columbia Geological Survey Paper 2018-1, pp. 83-128.

Abstract

The Turtle Lake map area straddles the boundary between exotic, oceanic crustal and mantle rocks of the Cache Creek terrane, and Laberge Group (Early Jurassic) Whitehorse trough forearc strata atop the Stikine terrane. Exposed in the Turtle Lake area are extensive platformal carbonate rocks of the Horsefeed Formation, a regional hallmark of the Cache Creek terrane, that were deposited over at least 25 m.y. Juxtaposition of Stikine and Cache Creek terranes was accommodated by collapse of the Whitehorse trough in mid-Middle Jurassic (starting ~174 Ma) and creation of a fold and thrust fault belt. This belt was cut by the Fourth of July batholith (~172 Ma) and lamprophyre dikes, emplaced and cooled by ~162 Ma, and followed by a magmatic lull between ~165-130 Ma. In the Turtle Lake area, we find a single granitic dike that crystallized in this time interval, at ~145 Ma. By 125 Ma, the Coast Belt arc had ignited, as recorded by voluminous volcanic and intrusive rocks in the west, and persisted until ~50 Ma. In the Turtle Lake area, volcanism accompanied uplift by ~110 Ma, as indicated by a unimodal detrital zircon population in karst deposits. The youngest known representative intrusions are ~56 Ma quartz diorite stocks. One of these stocks cuts the faulted contact between Whitehorse trough strata and harzburgite mantle tectonite. An analogous geological setting hosts epithermal gold-silver vein mineralization at the Engineer Mine, ~30 km to the south-southwest. The youngest rocks affected by crustal scale faulting and linked, mainly south-side-down, extensional faults are the ~80 Ma Windy-Table suite volcanic strata. We have yet to properly document the extensional faulting episode, but future work aimed at doing so will have important implications for regional tectonic reconstruction, and evaluation of mineral potential.

Keywords: Cache Creek terrane, Stikine terrane, Laberge Group, Horsefeed Formation, Kedahda Formation, Windy-Table suite, mantle tectonite, Turtle Lake, Tagish Lake, Atlin, regional mapping, conodont, geochronology, geochemistry

1. Introduction

The Turtle Lake map area of northern-most western British Columbia overlaps the boundary between Stikine and Cache Creek terranes on existing terrane assemblage maps (Fig. 1a; Wheeler et al., 1988; Colpron and Nelson, 2011). The Stikine terrane is characterized by Late Devonian to Early Permian and Middle Triassic to Lower Early Jurassic volcanic arc magmatic rocks. In the Turtle Lake area (Figs. 1b, 2), immature volcanic wacke to fine siliciclastic rocks of the Laberge Group (Lower to Middle Jurassic) are presumed to overlap and completely blanket the Stikine terrane. Farther west, Stikinia is represented by Late Triassic (and older?) arc rocks of the Stuhini Group (Souther, 1971; Mihalynuk et al., 1999; Lewes River Group in Yukon, Wheeler, 1961). To the east (Fig. 1b), platformal limestone, pelagic sedimentary, and ophiolitic rocks were

historically included in the Cache Creek terrane (Carboniferous to Lower Jurassic). However, parts of Cache Creek terrane may be related to Stikinia (English et al., 2010; Zagorevski et al., 2016; McGoldrick et al., 2017).

Systematic regional mapping in the Turtle Lake map area (Fig. 2) was conducted as part of the provincial-federal Geomapping for Energy and Minerals (GEM2) program. A major objective of the mapping was to resolve the age, kinematics, and magnitude of displacement along the Stikine-Cache Creek terrane boundary. Addressing these problems is critical to deciphering what happens to the northern extent of the mineralized Late Triassic-Early Jurassic porphyry belt, which is well-developed 200 km to the south but appears to be cut out by faults near the British Columbia-Yukon border. A re-evaluation of geological relationships along previously known faults led

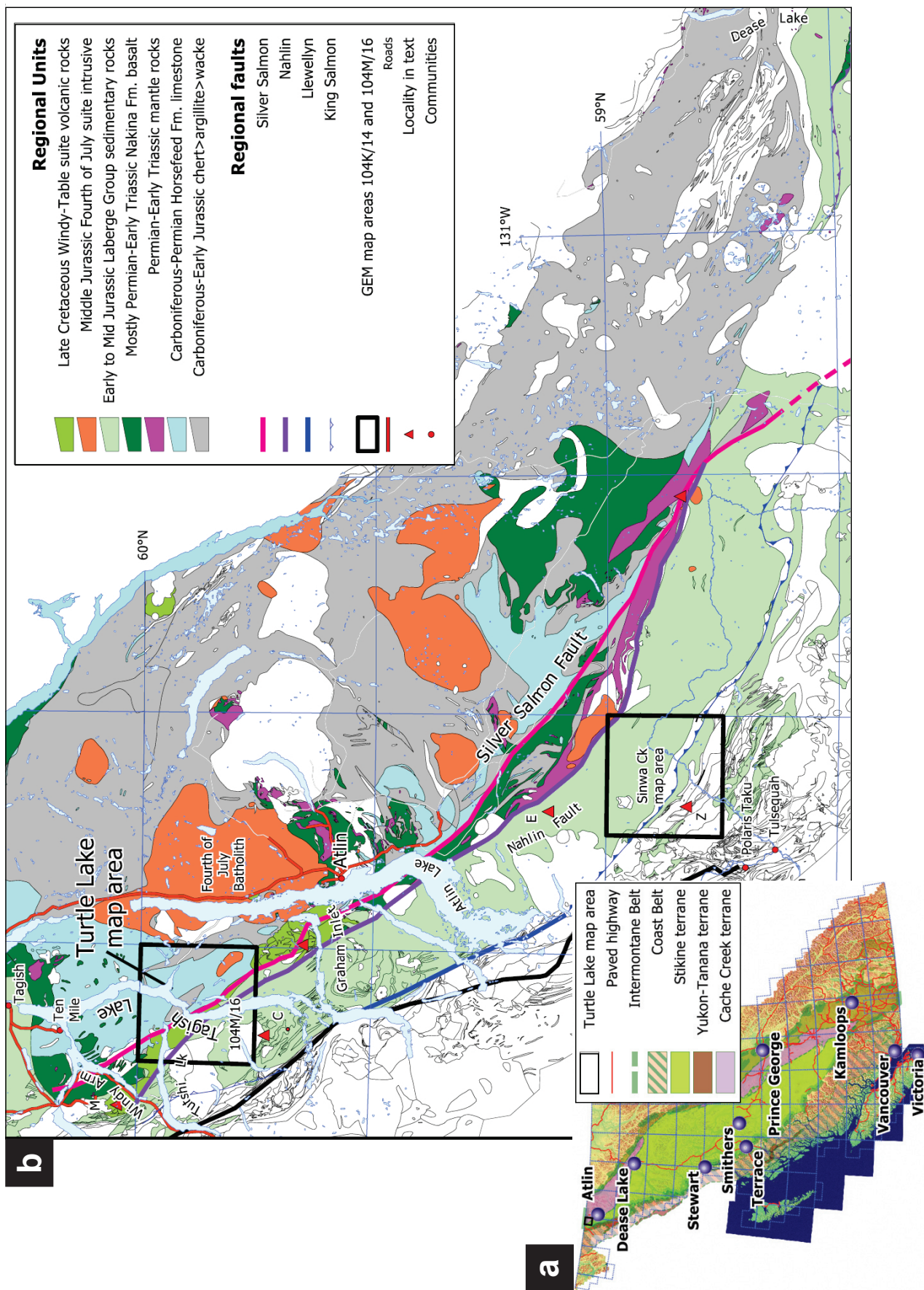


Fig. 1. a) Tectonic setting and location of the Turtle Lake map area in northwestern British Columbia. b) Regional geological setting showing the location of the quadrangles mapped as part of the Geomapping for Energy and Minerals initiative. Localities mentioned in the text are shown as labelled triangles: C – Mount Clive, E – Eclogite Ridge, M – Montana Mountain, Z – site of ~242 Ma detrital zircons in Mihalynuk et al. (2017).

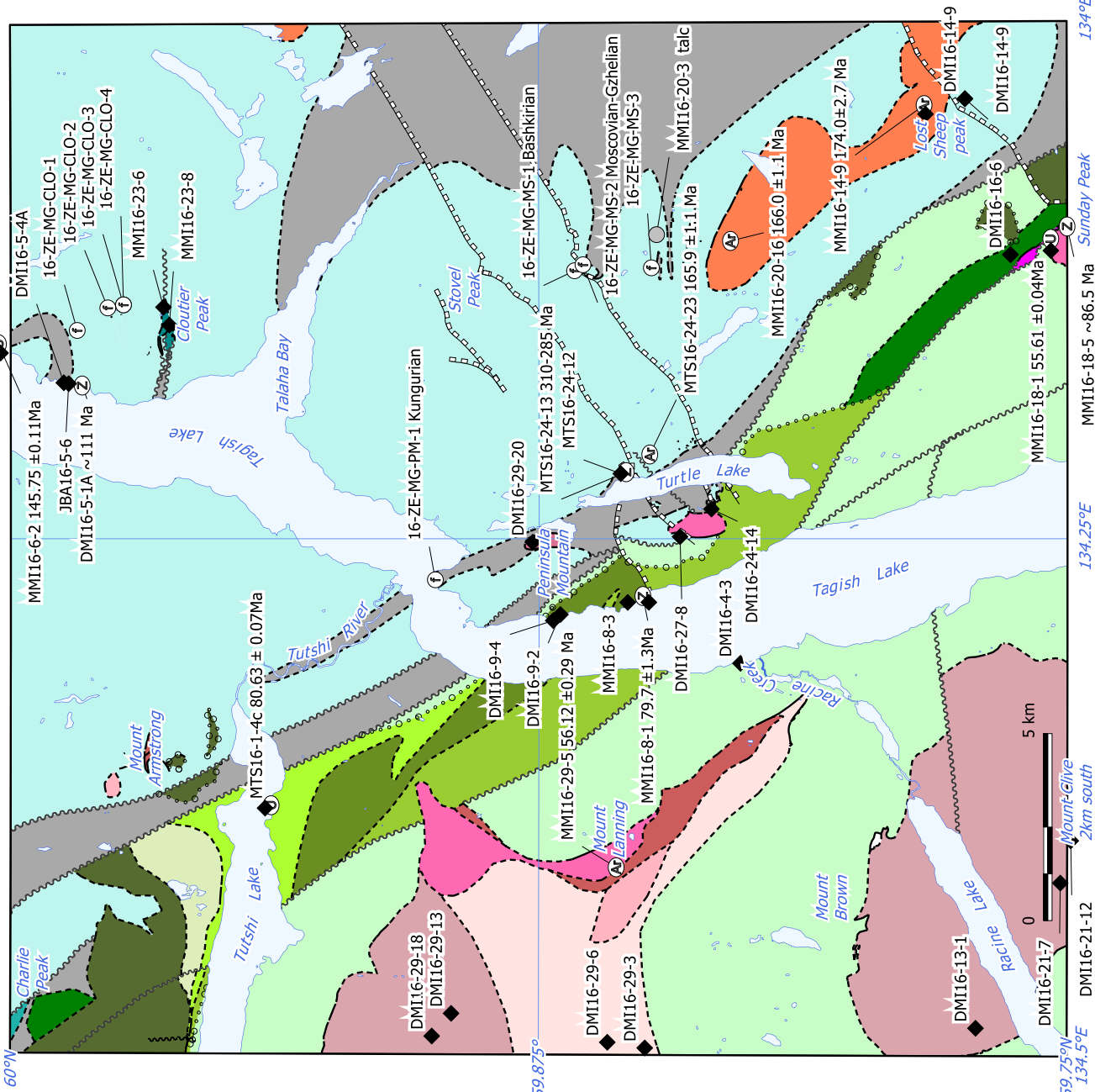


Fig. 2. Simplified geological map of the Turtle Lake map area updated from Mihalynuk et al. (1996, 1999) with location of samples for which geochronology and geochemistry results are reported herein.

to extension of the Silver Salmon fault from the Nakina area to northern British Columbia and southern Yukon, where it marks the present Stikine-Cache Creek boundary (Turtle Lake fault of Zagorevski et al., 2017). Herein we present results of systematic mapping, geochronology, geochemistry, and paleontology in the Turtle Lake area. Our data indicate that motion on the Silver Salmon fault affects rocks as young as Late Cretaceous and that fault zone fabrics are cut by an Early Eocene diorite stock. More regional work will be needed to evaluate offsets and make meaningful predictions about the apparent northward disappearance of the Late Triassic porphyry belt.

2. Physiography and previous work

The Turtle Lake map area is bisected by the main branch of Tagish Lake, which extends ~70 km southward from the northern border of the map area, adjacent Yukon (Fig. 1b). The lake provides excellent boat access; with boat launches at the community of Tagish or at Ten Mile, 22 km north of the British Columbia-Yukon border. The northwestern part of the map area can also be accessed by boat using Tutshi Lake, which is accessed from the Klondike Highway, ~17 km west of the map area. Tutshi Lake trends east across the northwest part of the Turtle Lake map area and drains into Tagish Lake via Tutshi River. Racine Lake, extends east-northeast across the southwestern corner of the map area, draining into Tagish Lake via cataract-laden Racine River. It is accessible via aircraft.

Whereas most of the area can be accessed by multi-day foot traverses, the most efficient mode of travel is by helicopter from a base in Atlin, 45 km southeast of the its central part. Extensive tree cover and brushy swamps in the northeastern part of the map area render large regions without helicopter landing sites, so the only option is foot traverse.

East of the high Coast Mountains, the Turtle Lake area is part of an orographic dry belt that receives only moderate winter snow and lacks glaciers. The highest points are Stovel Peak (1825 m) and Sunday Peak (1920 m) east of Tagish Lake and Mount Lanning (1902 m) and Mount Brown (2010 m) west of Tagish Lake, which all rise from the Tagish Highland plateau. Less than 20% of the area is above tree line, but the forests are relatively open, and usually easily navigated. Most of the eastern part of the map area is underlain by carbonate rocks with subterranean drainage and, by late summer, running surface water above treeline is almost non-existent.

Early systematic surveys of the area were conducted by Gwillim (1901), and Cairnes (1913). Quadrangle mapping covered the area at 1:250,000 scale as part of the Bennett sheet (104M) by Christie (1957). Bultman (1979) mapped the boundaries of the Whitehorse Trough through the region as part of an unpublished Ph.D. thesis, having a footprint that extended well beyond the Turtle Lake area. More detailed surveys at 1:50,000 scale almost surround the Turtle Lake map area (Mihalynuk and Rouse, 1988; Bloodgood et al., 1989; Mihalynuk and Mountjoy, 1990; Mihalynuk and Mountjoy, 1990; Mihalynuk et al., 1991; Mihalynuk and Smith, 1992a). Only the area north of the Turtle Lake mapsheet lacks systematic

quadrangle mapping at scales greater than 1:250,000 (Wheeler, 1961), although Monger (1975) covered much of the area at a 1:63,360 scale.

3. Regional geology and nomenclature

The eastern ~2/3 of the map area is underlain by extensive carbonate and lesser chert and argillaceous strata of the Cache Creek terrane (Fig. 2). Most abundant are limestones of the Horsefeed Formation (Carboniferous to Permian). They are the oldest known rocks in the Turtle Lake area (Late Carboniferous) as established by fusilinids (see Monger, 1975) and to a lesser extent, by conodonts (Golding and Orchard, 2017; see below). The western ~1/3 of the map area is underlain by coarse siliciclastic marine strata of the Laberge Group, the age of which is well-established, predominantly by ammonites (e.g., Mihalynuk et al., 1999; Johannson et al., 1997). Along most of their mapped extent, these two major rock packages are separated by the Nahlin fault zone, which trends northwest. However, Late Cretaceous volcanic strata of the Windy-Table suite and Peninsula Mountain suite (that we show here to largely belong to the former), and slivers of oceanic crustal rocks and mantle, are caught in between. Large (several tens of km²) homogeneous plutons at the western edge of the map area are outliers of the Coast Plutonic complex (~55 to 120 Ma).

Monger (1975) and Mihalynuk et al. (1999) reviewed the history of Cache Creek terrane nomenclature, which is not repeated here. However, we reiterate concerns raised by Zagorevski et al. (2016), that the present extent of Cache Creek terrane must include a major suture. Accordingly, it is a composite terrane in need of redefinition.

Mafic and minor intermediate volcanic rocks in sharp fault contact with Cache Creek limestones along eastern Tagish Lake were interpreted as the older of two volcanic packages. These rocks were mapped as Pennsylvanian to Triassic by Christie (1957), Upper Paleozoic by Monger (1975), and Middle to Late Triassic by Bultman (1979). Along strike in adjacent map sheets, they were mapped as Middle to Late Triassic (Mihalynuk et al., 1991, 1999; Mihalynuk and Smith, 1992a, b; Zagorevski et al., 2017). The younger package is mafic to felsic in composition and gently dipping where best exposed north of Tutshi Lake. It was included with “volcanic rocks of uncertain age” by Christie (1957), Late Cretaceous and/or Early Tertiary Sloko Group by Monger (1975), Middle to possibly Late Cretaceous Hutshi Formation by Bultman (1979) and, in adjacent areas, as either Lower to Middle Jurassic volcanic suite, or Late Cretaceous Windy-Table suite by Mihalynuk et al. (1999) and Zagorevski et al. (2017). Based on new geochronological data reported here, we suggest that most, if not all, of these rocks should be assigned to the Windy-Table suite.

3.1.1. Cache Creek terrane

In the Turtle Lake map area, Cache Creek terrane comprises the Horsefeed Formation limestone, Kedahda Formation chert (Watson and Mathews, 1944), and minor Nakina Formation mafic volcanic rocks (Monger, 1975). Although major

problems with this stratigraphic nomenclature exist (Monger, 1975; Mihalynuk et al., 1999; Zagorevski et al., 2016), we follow it for regional consistency until a thorough redefinition of the Cache Creek terrane is undertaken.

3.1.2. Horsefeed Formation limestone

The Horsefeed Formation is the most extensive unit in the Turtle Lake map area. These rocks have been described in detail by Monger (1975) who estimated their original thickness to be 1.5 km and obtained fossil ages ranging from Late Carboniferous (Middle Pennsylvanian) to Late Permian. The Horsefeed Formation is a mostly massive, variably recrystallized limestone, generally cream-coloured, but ranges to yellow and grey with local zones of red or black (Fig. 3). Layering that is apparent at a distance is commonly not discernable up close. Bioclasts, especially crinoids, can be locally found. However, well-preserved fossils are rare due to recrystallization, which is especially intense south of Stovel Peak where radiating talc splays are abundant in hydrothermally altered limestones in the contact metamorphic aureole of a Middle Jurassic pluton (Fig. 4a). Local variants of the Horsefeed Formation include well-bedded limestone (Figs. 3a, b), limestone interbedded with chert (Figs. 3b, c, d), limestone breccia (Figs. 3e, f), fusulinid packstone (Fig. 3g) and tuffaceous limestone (Fig. 3h).

Well-bedded limestone, with layers 0.05 to 2 m thick, tend to be darker grey (Fig. 3b) where bedding is thinnest, perhaps due to greater organic content. At two localities, thin (0.1-0.4 m) beds of packstone (Fig. 3a) contain fusulinids up to 1 cm in diameter (Fig. 3g). Fusulinids range from well preserved (where individual living chambers can be discerned with an unaided eye) to strongly deformed (Fig. 3g). Monger (1975) reported a late Early Permian fossil age from one of these localities. Limestone locally contains chert nodules, lenses and discontinuous layers up to 0.5 m thick that are grey to black (Figs. 3b, c). Chert layers are locally boudinaged within the recrystallized carbonate. Sparse younging indicators suggest a general increase in chert upsection towards the Kedahda Formation, consistent with the observations of Monger (1975).

Limestone breccias are common and likely have more than one origin. Conformable breccia beds have thicknesses in excess of 10 m. Most are clast supported, and whereas some layers appear uniform, with mm to cm-scale angular clasts set in a carbonate cement (Fig. 3e), they can contain outsized blocks up to several m in diameter. Other layers contain cm-dm clasts (Fig. 3f). Still others locally form semi-concordant sill and dike-like bodies in ribbon cherts (Fig. 5a; see below), some with blocks of deformed chert metres across floating in carbonate breccia. Other discordant breccia bodies, generally cemented by carbonate, are along brittle fault zones. All are likely produced by mass flow. Monger (1975) attributed isoclinally folded blocks of chert and interlayered limestone west of Mt. Cloutier to similar syn-sedimentary gravity sliding. In the Tagish area, fossils in breccia blocks tend to be of the same age as the fossils in the contiguous main mass of limestone (Monger, 1975). Immediately east of Turtle Lake, a

several metre-thick bed containing angular clasts of limestone, minor chert, and sparse rhyolite was sampled for detrital zircon age determination. Zircons recovered from this bed range from Middle Pennsylvanian through Early Permian (see below).

Exposed on a low ridge south of Stovel Peak, and at two sites along the east shore of Tagish Lake (Fig. 2), are limestone breccias with a calcarenite matrix containing a maroon hematitic cement that stands out against a backdrop of mainly white-weathering Horsefeed Formation (Figs. 4b, c). South of Stovel Peak, the calcarenite matrix is well laminated (Fig. 4c) and consists of spherical and round grains. The laminae drape and are folded around breccia clasts. Lamination in the matrix material indicates post-brecciation sedimentary infill, suggestive of a paleokarst origin, which is supported by Early Cretaceous detrital zircons from one sample of the laminated matrix (see below).

Green and maroon tuffaceous beds that are centimeters to a few metres thick form inconspicuous low outcrops on the northwest flank of Mt. Cloutier (Fig. 3h) and along eastern Tagish Lake, across from the mouth of the Tutshi River. These contain angular lapilli and ash-sized, aphanitic to finely plagioclase-phyric clasts in a carbonate matrix. Fine calcite-filled amygdales are common. Fine tuff layers are typically foliated, and the foliation is locally crenulated. Tuffaceous strata on Cloutier Peak are roughly along strike with Early Permian limestone (Monger, 1975). However, our samples of limestone interbedded with tuff did not yield conodonts (see below). Tuffaceous limestone breccia east of Turtle Lake contains detrital zircons that cluster at ~285 Ma, which we interpret as the best estimate of the maximum depositional age (see below), consistent with Early Permian deposition.

3.1.3. Kedahda Formation chert

The Kedahda Formation is best exposed on the east shore of Tagish Lake (northwest of Cloutier Peak, Figs. 5a, b), on the low ridges south of Stovel Peak, and north and east of Turtle Lake (Fig. 2). In these areas, well-bedded Kedahda Formation comprises 2-15 cm thick layers of black chert and 0.5-2 cm thick layers of argillite. The chert, locally varies from black to tan or nearly white. Radiolaria have been generally destroyed by recrystallization. Chert is generally more abundant than argillite. However, this may be due to recessive weathering of argillite such that it is only exposed in creek bottoms or low-profile outcrops along lake shores. Syn-sedimentary deformation structures include clastic dikes (Fig. 5a) and gravity slides.

Direct age determinations from chert in the Turtle Lake area are lacking. An early Early Permian fossil age (Monger, 1975) was determined for a breccia block contained in the chert unit north of Turtle Lake (where exposed on Tagish Lake), indicating that chert at that locality is early Permian or younger. Along strike, ~20 km southeast of the Turtle Lake map area (north of Graham Inlet), chert interbedded with wacke yielded Middle to Late Triassic radiolaria (Mihalynuk et al., 1999). Regionally, chert ranges from Paleozoic to Late Triassic, with abundant

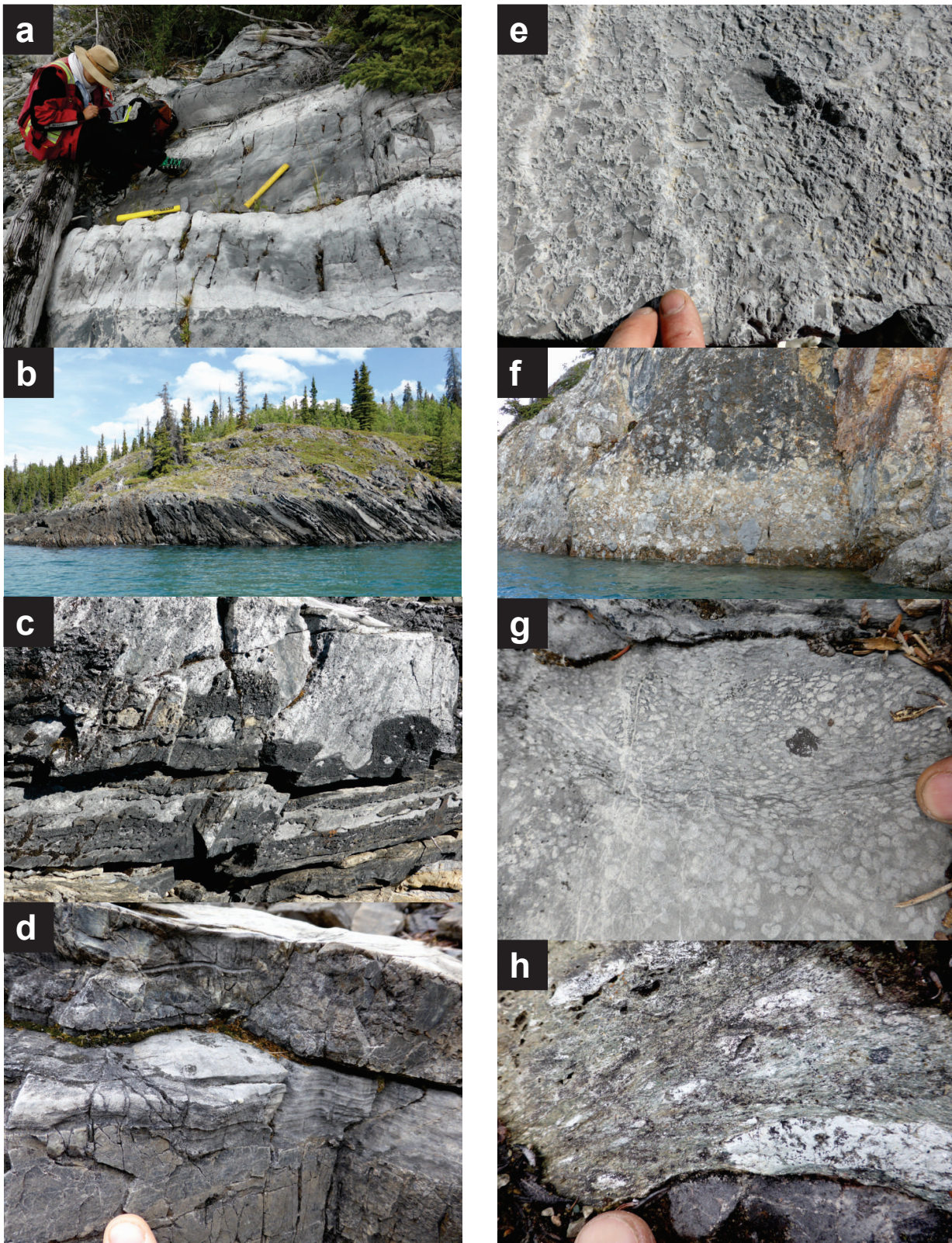


Fig. 3. Examples of Horsefeed Formation limestones, which are generally massive, that display structures. **a)** Thick bedded, fusulinid-rich bioclastic limestone. **b)** Massive chert grading to medium- to thin-bedded, grey cherty limestone upsection, to the right of photo (south). **c)** Straight and irregular zones of chert and limestone. **d)** Laminae from limestone continues into chert lens (above finger) indicating diagenetic replacement of limestone. **e)** Fine, homogeneous monomictic limestone-clast breccia. **f)** Coarse, mainly monomictic limestone-clast breccia. **g)** Fusulinid packstone; finger on high-strain zone. **h)** Foliation in green tuffaceous limestone wraps around flattened, white lapilli; in sharp contact with a grey limestone bed at bottom of photo.

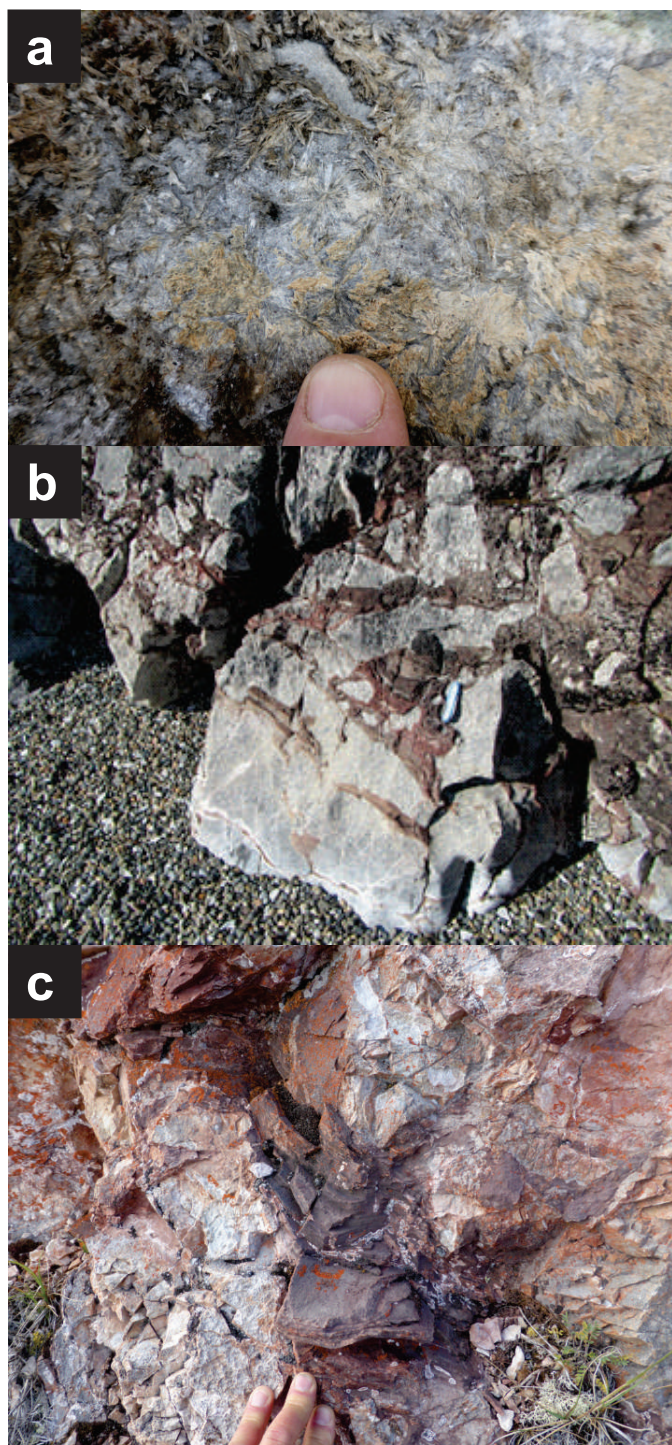


Fig. 4. a) Radiating talc crystals grow in thermally metamorphosed Horsefeed Formation. **b), c)** Bioclastic framework-intact limestone breccia with laminated, hematitic calcarenite matrix. Detrital zircons extracted from the matrix yielded an Early Cretaceous population, supporting the interpretation of the breccia as a paleokarst deposit (see below).

Middle Triassic chert in the Nakina Lake area (Mihalynuk et al., 1999, 2003), and voluminous Late Triassic chert in the Teslin area (Cordey et al., 1991). Probably the most common

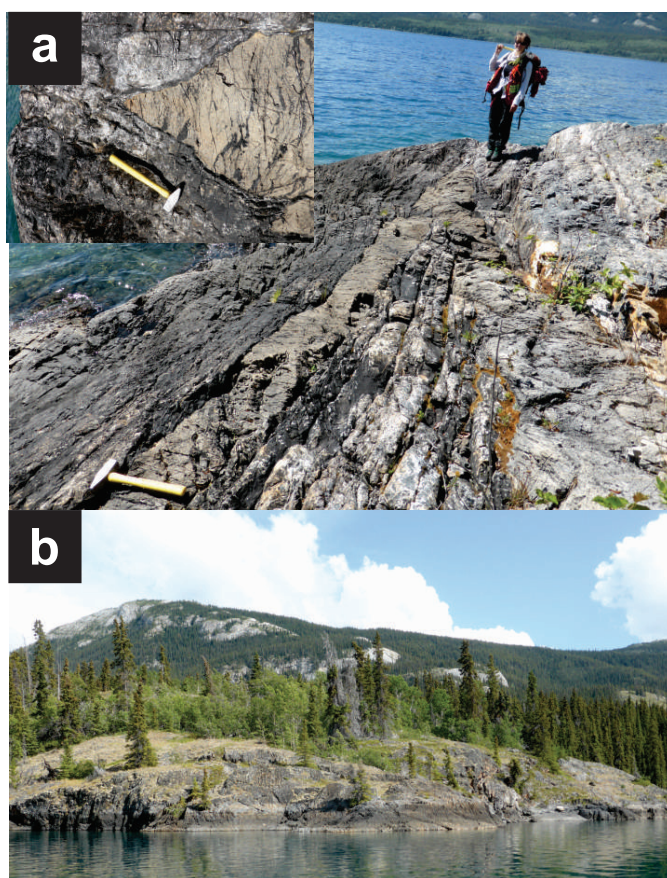


Fig. 5. a) Tan-weathering clastic carbonate intrusions cut well-bedded Kedahda Formation chert. Inset shows sill termination (in front of person). View to the northwest. **b)** Well-bedded Kedahda Formation ribbon chert along the eastern shore of Tagish Lake. View along strike to the southeast. On horizon is massive carbonate underlying the northern ridge of Mount Cloutier.

age of chert in the Tagish-Atlin region in British Columbia is Middle Triassic.

3.1.4. Nakina Formation basalt

Dark green to black, highly fractured to blocky weathering, aphanitic to finely feldspar- and pyroxene-phyric mafic rocks are well exposed on the east flank of Sunday Peak, extending in a belt toward Peninsula Mountain (Fig. 2). The Nakina Formation comprises rocks interpreted as basalt flows and tuff (Mihalynuk et al., 1999). Pillow basalt is locally exposed, but there is a substantial volume of hypabyssal diabase sills and dikes with very similar petrographic characteristics. Sparse geochemical data suggest that these mafic rocks have island arc to backarc tholeiite characteristics. These volcanic and shallow intrusive rocks are adjacent to a fault-bound sliver of mantle tectonite and both have previously been included in the Graham Creek suite (Mihalynuk et al., 1999). Elsewhere in the Cache Creek terrane, the association of island arc tholeiites and mantle tectonites has been interpreted to represent a structurally dismembered ophiolite (English et al., 2010; Zagorevski et al., 2016; McGoldrick et al., 2017). Graham Creek rocks were

previously considered probable correlatives of the Cache Creek ophiolitic rocks, but were separated because a gradational contact with overlying Laberge Group could be inferred (Mihalynuk et al., 1999), whereas, evidence for Cache Creek terrane basement was, at the time, more equivocal. Recent detrital zircon evidence from with wacke deposited on the Cache Creek terrane supports correlation with Laberge Group (Colpron et al., 2015), and a stratigraphic linkage of Cache Creek and Laberge Group by earliest Jurassic.

3.2. Laberge Group

Descriptions of the Laberge Group strata in areas immediately adjacent to the Turtle Lake mapsheet are detailed in Mihalynuk et al. (1999). The sedimentology, depositional setting, and paleontology of the Laberge Group have been addressed by many studies (e.g., Wheeler, 1961; Tempelman-Kluit, 1978; Tempelman-Kluit, 1984; Dickie and Hein, 1995; Hart et al., 1995; Hart, 1997; Johannson et al., 1997; Mihalynuk et al., 1999; Lowey, 2003; Lowey, 2004; Colpron et al., 2015). In the Turtle Lake area, the Laberge Group consists mainly of thick-bedded coarse wackestone, thin-bedded siltstone, and lesser rhythmically bedded sandstone and mudstone. The scale of interlayering is too fine to resolve at the 1:50,000 scale of our mapping.

3.2.1. Rhythmic sandstone-mudstone couplets (Richthofen formation)

Distinctive, rhythmically bedded, tan and black, sandstone-mudstone couplets (Fig. 6a) comprise what is possibly the lowest exposed unit of the Laberge Group in the Turtle Lake map area. Thin parallel beds are typically 2-5 cm thick, normally graded, and display bioturbation. Syndepositional folds and faults as well as intraformational angular unconformities are common. Outcrops are commonly well-cleaved.

This unit is a characteristic component of the informal Richthofen formation, which is recognized as forming the Early Jurassic base of the Laberge Group in the type area of Yukon (Hettangian to Pliensbachian; Tempelman-Kluit, 1984), consistent with observations in the Turtle Lake area. However, this unit is also observed at localities that are well above the base of the Laberge Group, in agreement with the suggestion of Lowey (2004), that it ranges to Toarcian (upper Lower Jurassic).

3.2.2. Thick-bedded coarse greywacke

Orange to brown or grey, blocky weathering greywacke is the most common Laberge Group rock type in the map area. Beds are generally 0.3-2 m thick, but are locally >10 m thick. Coarse feldspar and lithic grains predominate, although quartz grains can comprise up to ~15% of the rock. Rare beds of arkosic or lithic sandstone contain only minor muddy matrix. Sparse pebbles and cobbles of arc-like magmatic and sedimentary rocks are common. Northwest of Sunday Peak, greywacke contains conspicuous black volcanic clasts with blocky feldspar phenocrysts (Fig. 6b). These resemble volcanic clasts that are

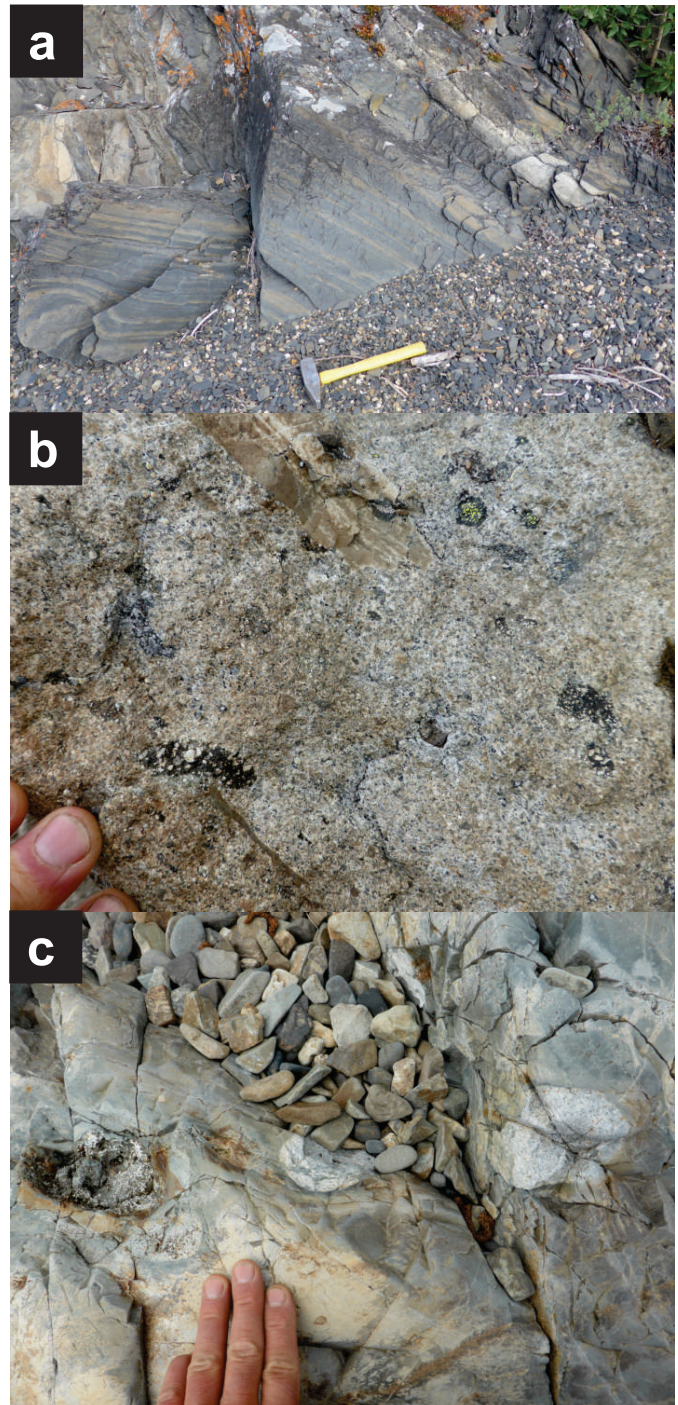


Fig. 6. Variation of Laberge Group lithologies. **a)** Rhythmically bedded tan wackestone and black argillaceous siltstone is typically bioturbated and strongly cleaved. **b)** Very coarse wacke to granule conglomerate with sparse oversized boulders. Distinctive, flattened black clasts with blocky feldspars are interpreted as collapsed pumaceous blocks. **c)** Polymictic matrix-supported conglomerate. Clasts range from diorite to granite and (outside of view) conglomerate to limestone.

common in the Eclogite Ridge section of the Laberge Group, about 100 km to the south (Canil et al., 2005). In other places, cobbles of arc provenance can comprise over 10% of the unit (Fig. 6c).

3.2.3. Thin-bedded siltstone

Rusty-weathering, indurated, well-bedded siltstone erodes to form slopes of fine angular talus. This unit consists of siltstone and argillaceous siltstone in beds that are typically less than 10 cm thick and may locally be cross stratified.

3.3. Windy-Table suite

The Windy-Table suite (Late Cretaceous; Mihalynuk et al., 1999) was first defined in the Windy Arm (western branch of Tagish Lake in Yukon) and Table Mountain areas (Fig. 1b). In the Turtle Lake area, the Windy-Table suite is exposed in a belt extending northwest from Sunday Peak. The base of the Windy-Table suite is seen at Sunday Peak and eastern Tutshi Lake (Fig. 7), where basal reworked rhyolite breccia (Figs. 7a, b) unconformably overlies Laberge Group and harzburgite tectonite. Three units predominate the suite near Tutshi Lake: a basal rhyolite to trachyte (Fig. 8a), overlying andesitic flows and interflow breccia and tuff (Fig. 8b), and heterolithic lapilli tuff and breccia (Fig. 8c). Near Peninsula Mountain, monomict volcanic conglomerate is predominant. Thinner units of fine-grained basalt and grey and green tuff are not divisible at the scale of Figure 2, where they are shown combined.

3.3.1. Rhyolitic rocks

Two types of rhyolitic rocks crop out in the Turtle Lake area: breccia at Sunday Peak (Fig. 7b), and rhyolite tuff at Tutshi Lake (Fig. 8a). New geochronologic and stratigraphic evidence that we report (see also Zagorevski et al., 2017) suggest that the units belong to the lower and middle parts of the Windy-Table suite.

On the eastern side of Sunday Peak (Fig. 7a), rhyolite breccia (Fig. 7b) marks the contact between mantle rocks (Figs. 7a, c) of the Cache Creek terrane and Whitehorse trough strata. Rhyolite breccia displaying finely embayed clasts (Fig. 7b) is in fault contact with strongly foliated serpentinized harzburgite to the east (Fig. 7c). Near its western limit of exposure, the rhyolite breccia is in contact with Laberge Group strata. At this locality, subangular fragments of the Laberge Group appear mixed with the rhyolite and may be conglomeratic, indicating an unconformable relationship, but thermal alteration caused by the nearby Sunday Peak stock (Fig. 7d) obscures relationships. A pebble dike or surface fissure infill contains a mix of rhyolite breccia and clasts of harzburgite within harzburgite (Fig. 7a inset). A sample of the main breccia layer yielded new U-Pb data that suggest an age of ~86.5 Ma (see below).

Along the shores of eastern Tutshi Lake, white and orange, rubbly-weathering rhyolite tuff (Fig. 8a) and trachytic flows occupy the structurally lowest exposed parts of the suite. Rhyolite tuff is composed of aphanitic cream and tan lapilli and blocks in layers up to tens of metres thick. Locally the unit contains a few percent of medium-grained, pinkish orthoclase crystals and rare medium-grained quartz eyes. Wispy chlorite layers are likely relicts of flattened pumice lapilli.

Near the base of the precipitous south face of Charlie Peak, along the western edge of the map area, a discontinuous section

is exposed. Starting at lake level, poorly bedded Laberge Group wacke becomes red and oxidized up section, until it is overlain by well-bedded, shallowly north-dipping, maroon and green volcanic sandstone containing granules of underlying Laberge Group and rhyolite and green felsic tuffaceous interbeds that have a waxy luster. Above is the main mass of Windy-Table volcanic strata with rhyolite at its base. The contact is interpreted as an angular unconformity even though definitive bedding could not be found in immediately underlying Laberge Group strata, which are extensively folded in most other localities. Below we report a new U-Pb zircon age from the thickest mapped part of the rhyolite unit.

3.3.2. Coarse volcanic wacke

Coarse-grained volcanic wacke to feldspar-phyric granule conglomerate displays poorly developed layering. This unit may be a fine-grained equivalent of the conglomerate along the southwest side of the Peninsula Mountain where it is separated from Kedahda Formation chert by covered intervals. However, volcanic wacke and Middle to Late Triassic chert are interbedded near Graham Inlet to the southeast (Mihalynuk et al., 1999; Zagorevski et al., 2017), demonstrating the difficulty in correlating this unit regionally.

3.3.3. Fine-grained to aphanitic basalt

Dark grey to black, tan weathering, fine-grained to aphanitic amygdaloidal basalt is typically grey to mint green on fresh surfaces and brecciated, forming massive intervals tens of metres across. In some localities, probable flows display vague pillow forms (Fig. 9a), but these are obscured by autoclastic and subsequent fracturing. The basalts contain fine phenocrysts of augite, and very fine-grained needles of plagioclase, indicating that clinopyroxene preceded plagioclase on the basalt liquidus. Most of these rocks have island arc tholeiite affinity, serving to distinguish them from E-MORB basalts of the Horsefeed Formation, but they are difficult to distinguish lithologically and geochemically from Nakina Formation, and may be partly correlative (see below).

3.3.4. Grey and green tuff

Angular block to lapilli tuff is dark green to black-weathering, and where wave-washed or fresh, displays a lighter grey (Fig. 9b) or green ash-rich matrix. Clasts tend to be sparsely pyroxene-phyric, some with fine feldspar, or aphanitic. Matrix-deficient samples have a basaltic composition. In a few localities, sparse, irregular black clasts of indurated rock may be siltstone. Some clasts display white rims. Rarely this unit contains aphanitic clasts that are entirely white and may be of felsic composition (Fig. 9c). At one locality, light-coloured clasts predominate the rock (Fig. 9d), but here they contain coarse prismatic crystals that are probably hornblende, and ghosts of green to white crystals, probably feldspars that were chloritized and then further altered and bleached. Below we report an age from this unit of 79.7 Ma.

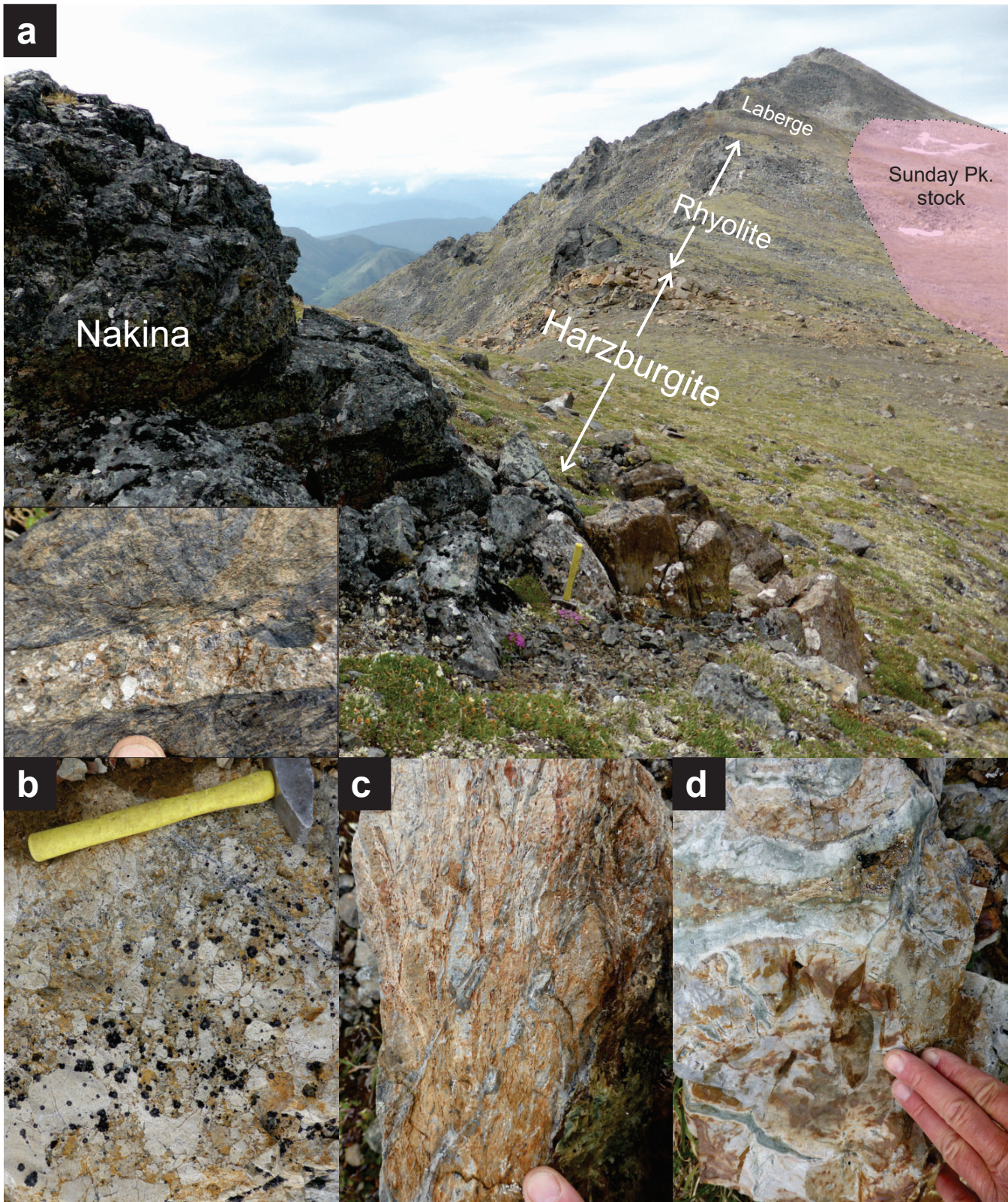


Fig. 7. Contact relationships in the saddle east of Sunday Peak. **a)** View to the southwest parallel to the steep face of the peak shows dun-weathering harzburgite extending from near foreground to just beyond the low point of the saddle. Immediately beyond the far harzburgite outcrop is a resistant knob of rhyolite breccia (close up view in **b**), which is foliated and in direct contact with serpentinite (exact contact beneath finger in **c**). Light weathering-resistant breccia gives way to rusty weathering, rounded ridge underlain by Laberge Group. clastic rocks. Light weathering rocks along the far right side of the photo (**a**) are thermally altered (as in **d**) by the Sunday Peak stock that partly underlies the far snow patch (approximate distribution is shown).

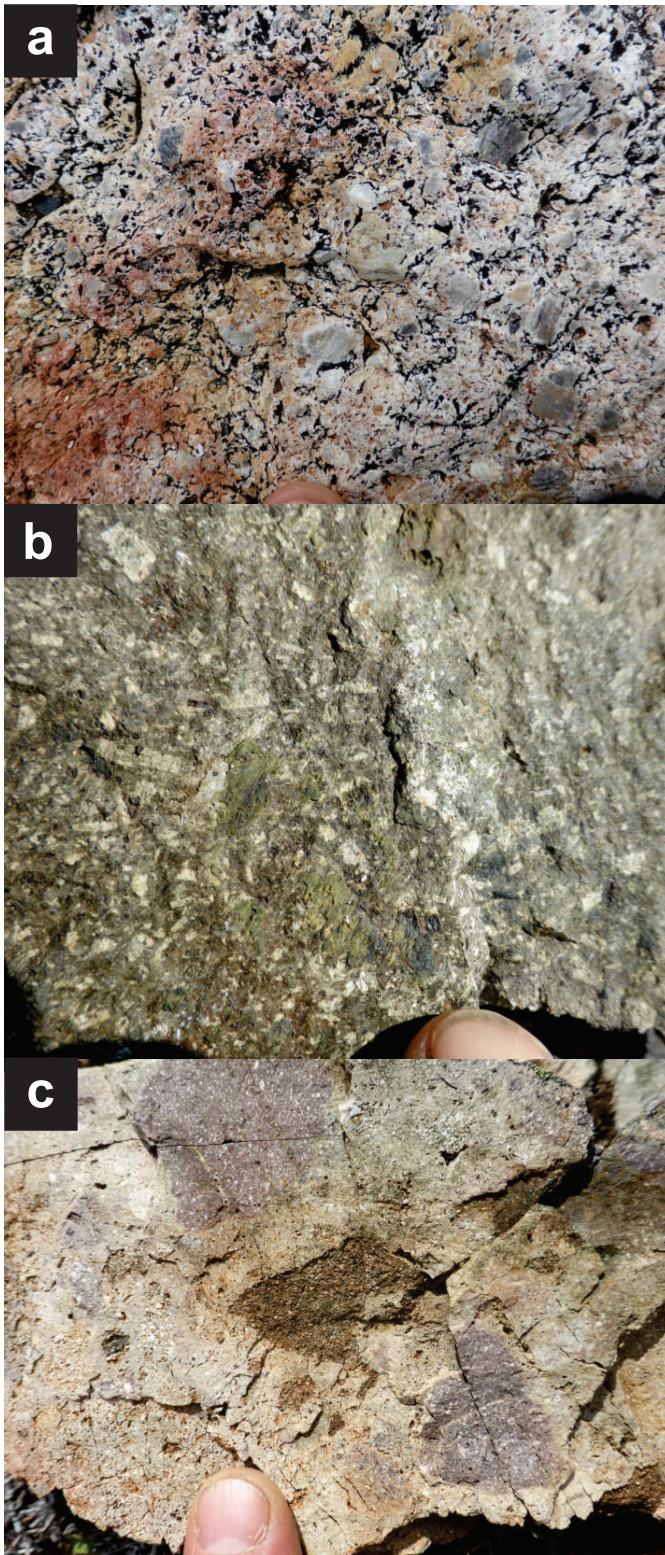


Fig. 8. Characteristic Windy-Table suite rock types near eastern Tutshi Lake. **a)** Rhyolite at the base of the section, south shore, eastern Tutshi Lake. **b)** Tabular feldspar porphyry of autoclastic flows above the rhyolite, north of eastern Tutshi Lake. **c)** Variegated fine- to medium-grained, tabular plagioclase porphyry tuff near Sunday Peak is similar to units north and south of eastern Tutshi Lake, and if reworked, the conglomerate facies near Peninsula Mountain (Figs. 9 e, f).

3.3.5. Monomictic volcanic conglomerate

Rounded blocks up to 1 m in diameter of orange or green-weathering, (Figs. 9e, f) brown to green pyroxene-feldspar porphyry typically float in a matrix of medium-grained grey volcanic wacke to angular granulestone. Pyroxene crystals are medium- to coarse-grained, black, chloritized and comprise up to ~5% of the volcanic clasts. Feldspar is mainly fine- to medium-grained and comprises up to ~30% of the clasts. Clasts vary in colour, grain size, and angularity, but have a uniform mineralogy and are presumably derived from a single volcanic source.

3.3.6. Feldspar-phyric flows and interflow breccia

Coarse, white tabular feldspar crystals up to ~1 cm in length comprise ~20% of the rock. An olive brown matrix contains ~1% fine black blocky relicts of mafic crystals, probably pyroxene or hornblende, altered to chlorite. Epidote alteration and veins are common (Fig. 8b). Flows range from a few m to probably more than 10 m thick. Although the rubbly nature of most outcrops makes definition of upper and lower flow surfaces uncertain, the relatively resistant flows form subhorizontal topographic benches. Recessive interflow breccia is the same composition as the flows and is generally massive with internal bedding and reworking of clasts to form conglomerate observed in a few localities.

3.3.7. Heterolithic tuff

Rocks of the Windy-Table suite, which are not mapped as parts of the foregoing units, are predominantly fine- to medium-grained feldspar-phyric block and lapilli ash tuff (Fig. 8c, included on Figure 2 with 'undivided volcanic') of probable intermediate composition, and containing varying proportions of felsic volcanic clasts. Other distinctive lithologies, which are too isolated to map at 1:50,000 scale, are also included. Some examples are: discontinuous rhyolitic tuff layers (locally containing coarse biotite); and andesitic flows (in one case displaying indistinct pillows).

4. Intrusive rocks

Elliptical to irregularly-shaped stocks of quartz diorite to granite composition are less than one to several km² in size where they cut the eastern margin of the Cache Creek terrane between Sunday Peak (Fig. 10a) and Mount Lanning. Larger bodies, tens of km² in size and mainly of granodioritic composition, cut rocks of the Whitehorse trough farther west and closer to the main mass of the Coast Plutonic complex. Based on geological relationships and K-Ar cooling ages of other bodies in the suite, the ages of stocks and plutons in the Turtle Lake map area were assumed to be Late Cretaceous to Early Tertiary (Mihalynuk et al., 1996), but based on our new isotopic age determinations, are now known to extend from Middle Jurassic to Eocene.

Most stocks and plutons are heterogeneous. For example, the Middle Jurassic (174 ± 2.7 Ma) elongate pluton extending from Lost Sheep peak ~10 km northwest, is compositionally and

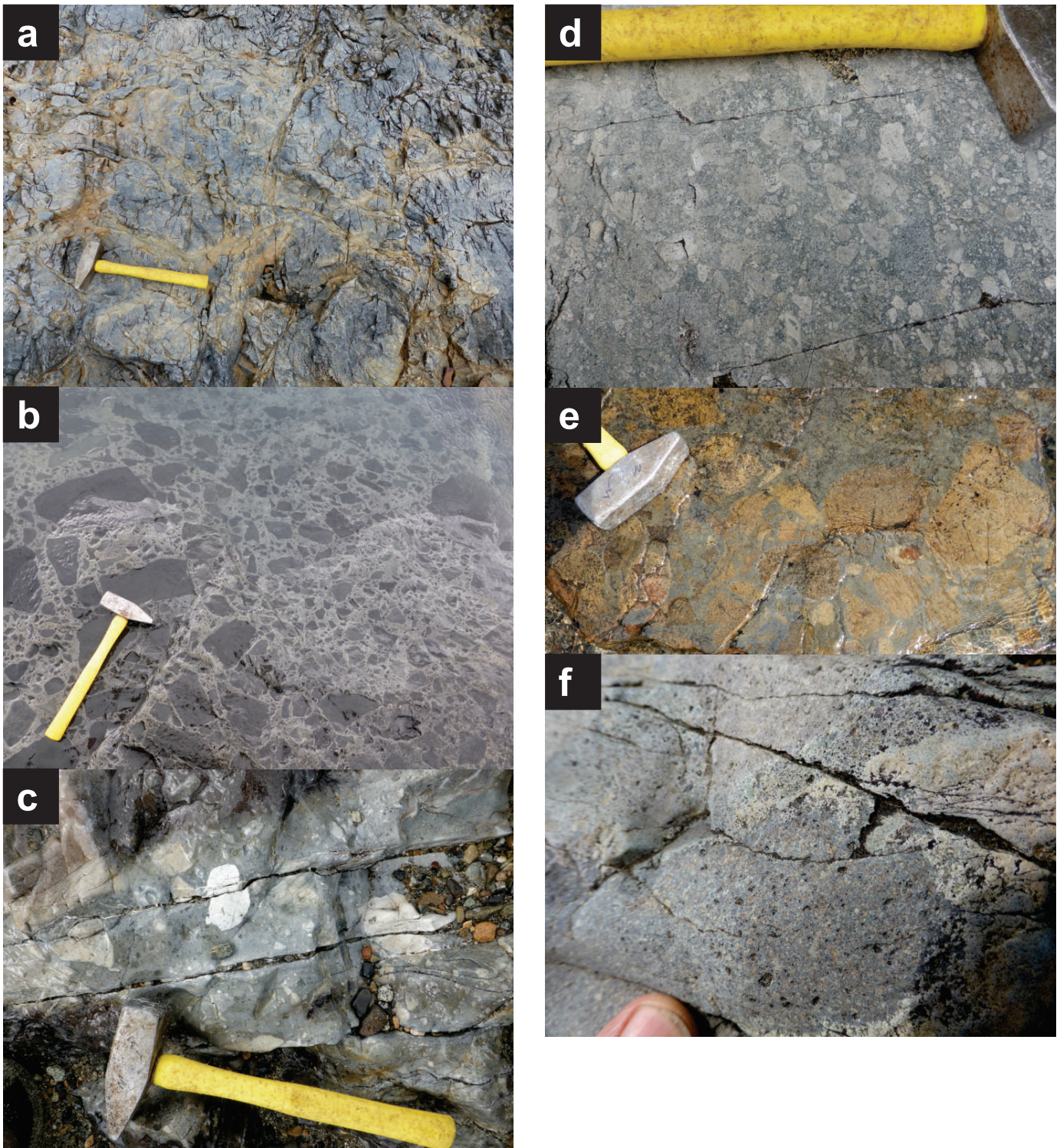


Fig. 9. Variations in the Windy-Table suite at Peninsula Mountain. **a)** Aphanitic brecciated basalt with vague pillow forms. **b)** Angular breccia blocks floating in an ash tuff matrix. **c)** Heterolithic tuffaceous conglomerate with light and dark clasts. Clasts are light coloured due to alteration, but also due to more felsic compositions. **d)** Felsic tuffite is composed largely of angular fragments. **e)** Monomictic volcanic conglomerate. Despite colour and grain size variation, the phenocryst assemblage is consistent. **f)** Close-up of conglomerate showing homogeneous pyroxene-feldspar-phyric clasts and greywacke to granulestone matrix.



Fig. 10. Variability of Cretaceous intrusive rocks in the Turtle Lake area. **a)** Quartz diorite marginal phase of the Sunday Peak stock. **b)** Dark-weathering lamprophyre dike is extensively back-veined by the light pink granitic phase of the intrusion at Lost Sheep peak that it cuts, suggesting that the granitic and lamprophyre melts are synchronous. Because of the higher melting temperature of lamprophyre, it breaks into blocks while the granitic melt flows between blocks. **c)** Foliated and pegmatitic phases of Lost Sheep peak intrusion close to its northwestern end. **d)** Extensive dikes cut strongly recrystallized Horsefeed Formation on the valley side east of Turtle Lake. The northwest extension of the intrusion at Lost Sheep peak, or a related body is interpreted to lie beneath. **e)** Spongy texture of miarolitic granite at Mount Lanning.

texturally variable with multiple cross-cutting phases ranging from aplite to lamprophyre (Fig. 10b). Near its northern limit, medium-grained granodioritic phases can be strongly foliated and cut by non-foliated quartz diorite to granite or pegmatite (Fig. 10c) with hornblende and biotite cooling ages of ~166-162 Ma (see below). Continuation of this elongate body in the subsurface is indicated by a zone of strong recrystallization and

extensive dike emplacement in Horsefeed Formation limestone east of Turtle Lake (Fig. 10d), and by its aeromagnetic response, which extends the belt across an area with little outcrop.

Underlying northern Sunday Peak is a semi-circular granodioritic stock with a quartz-dioritic border phase (Fig. 10a). Crystallization of its northern border is now precisely dated at 56.01 ± 0.04 Ma (see below).

Large plutons west of Tagish Lake tend to be more isotropic and granodioritic in composition (ranging from quartz diorite to granite), although separate composite zones can be mapped. For example, between Mount Lanning and Racine River, northwest-trending porphyritic and quartz-dioritic belts can be mapped (Fig. 2). East of Mount Lanning a zone of spectacularly miarolitic granite crops out over at least 2 km² (Fig. 10e). From a late quartz dioritic phase we obtained a new cooling age of 56.12 ± 0.29 Ma (see below).

Most plutons have a high magnetic susceptibility relative to the rocks that they intrude and are well defined by a recent regional aeromagnetic survey (Boulanger and Kiss, 2017). However, the elongate, composite body that extends from Racine River, across Mount Lanning to the ridges south of Tutshi Lake, shows only a muted magnetic response. Approximately 3 km² of the plateau between Mount Lanning and Mount Brown is covered with granitic boulders, commonly more than a metre in diameter. The total lack of a regional aeromagnetic response is consistent with the interpretation that these boulders are coarse moraine overlying Laberge Group sedimentary rocks rather than of local derivation from a nearby intrusion in the subsurface. Currently unexplained is an aeromagnetic high in the northeast corner of the Turtle Lake sheet that was not mapped during the course of our survey. We suspect that this belongs to an apophysis of the Fourth of July batholith, the contact of which is currently mapped 5 km to the east.

4.1. Lamprophyre dikes

Dark green biotite-rich lamprophyre dikes extensively cut rocks in the Turtle Lake map area and are especially conspicuous where they cut granitoid bodies or Horsefeed Formation limestone. They range from centimetres to about 15 m in thickness and commonly display chilled margins and parallel internal zones with varying contents and compositions of xenoliths or amygdales. Differences in relative resistance to weathering of the xenoliths and amygdales give the weathered dikes a knobby appearance. At one locality on northeast Lost Sheep peak, chrome diopside xenocrysts were tentatively identified in outcrop, but could not be confirmed petrographically. A southeast-trending set of these dikes cut a granitic phase of the intrusion at Lost Sheep peak and are back-veined by that phase (Fig. 10b), suggesting that the two are penecontemporaneous. Cooling ages of ~168-174 Ma from biotite and hornblende separates of two dikes are presented below.

5. Structure

A lack of distinctive marker horizons challenges structural interpretation of the Turtle Lake area. Nevertheless, outcrop-scale structure can be observed and, in some cases, can be reasonably linked to map-scale structures.

5.1. Folds

Massive Horsefeed limestone of the Cache Creek terrane does not reveal mountain-scale folds; whereas, in the well-stratified

Laberge Group, west-verging folds and thrust faults are clearly displayed (Fig. 11a). However, argillaceous or chert-rich layers outline km-scale folds along Tagish Lake, and spectacular refolded folds are displayed at outcrop scales where Horsefeed Formation limestone has been strongly recrystallized in the thermal aureole of intrusions (Fig. 11b). At one locality, we interpret chaotic infolding of limestone breccia and chert as due to soft sediment deformation, but that tightening of such folds has resulted in refolding with an axial cleavage (Fig. 11c).

Outcrop-scale folds in fault zones are common in the Cache Creek terrane. Such folds are readily apparent in bedded chert-argillite of the Kedahda Formation and near the contact between Kedahda and Horsefeed formations (Fig. 11d). Steep easterly plunges of folds in fault zones are common.

5.2. Faults

Fault styles in the Cache Creek terrane and Whitehorse trough contrast strongly. Late Middle Jurassic collapse of the Whitehorse Trough (Thorstad and Gabrielse, 1986; Mihalynuk et al., 2004) produced a fold and thrust belt characterized by transport of the interior parts of the trough over its southwest margin (Mihalynuk et al., 1999; English, 2004). Bedding-parallel thrusts can be identified by close examination of outcrops, or are clear at mountainside scale where hangingwall or footwall cutoffs are displayed (Fig. 11a). Such fold and thrust belt style of deformation is not apparent in the Cache Creek terrane of the Turtle Lake area, although, along strike to the northwest, Monger (1975) mapped a thrust belt along Windy Arm where structural repetition of stratigraphy is confirmed by fossil age determinations.

High-angle faults that cut Cache Creek terrane rocks at the outcrop scale are common, but identification of marker horizons and quantifiable offset by faults that can be mapped at 1:50,000 scale, are lacking. Zones of disruption m to 10s of m across that juxtapose disparate rock packages are also common, with implied large (hundreds of metres to many kilometres), but unquantified offsets. Faults with outcrop-scale offset include zones of brittle and ductile shear, which are especially well displayed by Horsefeed Formation carbonates. At one locality, a fusulinid packstone has been subjected to ductile deformation recorded by elongation of originally ovoid fusulinids (Fig. 3g). Major faults within the Horsefeed Formation show admixture of other lithologies such as angular aphanitic felsic or deformed shale and chert fragments (Fig. 12a). Within other Horsefeed Formation faults, carbonate blocks are milled and rounded with only sparse extraformational fragments (Fig. 12b).

Faults in the Kedahda Formation are extensively developed across strike widths of 10s to 100s of m. Chaotic folds (Fig. 12c), small-scale duplexing, and disaggregation of layers and milling of fragmented bed segments (Fig. 12d), are common. Such widespread disruption of the Kedahda Formation suggests that either strain is preferentially partitioned into this unit, or that the unit is comprised of, and originally accumulated as, a series of fault slivers, such as in an accretionary complex.

Within the volcanic rocks at Peninsula Mountain, one major

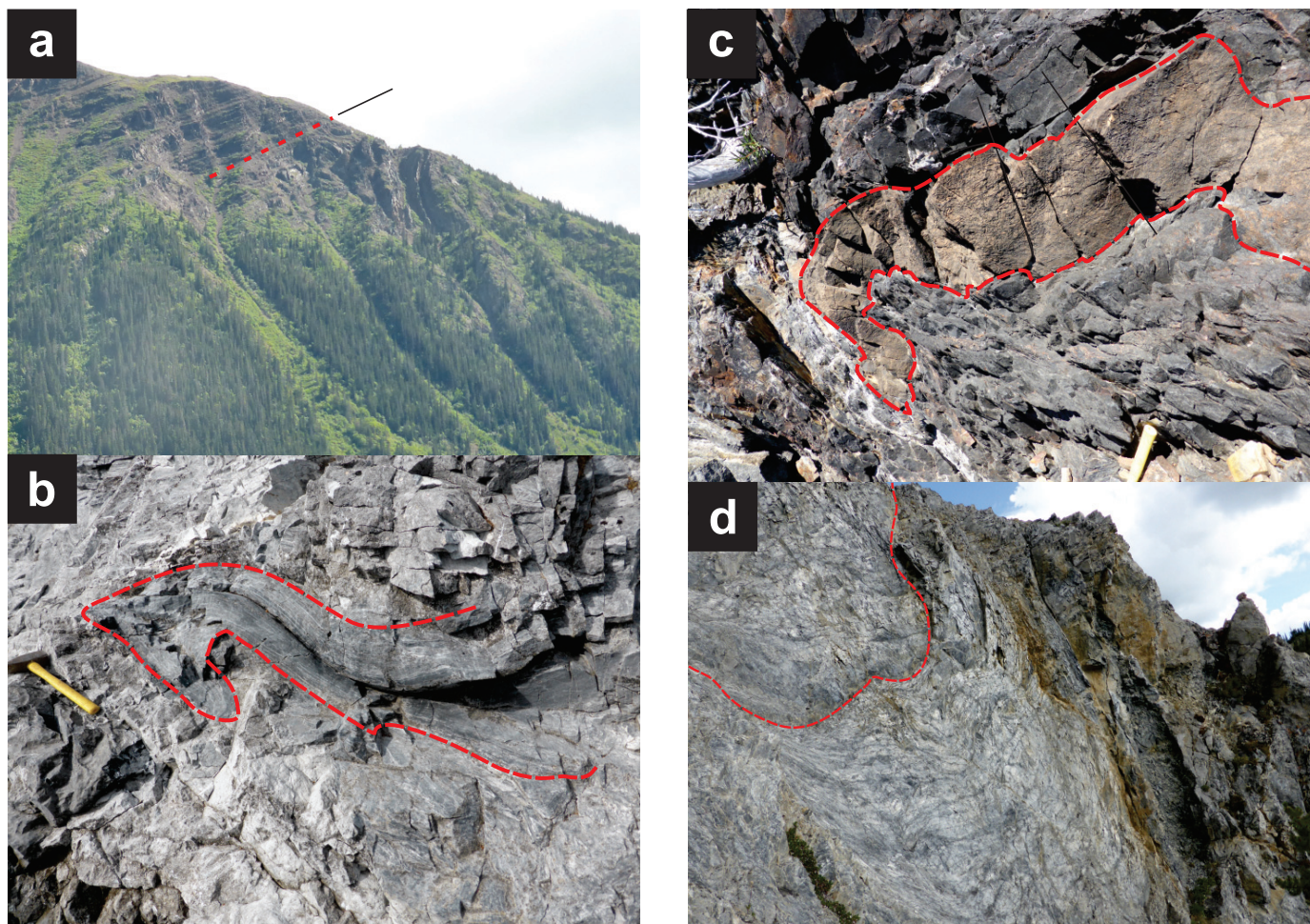


Fig. 11. Folds in the Turtle Lake map area. **a)** Southerly view of well-bedded Laberge Group strata extensively folded in the mid-right part of the photo (between the treeline and skyline, below projection of line) in the footwall of thrust with hangingwall of consistently east-dipping planar strata. **b)** Multiply-folded Horsefeed Formation limestone where thermally metamorphosed along western shore of Tagish Lake. **c)** tan carbonate layer and infolded grey bedded chert are refolded and cleaved. **d)** Steeply plunging fold in the Horsefeed Formation near the contact with the Kedahda Formation south of Stovel Peak.

fault has been mapped. It is a ~40 m wide zone displaying an anastomosing scaly fabric (Fig. 12e) around blocks of volcanic and extraformational fragments such as dioritic intrusive, serpentinized ultramafite (Fig. 12e inset) and carbonate. Dikes extensively intrude the fault zone, subparallel with the fabric. One dike has been deformed within the fabric and cut by a subsequent dike with an average strike of ~245° and dip of ~75°. At least during dike emplacement, the fault was probably extensional towards the southeast (~155°).

In outcrops across Tagish Lake, along its west shore, quasi-ductile extensional fabrics are also developed where dikes extensively cut and thermally metamorphose Laberge Group strata (Fig. 12f). A locally pervasive fabric (striking 160°, dipping ~65° WSW) cuts folded bedding (striking ~340° and dipping moderately to steeply overturned), and layers developed within that fabric are extended and rotated sinistrally. A top to the south-southeast sense of motion is indicated.

Faults between major lithologic packages can also be discrete. For example, along the eastern shore of Tagish Lake,

north of Tutshi Island, orange-weathering volcanoclastic rocks that we map as Windy-Table suite (Fig. 2), are abruptly juxtaposed across a decimetre-thick breccia zone with massive Horsefeed Fm. carbonate (Fig. 12g). There is little evidence of shearing during or after juxtaposition of these lithologies. One possibility is that the contact is part of an unconformity surface that has been repeated to the west by faulting. In contrast, near Sunday Peak, juxtaposition of Windy-Table rhyolite breccia with harzburgite is accompanied by a locally strong ductile fabric (Fig. 7c) that suggests significant syn- or post-juxtaposition movement. Rhyolite breccia west of the harzburgite is separated from the nearest main mass of Windy-Table volcanic rocks to the southeast by the nearly 500 m vertical elevation of the cliffs of southeastern Sunday Peak. A down-to-the-southeast fault separation is suggested, consistent with other indications of extensional faulting.

Limestone underlying Stovel Peak and the two unnamed mountains to the south is tentatively interpreted to be roughly equivalent and repeated by extensional faulting. However,



Fig. 12. Faults in the Turtle Lake map area. **a)** Heterolithic foliated breccia (located at arrow, Fig. 13, along strike of tectonic zone of Fig. 11d). **b)** Milled carbonate blocks within fault zone cutting Horsefeed Formation. **c)** Chaotic folds in a broad fault zone cutting the Kedahda Formation that contains a variety of clast types. **d)** Disrupted Kedahda Formation is strongly foliated, and chert beds are disaggregated and milled. **e)** Heterolithic scaly fault zone at Peninsula Mountain. Inset shows a close-up view of a serpentinized block. **f)** Extensional quasi-ductile strain zone within thermally metamorphosed Laberge Group strata. **g)** Abrupt fault contact between orange volcaniclastic rock and light grey carbonate (above finger in top close-up, and in bottom at mid photo).

support for this interpretation is currently limited to: aerial reconnaissance (Fig. 13); identification of a dip slope fault zone that crops out along one of the inferred fault traces (Fig. 12a); and extrapolation of the fault zones to faults previously mapped in areas adjacent to the Turtle Lake map sheet (Figs. 1b, 2). Testing this idea is important because extensional faults with nearby syn-kinematic magmatic rocks is a setting in which gold-silver deposits are known to form, for example, in the Republic graben, southern BC, and northeast Washington State (e.g., Boleneus et al., 2001).

6. Geochronology

Accurate age determination is especially useful in outcrop impoverished areas like the Turtle Lake map sheet, where geological relationships that could be used to establish relative age progression are not exposed. Here we report on biochronological (conodont) and isotopic age determinations.

6.1. Conodonts

Eight samples were collected from Horsefeed Formation limestone where bioclastic grains were evident. All conodont samples were processed at the Geological Survey of Canada in Vancouver, using standard techniques as outlined in Stone (1987) and (Jeppsson et al., 1999) with results summarized in Table 1. Of these samples, three yielded conodonts (a 37.5% success rate). These conodonts date from the early (Bashkirian)

and middle-upper (Moscovian-Gzhelian) parts of the Late Carboniferous (Pennsylvanian), and the last stage of the Early Permian (Kungurian).

These new conodont age determinations extend the ages of fossils at Stovel Peak, formerly known to contain late Early Permian fusulinids (Monger, 1975), to Late Carboniferous (Bashkirian). Also extended is the range of ages of fossils at Peninsula Mountain, formerly ranging from middle to upper Late Carboniferous (Monger, 1975), and now ranging to Early Permian, confirming an early Early Permian age previously obtained from a clast (Monger, 1975). Such revisions from a limited number of samples demonstrates that the sections are more age-extensive and/or interleaved at both localities and that our understanding of the Horsefeed Formation remains rudimentary.

6.2. Isotopic analyses

We used multiple isotopic systems and dating techniques for which laboratory procedures are well established. To date zircons extracted from igneous rocks, we used chemical abrasion-thermal ionization mass spectroscopy (CA-TIMS) at the Pacific Centre for Isotopic and Geochemical Research (PCIGR) at The University of British Columbia. Sample preparation and analytical procedures are reported in Friedman et al. (2016; abridged in Mihalynuk et al., 2016). For detrital zircons, high-quality portions of single zircon grains were analyzed by laser

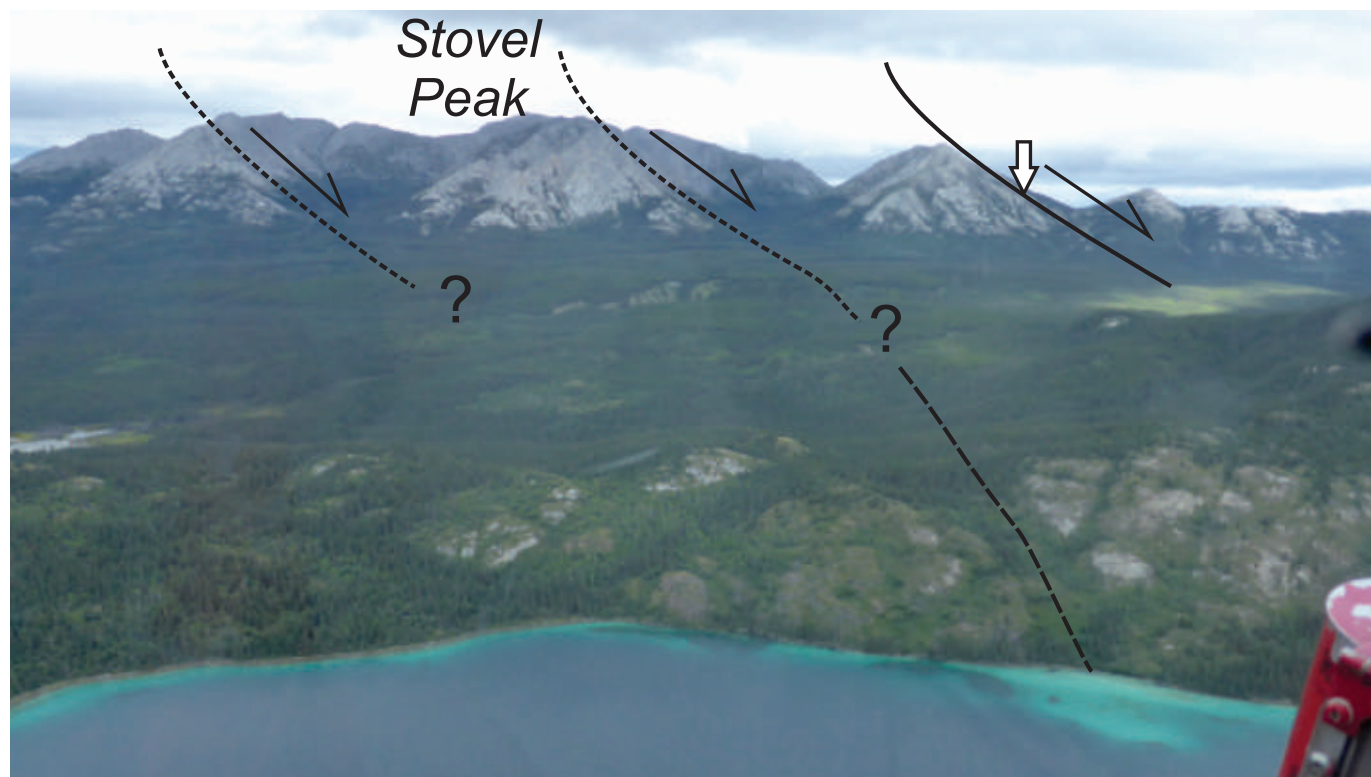


Fig. 13. A view from above northern Turtle Lake toward the northeast, of Stovel Peak and ridges to the south. Inferred south-side-down extensional faults repeat thick Horsefeed Formation limestone. During our mapping, traverses crossed only the southern inferred structure, but there we observed a dip-slope fault (approximate location indicated by white arrow, see also Figs. 11d and 12a). One of the faults is interpreted to track westward to offset limestone near Turtle Lake (see Fig. 2).

Table 1. Results from samples collected for conodont extraction and identification (see Fig. 2 for locations).

Curation Number	Field Number	UTM E	UTM N	Microfossil Content	Locality	Formation	Conodont Fauna	New Age
V-003694	16-ZE-MG-MS-1	549273	6636880	conodont	Mount Stovel	Horsefeed Fm.	<i>Idiognathoides</i> cf. <i>corrugata</i> (Harris and Hollingsworth, 1933); <i>Idiognathoides</i> sp.; <i>Neognathodus</i> cf. <i>symmetricus</i> (Lane, 1967)	Bashkirian
V-003695	16-ZE-MG-MS-2	549438	6636661	conodont	Mount Stovel	Horsefeed Fm.	<i>Gondolella</i> sp.	Moscovian-Gzhelian
V-003696	16-ZE-MG-MS-3	549375	6634857	barren	Mount Stovel	Horsefeed Fm.	None	Indeterminate
V-003716	16-ZE-MG-CLO-1	547505	6649965	barren	Mount Cloutier	Horsefeed Fm.	None	Indeterminate
V-003717	16-ZE-MG-CLO-2	548126	6649166	barren	Mount Cloutier	Horsefeed Fm.	None	Indeterminate
V-003718	16-ZE-MG-CLO-3	548213	6648754	barren	Mount Cloutier	Horsefeed Fm.	None	Indeterminate
V-003719	16-ZE-MG-CLO-4	548213	6648754	barren	Mount Cloutier	Nakina Fm.	None	Indeterminate
V-003720	16-ZE-MG-PM-1	540846	6640452	conodont	Peninsula Mtn.	Horsefeed Fm.	<i>Mesogondolella idahoensis</i> (Youngquist et al., 1951); <i>Streptognathodus</i> sp.	Kungurian

ablation-inductively coupled plasma mass spectrometry (LA-ICPMS) for U-Th-Pb isotope contents (see Friedman et al., 2016 for techniques). Two samples were analyzed by Sensitive High Resolution Ion MicroProbe (SHRIMP) at the Geological Survey of Canada in Ottawa, Ontario, and the procedures used were those reported in Mihalynuk et al. (2017; with analytical and calibration details in Stern, 1997; Stern and Amelin, 2003). $^{40}\text{Ar}/^{39}\text{Ar}$ age determinations were carried out at the University of Manitoba Geochronology Laboratory in Winnipeg, Manitoba; methods are described below.

6.2.1. $^{40}\text{Ar}/^{39}\text{Ar}$ methods

Samples containing the freshest hornblende and biotite were broken in to pea-sized pieces using a hydraulic splitter and the pieces were pulverized in a hardened steel piston and sleeve apparatus. Single crystals were handpicked before irradiation. Standards and unknowns were placed in 2 mm deep wells in 18 mm diameter aluminium disks for irradiation in the cadmium-lined, in-core CLICIT facility of the Oregon State University TRIGA reactor. Standards were placed strategically so that the lateral neutron flux gradients across the disk could be evaluated. Irradiation duration was 10 hours. Standards used were Fish Canyon sanidine (28.2 Ma; Kuiper et al., 2008) and GA1550 biotite (98.5 Ma; Spell and McDougall, 2003). Planar

regressions were fit to the standard data, and the $^{40}\text{Ar}/^{39}\text{Ar}$ neutron fluence parameter, J, interpolated for the unknowns. Uncertainties in J are estimated at 0.1-0.2% (1s), based on Monte Carlo error analysis of the planar regressions (Best et al., 1995).

All $^{40}\text{Ar}/^{39}\text{Ar}$ analytical work was performed using a Thermo Fisher Scientific ARGUSVI multi-collector mass spectrometer, linked to a stainless steel Thermo Fisher Scientific extraction/purification line and Photon Machines (55 W) Fusions 10.6 CO₂ laser. Argon isotopes (from mass 40 to 37) were measured using Faraday detectors with low noise $1 \times 10^{12} \Omega$ resistors and mass 36 was measured using a compact discrete dynode (CDD) detector. Irradiated samples were placed in a Cu sample tray, with a K-Br cover slip, in the extraction line under high vacuum and baked with an infrared lamp for 24 hours. Biotite analyses were performed on single crystals whereas hornblende analyses were performed on aliquots consisting of 3 crystals that were either fused or step-heated using the laser, and reactive gases were removed, after ~3 minutes, by three NP-10 SAES getters (two at room temperature and one at 450°C) before being admitted to an ARGUSVI mass spectrometer by expansion. Five argon isotopes were measured simultaneously during a period of 6 minutes. Measured isotope abundances were corrected for extraction-line blanks, which were determined

before every sample analysis. Line blanks averaged ~ 3.05 fA for mass 40 and ~ 0.01 fA for mass 36. The sensitivity for argon measurements is $\sim 6.312 \times 10^{17}$ moles/fA as determined from measured aliquots of Fish Canyon Sanidine (Dazé et al., 2003; Kuiper et al., 2008).

Mass discrimination was monitored by online analysis of air pipettes and gave a mean of $D=1.0035 \pm 0.0014$ per amu, based on 39 aliquots interspersed with the unknowns. A value of 295.5 was used for the atmospheric $^{40}\text{Ar}/^{36}\text{Ar}$ ratio (Steiger and Jäger, 1977) for the purposes of routine measurement of mass spectrometer discrimination using air aliquots, and correction for atmospheric argon in the $^{40}\text{Ar}/^{39}\text{Ar}$ age calculation. Corrections were made for neutron-induced ^{40}Ar from potassium, ^{39}Ar and ^{36}Ar from calcium, and ^{36}Ar from chlorine (Roddick, 1983; Renne et al., 1998; Renne and Norman, 2001). Data collection was performed using Pychron (Ross, 2017) and data reduction, error propagation, age calculation and plotting were performed using MassSpec software (version 8.091). The decay constants used were those recommended by Steiger and Jäger (1977).

6.3. Isotope geochronology results

Below we summarize the results of our geochronologic studies. A comprehensive set of isotopic data tables and photomicrographs is presented elsewhere (Mihalynuk et al., 2018).

6.3.1. CA-TIMS

The three samples analyzed by the CA-TIMS method were collected from: 1) a granitic dike that cuts the deformed chert-argillite section along the eastern shore of Tagish Lake; 2) a rhyolite tuff along the southern shore of Tutshi Lake; and 3) a weakly altered quartz diorite that underlies Sunday Peak. Locations are plotted on Figure 2 and UTM coordinates are provided along with isotope data in Table 2.

6.3.1.1. Granitic dike, Tagish Lake; MMI16-6-2

On the east shore of Tagish Lake, at a latitude of 60.003°N , a northwest-trending, orange-weathering, felsic, altered, medium- to coarse-grained feldspar porphyritic, ~ 40 cm thick dike cuts a strongly folded, cleaved and faulted section of chert and graphitic argillaceous strata (Fig. 14a) to form rounded phacoids within a strongly sheared argillaceous matrix. Only brittle fractures with millimetres of offset affect the dike, which was collected to constrain the minimum age of deformation, as well as the crystallization age of the unusual dike lithology.

Analyses from four grains (Table 2) overlap concordia at 145.75 ± 0.11 Ma (Fig. 14c), and this precise date is considered the crystallization age of the dike.

6.3.1.2. Windy Table suite, rhyolite tuff, Tutshi Lake; MTS16-1-4c

A white and rust-weathering rhyolite lapilli tuff (Fig. 8a) on the south shore of eastern Tutshi Lake is interpreted as the lowest volcanic unit of the Windy Table suite exposed in that

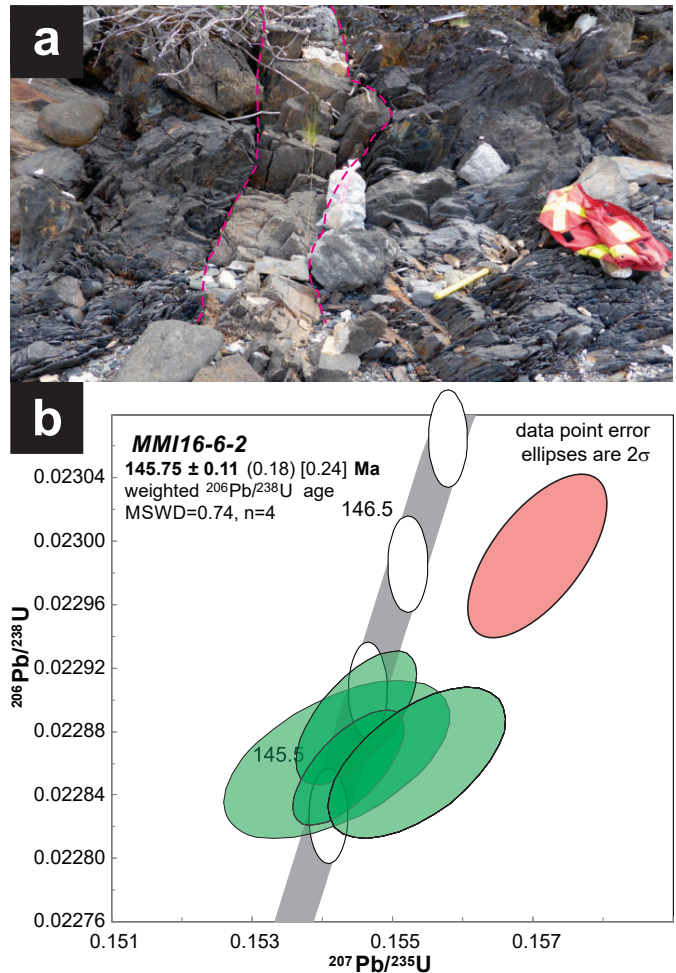


Fig. 14. a) Dike cuts almost orthogonal to strong cleavage and foliation in chert-argillite section (dike contacts are approximately outlined by fuschia dashed lines). b) Concordia diagram showing cluster of 4 concordant grains at 145.75 ± 0.11 Ma.

part of the map area (Fig. 2). We collected about 40 kg of fresh material from which zircons were separated. Five zircons were analyzed (Table 2). Analytical results from the grains fall into two populations, with concordant U-Pb isotopic ratios and mutually overlapping error 2s ellipses. Two grains are between 80.8 and 81 Ma, and three grains are at 80.63 ± 0.07 Ma (Fig. 15), which we interpret as the crystallization age of the unit. The older population likely represents precursor magmatic products cannibalized during migration and eruption of the rhyolite magma.

6.3.1.3. Sunday Peak stock quartz diorite; MMI16-18-1

The Sunday Peak pluton is one of a suite of zoned granodioritic to dioritic intrusions that cut the Whitehorse trough. On the basis of lithologic similarity and sparse K-Ar geochronology (e.g., Bultman, 1979, recalculated in Breitsprecher and Mortensen, 2004), these intrusions have formerly been considered mainly Late Cretaceous (Mihalynuk et al., 1996, 1999). At Sunday Peak, a ~ 0.6 km² stock cuts and thermally metamorphoses

Table 2. U-Pb zircon TIMS analytical results and computed ages for samples MMI16-6-2 (UTM 546011E, 6649818N), MTS16-1-4c (UTM 534680E, 6644710N), and MMI16-18-1 (UTM 550280E, 6624344N).

Sample (a)	Compositional Parameters										Radiogenic Isotope Ratios						Isotopic Ages							
	Wt.	U	Pb	Th	$^{206}\text{Pb}^*$	mol %	Pb*	Pb _c	^{206}Pb	^{204}Pb	^{208}Pb	^{207}Pb	^{206}Pb	^{235}U	^{206}Pb	corr.	^{207}Pb	^{235}U	^{207}Pb	^{238}U	^{206}Pb	^{238}U		
	mg	ppm	ppm	U x10 ⁻¹³	mol $^{206}\text{Pb}^*$	(e)	(e)	(e)	(g)	(f)	(g)	(g)	(g)	(h)	(g)	(h)	(g)	(h)	(i)	(h)	(i)	(h)	(i)	(h)
MMI-16-6-2																								
A	0.0021	388	9.0	0.260	0.7608	98.87%	25	0.71	1639	0.083	0.048912	0.770	0.154486	0.852	0.022863	0.178	0.546	143.60	18.05	145.60	116	145.72	0.26	
B	0.0014	682	15.6	0.250	0.9320	99.12%	32	0.68	2093	0.080	0.048946	0.373	0.154472	0.454	0.022889	0.151	0.654	145.23	8.76	145.85	0.62	145.89	0.22	
C	0.0028	369	8.4	0.237	0.9689	99.27%	38	0.59	2528	0.076	0.048978	0.345	0.154362	0.449	0.022858	0.129	0.680	146.80	8.08	145.76	0.57	145.69	0.19	
D	0.0018	587	13.6	0.224	0.9862	98.58%	19	1.17	1300	0.072	0.049279	0.580	0.155332	0.662	0.022861	0.171	0.581	161.14	13.56	146.61	0.90	145.71	0.25	
E	0.0012	537	12.4	0.224	0.6232	98.86%	24	0.59	1629	0.072	0.049542	0.426	0.157050	0.517	0.022991	0.185	0.627	173.56	9.93	148.12	0.71	146.53	0.27	
MMI-16-1-4c																								
A	0.0021	504	7.2	0.455	0.5428	96.86%	9	1.45	589	0.147	0.048005	2.186	0.083223	2.332	0.012573	0.191	0.781	99.53	51.69	81.17	182	80.55	0.15	
B	0.0066	260	3.4	0.319	0.8981	98.29%	17	1.29	1080	0.103	0.047942	0.719	0.083615	0.795	0.012649	0.135	0.620	96.39	17.01	81.54	0.62	81.03	0.11	
C	0.0073	563	7.2	0.274	2.1440	98.98%	28	1.82	1811	0.088	0.047508	0.412	0.082416	0.488	0.012582	0.144	0.638	74.85	9.78	80.41	0.38	80.60	0.12	
D	0.0028	104	14.1	0.285	1.5949	99.03%	29	1.28	1914	0.091	0.047607	0.374	0.082671	0.449	0.012595	0.134	0.667	79.77	8.87	80.65	0.35	80.68	0.11	
E	0.0044	228	3.2	0.398	0.5298	97.60%	12	1.07	770	0.128	0.047829	0.931	0.083522	10.16	0.012665	0.140	0.646	90.84	22.05	81.45	0.79	81.13	0.11	
MMI-16-18-1																								
A	0.0064	480	4.4	0.470	1.1113	99.04%	31	0.89	1923	0.151	0.04781	0.415	0.056325	0.494	0.008658	0.152	0.627	58.38	9.90	55.64	0.27	55.57	0.08	
B	0.0048	602	5.5	0.486	1.0480	99.18%	37	0.71	2256	0.156	0.04708	0.358	0.056322	0.432	0.008671	0.131	0.670	54.72	8.53	55.64	0.23	55.66	0.07	
D	0.0104	173	17	0.358	0.6485	97.02%	9	1.64	620	0.115	0.04719	1.177	0.056331	1.274	0.008667	0.166	0.629	56.28	28.05	55.64	0.69	55.63	0.09	
E	0.0041	704	6.4	0.388	1.0481	98.64%	21	1.19	1363	0.124	0.046837	0.756	0.055892	0.834	0.008655	0.161	0.562	40.91	18.07	55.22	0.45	55.55	0.09	

(a) A, B etc. are labels for fractions composed of single zircon grains or fragments; all fractions annealed and chemically abraded after Mattinson (2005) and Scoates and Friedman (2008).

(b) Nominal fraction weights estimated from photomicrographic grain dimensions, adjusted for partial dissolution during chemical abrasion.

(c) Nominal U and total Pb concentrations subject to uncertainty in photomicrographic estimation of weight and partial dissolution during chemical abrasion.

(d) Model Th/U ratio calculated from radiogenic $^{206}\text{Pb}/^{206}\text{Pb}$ ratio and $^{207}\text{Pb}/^{235}\text{U}$ age.

(e) Pb* and Pbc represent radiogenic and common Pb, respectively; mol % $^{206}\text{Pb}^*$ with respect to radiogenic, blank and initial common Pb.

(f) Measured ratio corrected for spike and fractionation only. Mass discrimination of $0.30 \pm 0.05\%$ amu based on analysis of NBS-982; all Daly analyses.

(g) Corrected for fractionation, spike, and all common Pb was assumed to be procedural blank. $^{206}\text{Pb}/^{204}\text{Pb} = 18.50 \pm 1.0\%$; $^{207}\text{Pb}/^{204}\text{Pb} = 15.50 \pm 1.0\%$; $^{208}\text{Pb}/^{204}\text{Pb} = 38.40 \pm 1.0\%$ (all uncertainties 1σ).

(h) Errors are 2σ , propagated using the algorithms of Schmitz and Schoene (2007) and Crowley et al. (2007).

(i) Calculations are based on the decay constants of Jaffey et al. (1971). $^{206}\text{Pb}/^{238}\text{U}$ and $^{207}\text{Pb}/^{235}\text{U}$ ages corrected for initial disequilibrium in $^{230}\text{Th}/^{238}\text{U}$ using Th/U [magma] = 3.

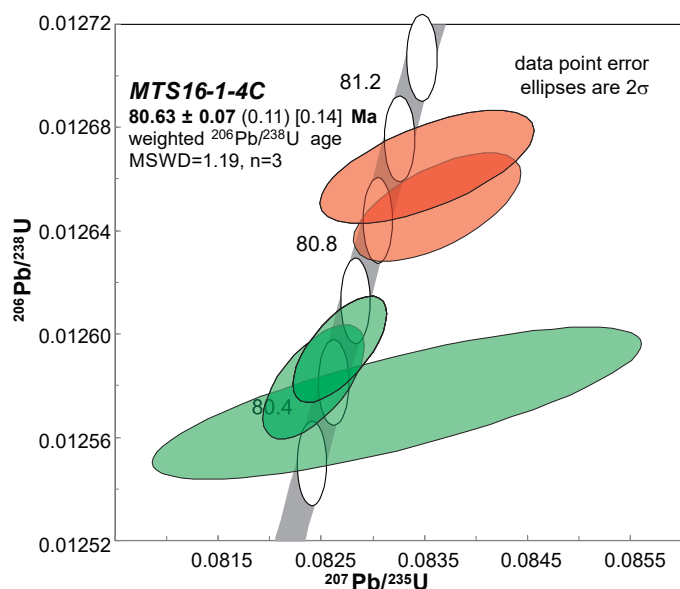


Fig. 15. Concordia plot showing cluster of three grains overlapping concordia at 80.63 ± 0.07 Ma.

rocks on both sides of a terrane-bounding fault: harzburgite of the Cache Creek terrane and wacke of Whitehorse trough (as well as overlapping Windy-Table suite felsic volcanic conglomerate). Thus, an age determination from the stock constrains the latest phase of major fault motion as well as the age of the conglomerate. Four zircons were analyzed (Table 2). All have concordant U-Pb isotopic ratios with mutually overlapping error 2s ellipses (Fig. 16), producing a precise age of 55.61 ± 0.04 Ma.

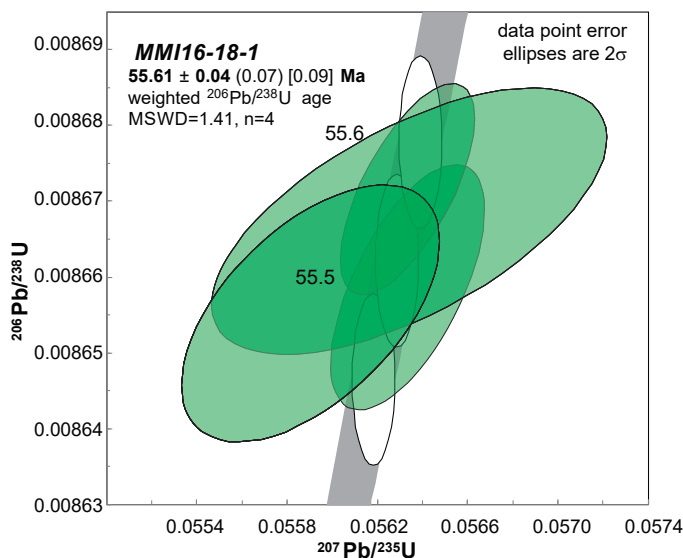


Fig. 16. Concordia diagram for sample MMI16-18-1 of Sunday peak quartz diorite (rock sampled is shown in Fig. 10a). Analyses plot as a 4-grain cluster that overlaps concordia at 55.61 ± 0.04 Ma.

6.3.2. Detrital zircon SHRIMP

Two samples were collected for analysis by the SHRIMP method: one from a volcanic conglomerate on Sunday Peak, and the other from the maroon sandstone matrix of a breccia consisting of Horsefeed Formation limestone blocks. Locations are plotted on Figure 2 and UTM coordinates are provided along with the data for age determinations in Table 3.

6.3.2.1. Horsefeed Formation hematitic breccia matrix; sample DMI16-5-1A

We collected samples of the laminated hematitic calcarenite matrix to breccias in the Horsefeed Formation from exposures along the eastern shoreline of Tagish Lake and from a low ridge south of Stovel Peak. Petrographic work showed that the ridge sample contains only rare quartz grains, so the lakeshore sample, with more abundant quartz grains, was analyzed with the expectation that detrital zircon contents would be proportional to the abundance of quartz grains.

Of the zircon grains recovered from the lakeshore sample, 124 grains were selected and mounted for analysis. Most of these grains are clear and pale brown, and are euhedral well-faceted equant, stubby, and elongate prisms. About 10% of the grains have rounded grain boundaries. Clear bubble- and rod-shaped inclusions, and brown bubble-shaped inclusions are relatively common. In SEM-cathodoluminescence (CL) images, most grains exhibit distinct oscillatory zoning, and lesser sector zoning (Fig. 17a). CL response from the grains varies from very dark (relatively high U content) to bright (relatively low U content). Cores are visible in ~10% of the grains. Of the zircon grains analyzed, the youngest population is 111 Ma (Table 3; $n=19$, MSWD=1.3, POF=0.17, and the youngest grain 107 Ma (Fig. 17b). This age is nearly 150 m.y. younger than the youngest known age limit of the Horsefeed Formation, based on Late Permian fossils south of the mouth of Talaha Bay (Monger, 1975). We interpret the hematitic breccia as Cretaceous karst infill representing a period exposure.

6.3.2.2. Windy-Table suite, felsic volcanic conglomerate and breccia at Sunday Peak; sample MMI16-16-9

Conglomeratic, reworked felsic volcanic breccia (Fig. 18a) occurs east of Sunday Peak between Laberge Group sedimentary rocks to the west and harzburgite mantle tectonite to the east (Fig. 2). An unconformable contact with the harzburgite was established on the basis of serpentinite clasts in the conglomerate and dikelets of volcanic breccia in the harzburgite (Fig. 7a inset). However, contact relations between the volcanic conglomerate and breccia and the adjacent rocks of the Laberge Group are masked by deformation and subsequent thermal alteration by the Sunday Peak intrusion (Fig. 7d). Consequently, it was unclear if the volcanic conglomerate was an intraclast-bearing layer within the Laberge Group that had lapped against harzburgite exposed in the Early to Middle Jurassic. If part of the Laberge Group, then stratigraphic and structural continuity since Middle Jurassic could be established (with strong post-deformational shearing along

Table 3. U-Pb zircon SHRIMP analytical results and computed ages for samples MMI16-18-5 (UTM 550621E, 6623917N) and DMI16-5-1 (UTM 546012E, 6649818N).

Spot name	U (ppm)	Th (ppm)	Th/U	²⁰⁶ Pb* (ppm)	²⁰⁴ Pb/ ²⁰⁶ Pb	²⁰⁸ Pb/ ²⁰⁶ Pb	²³⁸ U/ ²⁰⁶ Pb	²⁰⁷ Pb/ ²⁰⁶ Pb	²⁰⁷ Pb/ ²³⁵ U	²⁰⁶ Pb/ ²³⁸ U	Corr	²⁰⁷ Pb/ ²⁰⁶ Pb	²⁰⁶ Pb ± ²⁰⁶ Pb/ ²³⁸ U	²⁰⁶ Pb ± ²⁰⁶ Pb/ ²³⁸ U								
DMI16-5-1A; Lab#11838; Turtle Lake Sandstone; UTM 546012E, 6649818N																						
11838-119.1	265	68	0.27	3.8	1.3E-3	41	2.22	0.039	63.3	59.1	1.5	0.0542	5.4	0.080	24.4	0.0166	1.8	0.072	0.0351	24.3	107	2
11838-096.1	552	350	0.65	8.0	6.8E-4	41	1.18	0.197	9.7	58.7	1.7	0.0562	3.9	0.107	10.3	0.0168	1.8	0.174	0.0462	10.2	108	2
11838-094.1	224	139	0.64	3.3	5.1E-4	71	0.88	0.192	14.3	58.3	2.5	0.0566	6.4	0.115	13.4	0.0170	2.5	0.189	0.0492	13.1	109	3
11838-103.1	258	120	0.48	3.8	2.4E-4	100	0.41	0.158	15.1	58.3	2.1	0.0541	5.8	0.119	9.5	0.0171	2.1	0.221	0.0507	9.2	109	2
11838-089.1	585	393	0.69	8.6	2.3E-4	71	0.41	0.194	18.4	58.2	1.6	0.0516	4.2	0.114	7.0	0.0171	1.7	0.238	0.0482	6.8	109	2
11838-079.1	356	263	0.76	5.1	7.6E-4	50	1.32	0.198	12.8	58.6	1.8	0.0453	9.6	0.079	21.5	0.0168	1.9	0.091	0.0339	21.4	109	2
11838-124.1	1061	927	0.90	15.5	4.6E-4	35	0.80	0.276	5.2	58.3	1.5	0.0479	7.5	0.097	10.7	0.0170	1.6	0.147	0.0411	10.6	110	2
11838-121.1	311	243	0.81	4.5	1.1E-3	41	1.94	0.263	11.3	57.8	2.3	0.0528	5.1	0.084	20.8	0.0170	2.5	0.118	0.0361	20.7	110	3
11838-123.1	279	298	1.10	4.2	-3.9E-4	71	-0.68	0.370	7.8	57.6	1.8	0.0494	5.5	0.133	9.0	0.0175	1.9	0.211	0.0551	8.8	111	2
11838-110.1	196	168	0.89	2.9	8.4E-4	58	1.45	0.272	13.2	57.2	2.3	0.0527	6.3	0.096	20.0	0.0172	2.5	0.123	0.0403	19.8	111	3
11838-076.1	513	209	0.42	7.7	5.6E-4	50	0.97	0.126	14.3	57.0	1.5	0.0481	9.5	0.095	15.7	0.0174	1.5	0.098	0.0398	15.6	112	2
11838-107.1	674	394	0.60	10.1	3.1E-4	50	0.54	0.173	8.0	56.8	1.6	0.0480	3.4	0.105	6.7	0.0175	1.6	0.242	0.0434	6.5	112	2
11838-112.1	300	244	0.84	4.5	1.8E-4	100	0.31	0.213	19.0	56.4	2.2	0.0535	5.0	0.124	7.7	0.0177	2.2	0.282	0.0508	7.4	113	2
11838-080.1	460	341	0.77	6.9	4.4E-4	58	0.76	0.236	9.2	56.5	2.2	0.0529	4.6	0.113	9.9	0.0176	2.3	0.228	0.0465	9.7	113	2
11838-097.1	144	93	0.67	2.2	1.2E-3	58	2.14	0.204	20.7	54.8	2.5	0.0605	11.9	0.104	30.9	0.0179	2.8	0.090	0.0423	30.8	115	3
11838-084.1	170	101	0.62	2.6	1.5E-3	58	2.52	0.174	27.2	54.2	3.2	0.0697	7.7	0.120	28.8	0.0180	3.5	0.122	0.0483	28.6	115	4
11838-074.1	347	277	0.82	5.3	8.1E-4	45	1.41	0.287	15.6	55.1	1.5	0.0547	8.1	0.105	16.7	0.0179	1.6	0.096	0.0427	16.6	115	2
11838-104.1	1604	1556	1.00	28.1	5.9E-5	71	0.10	0.314	3.3	49.0	1.8	0.0497	2.1	0.137	3.1	0.0204	1.8	0.594	0.0488	2.5	130	2
11838-120.1	155	74	0.49	3.6	1.6E-3	38	2.77	0.105	28.8	36.1	2.2	0.0518	5.7	0.103	35.4	0.0269	2.4	0.068	0.0278	35.3	176	4
11838-100.1	245	109	0.46	6.3	-1.7E-4	100	-0.30	0.123	13.3	33.7	1.9	0.0555	4.8	0.238	6.6	0.0297	1.9	0.285	0.0580	6.3	187	3
11838-116.1	468	249	0.55	11.9	4.0E-4	45	0.69	0.160	9.1	33.7	1.9	0.0510	3.7	0.183	7.4	0.0295	2.0	0.265	0.0452	7.2	188	4
11838-092.1	263	133	0.52	7.2	1.1E-4	100	0.19	0.167	9.2	31.1	1.5	0.0542	4.0	0.233	5.4	0.0321	1.5	0.280	0.0526	5.2	203	3
11838-122.1	171	79	0.48	4.7	-1.9E-4	100	-0.33	0.153	12.4	31.2	1.9	0.0504	5.3	0.235	7.4	0.0321	2.0	0.263	0.0531	7.2	203	4
11838-085.1	1254	651	0.54	35.3	1.3E-4	45	0.22	0.161	4.4	30.4	1.5	0.0511	1.9	0.223	3.0	0.0328	1.5	0.490	0.0492	2.6	208	3
11838-088.1	233	72	0.32	6.6	1.1E-3	33	1.98	0.057	33.2	29.7	1.5	0.0506	4.8	0.153	18.9	0.0330	1.7	0.089	0.0335	18.8	214	3
11838-114.1	291	92	0.33	8.6	1.9E-4	71	0.32	0.088	12.3	28.9	1.8	0.0536	3.6	0.241	5.7	0.0344	1.8	0.319	0.0508	5.4	218	4
11838-083.1	394	126	0.33	11.8	5.2E-4	41	0.90	0.093	13.9	28.5	3.7	0.0516	7.1	0.211	11.7	0.0348	3.8	0.322	0.0439	11.1	222	8

Mount IP832, K100a spot size (13x16µm), 2.5 minute raster; 6 mass scans. Primary beam intensity ~3.0 nA

Spot name follows the convention x-y.z; where x = lab number, y = grain number and z = spot number

Uncertainties reported at 1σ and are calculated by using SQUID 2.50.11.10.15, rev. 15 Oct 2011

F(206)²⁰⁴ refers to mole percent of total ²⁰⁶Pb that is due to common Pb, calculated using the ²⁰⁶Pb-method; common Pb composition used is the surface blank (4/6: 0.05770; 7/6: 0.89500; 8/6: 2.13840)

* refers to radiogenic Pb (corrected for common Pb)

Error in ²⁰⁶Pb/²³⁸U calibration 1.35% (included). Standard Error in Standard calibration was 0.38% (not included in above errors but required when comparing data from different mounts).

Apparent ages shown in bold font are those which were used in the weighted mean age calculations

For sample DMI16-5-1A, analyses not included in the age calculation were those which exceeded 3.0% common Pb, or were from older populations

For sample MMI16-16-9, many analyses contained high common Pb, but the 3 youngest analyses clearly represent a young generation of growth and are therefore not disregarded on the basis of high common Pb

below detection limit analyses and those with relatively high common Pb excluded. Only data for apparent ages less than 220 Ma are shown, see Mihalynuk et al., 2018 for full listing of analytical data

Table 3. Continued.

MMH16-16-9; Lab#11839; Sunday Peak Conglomerate; UTM 550621E, 6623917N																			
11839-075.1	1327	687	0.54	14.9	0.195	5.7	76.6	1.5	0.0484	2.9	0.087	3.3	0.0131	1.5	0.446	0.0484	2.9	83.5	1.2
11839-097.1	2513	1198	0.49	29.0	0.157	4.8	74.3	1.4	0.0497	2.2	0.091	2.8	0.0134	1.4	0.492	0.0492	2.4	85.9	1.2
11839-081.1	1770	699	0.41	20.5	0.129	7.4	73.9	1.5	0.0495	6.0	0.083	8.0	0.0135	1.5	0.193	0.0447	7.8	86.5	1.4
11839-077.1	151	56	0.39	3.9	0.097	30.0	32.5	2.3	0.0587	5.2	0.150	25.7	0.0300	2.5	0.097	0.0362	25.6	194	4
11839-013.1	90	24	0.28	2.5	0.186	19.1	32.1	3.0	0.0591	14.1	0.365	17.3	0.0320	3.3	0.189	0.0826	17.0	195	6
11839-098.1	128	38	0.30	3.4	0.099	22.1	32.1	1.7	0.0586	5.7	0.219	12.1	0.0309	1.8	0.147	0.0514	12.0	196	3
11839-039.1	91	31	0.35	2.4	0.063	66.1	31.6	3.1	0.0687	10.6	0.152	43.8	0.0304	3.5	0.079	0.0361	43.7	196	6
11839-033.1	101	32	0.33	2.7	0.133	25.2	31.9	4.0	0.0602	11.6	0.189	26.4	0.0308	4.2	0.157	0.0446	26.0	197	8
11839-032.1	146	39	0.28	3.8	0.043	65.7	31.9	1.9	0.0555	5.5	0.125	33.8	0.0304	2.2	0.065	0.0297	33.8	198	4
11839-073.1	451	147	0.34	12.0	0.095	12.6	32.0	1.5	0.0524	3.2	0.191	7.7	0.0310	1.5	0.194	0.0447	7.6	198	3
11839-109.1	130	44	0.35	3.5	0.162	15.1	32.2	1.6	0.0477	6.1	0.268	12.1	0.0316	1.8	0.149	0.0615	12.0	198	3
11839-070.1	196	60	0.32	5.3	0.084	22.0	31.6	2.0	0.0568	9.4	0.203	15.7	0.0312	2.1	0.133	0.0470	15.6	199	4
11839-115.1	146	47	0.34	4.0	0.133	17.9	31.6	1.6	0.0566	5.7	0.314	11.0	0.0322	1.8	0.166	0.0708	10.8	199	3
11839-100.1	279	159	0.59	7.5	0.169	9.4	32.0	1.5	0.0478	4.1	0.191	7.1	0.0312	1.5	0.212	0.0445	7.0	199	3
11839-108.1	182	61	0.35	4.9	0.087	15.6	31.6	2.4	0.0538	4.6	0.224	6.9	0.0316	2.4	0.345	0.0515	6.4	200	5
11839-009.1	224	93	0.43	6.1	0.118	14.5	31.4	1.9	0.0561	4.2	0.217	9.0	0.0316	2.0	0.216	0.0498	8.8	201	4
11839-012.1	288	129	0.46	7.8	0.114	15.6	31.2	1.5	0.0575	6.6	0.203	12.9	0.0317	1.6	0.124	0.0466	12.8	202	3
11839-037.1	199	61	0.32	5.5	0.084	20.6	30.9	2.2	0.0568	4.6	0.219	10.3	0.0321	2.2	0.213	0.0495	10.1	204	4
11839-094.1	277	108	0.40	7.5	0.084	19.8	31.3	1.5	0.0462	4.4	0.153	14.2	0.0316	1.6	0.112	0.0352	14.1	204	3
11839-019.1	239	58	0.25	6.6	0.083	17.5	30.8	1.8	0.0528	4.5	0.216	8.1	0.0323	1.8	0.223	0.0486	7.9	205	4
11839-067.1	321	121	0.39	8.9	0.122	13.5	30.5	1.5	0.0582	9.1	0.202	15.4	0.0323	1.6	0.102	0.0453	15.3	206	3
11839-040.1	111	42	0.39	3.0	0.044	91.8	30.0	2.4	0.0619	16.2	0.089	84.9	0.0318	2.9	0.034	0.0204	84.8	209	6
11839-106.1	150	53	0.37	4.3	0.165	13.6	30.1	1.8	0.0491	5.3	0.277	10.0	0.0336	1.9	0.194	0.0597	9.8	211	4
11839-036.1	167	42	0.26	4.7	0.078	27.9	29.8	1.6	0.0546	8.5	0.186	19.1	0.0330	1.7	0.091	0.0410	19.0	212	3
11839-040.2	135	43	0.33	3.9	0.092	25.5	29.7	2.8	0.0541	5.7	0.202	15.5	0.0333	2.9	0.188	0.0439	15.3	213	6
11839-014.1	401	163	0.42	11.6	0.147	9.2	29.4	1.5	0.0574	5.1	0.239	7.9	0.0338	1.5	0.191	0.0514	7.7	214	3
11839-021.1	214	66	0.32	6.2	0.091	17.3	29.2	1.5	0.0581	7.6	0.235	11.9	0.0339	1.6	0.133	0.0502	11.8	215	3
11839-076.1	369	163	0.46	10.8	0.160	8.6	29.3	1.5	0.0574	3.3	0.246	6.0	0.0340	1.5	0.247	0.0526	5.9	215	3
11839-015.1	130	29	0.23	3.7	0.032	80.6	29.2	2.1	0.0586	5.4	0.179	22.9	0.0334	2.3	0.102	0.0389	22.8	215	5
11839-034.1	272	93	0.35	7.9	0.100	15.3	29.3	1.5	0.0528	4.3	0.207	9.9	0.0338	1.6	0.157	0.0446	9.8	215	3
11839-103.1	298	212	0.73	8.7	0.237	7.8	29.4	1.5	0.0503	8.4	0.212	11.4	0.0338	1.5	0.135	0.0454	11.3	216	3
11839-035.1	374	103	0.28	10.9	0.059	21.0	29.2	1.5	0.0543	3.4	0.212	8.7	0.0339	1.5	0.174	0.0454	8.6	216	3
11839-082.1	1110	255	0.24	32.5	0.073	7.5	29.3	1.4	0.0517	1.9	0.230	3.2	0.0341	1.4	0.436	0.0491	2.9	216	3
11839-044.1	120	40	0.34	3.6	0.102	19.8	29.0	1.7	0.0581	13.0	0.258	15.5	0.0344	1.7	0.111	0.0545	15.4	217	4
11839-107.1	343	298	0.90	10.0	0.264	6.9	29.2	1.8	0.0499	6.6	0.201	10.8	0.0339	1.8	0.168	0.0430	10.6	217	4
11839-018.1	302	80	0.28	8.8	0.075	16.6	29.1	1.5	0.0520	6.6	0.217	10.0	0.0341	1.5	0.153	0.0462	9.9	217	3
11839-042.1	375	389	1.07	10.9	0.337	6.4	29.0	1.5	0.0522	3.7	0.175	13.3	0.0339	1.6	0.118	0.0375	13.2	218	3
11839-022.1	452	129	0.30	13.3	0.091	9.3	29.1	1.4	0.0482	3.2	0.223	4.0	0.0343	1.4	0.358	0.0473	3.8	218	3
11839-024.1	263	97	0.38	7.8	0.107	24.8	28.9	2.1	0.0526	4.0	0.234	6.6	0.0344	2.1	0.314	0.0493	6.3	218	4
11839-025.1	281	63	0.23	8.3	0.066	14.8	28.9	1.8	0.0523	7.2	0.242	8.2	0.0345	1.8	0.223	0.0508	8.0	219	4
11839-081.2	421	175	0.43	12.4	0.128	10.4	28.8	1.5	0.0561	3.0	0.221	8.0	0.0343	1.5	0.189	0.0466	7.8	219	3
11839-020.1	313	85	0.28	9.3	0.087	13.9	28.7	1.7	0.0554	6.9	0.238	9.6	0.0346	1.8	0.183	0.0500	9.4	219	4
11839-029.1	306	67	0.22	9.0	0.034	39.6	28.8	1.5	0.0542	3.6	0.195	11.6	0.0342	1.6	0.135	0.0414	11.5	219	3
11839-065.1	133	55	0.43	3.9	0.110	26.8	28.6	1.6	0.0582	8.8	0.177	26.9	0.0341	1.9	0.072	0.0376	26.8	219	4

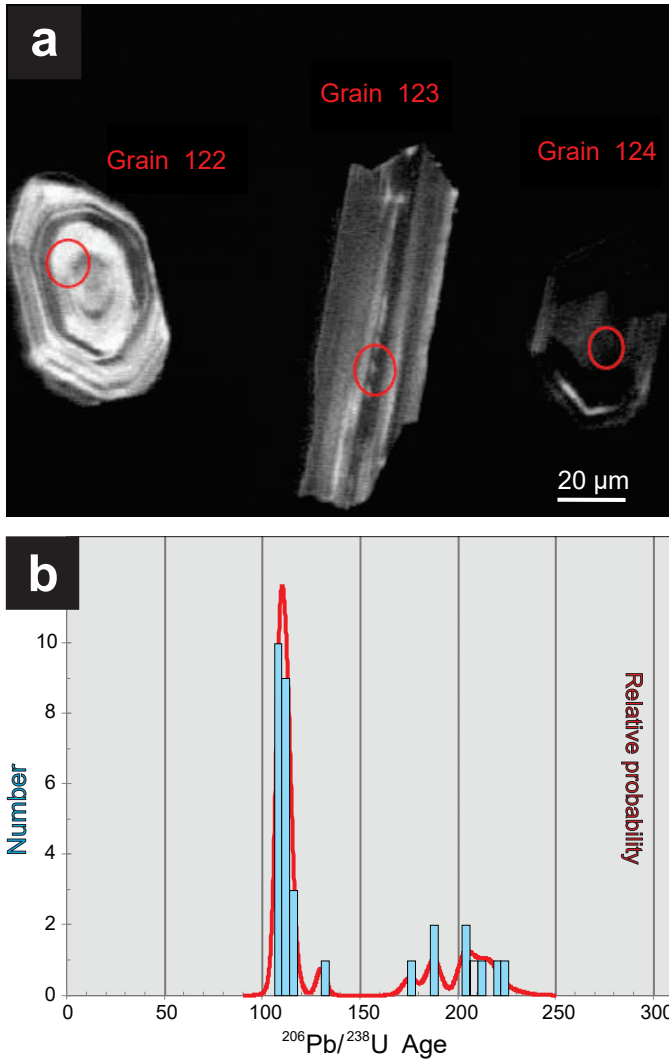


Fig. 17. Laminated maroon calcarenite between blocks of Horsefeed Formation limestone contain Early Cretaceous detrital zircons and are interpreted as karst collapse deposits. **a)** Cathodoluminescence images of representative zircons analyzed by SHRIMP. **b)** Zircon age distribution plot.

the Laberge wacke and Harzburgite-conglomerate contacts resulting in a relative offset that is less than the footprint of the felsic conglomerate unit). A sample ~25 cm in diameter of the stratigraphically lowest conglomerate containing almost entirely felsic volcanic clasts was collected for detrital zircon analysis.

Approximately 120 grains were mounted for analysis, representing a full range of zircon morphologies (a subset is shown in Table 3 and Fig. 18b). Most grains are clear and colourless, equant to stubby prisms with well-preserved facets and minor clear bubble-shaped inclusions. In SEM-CL images (Fig. 18b), most grains exhibit distinct oscillatory zoning. Sector zoning is present in one third of the crystals. Core-like regions are seen in ~10% of the grains. A maximum depositional age is given by three Late Cretaceous grains. The youngest of the three grains is 84 Ma, whereas their combined

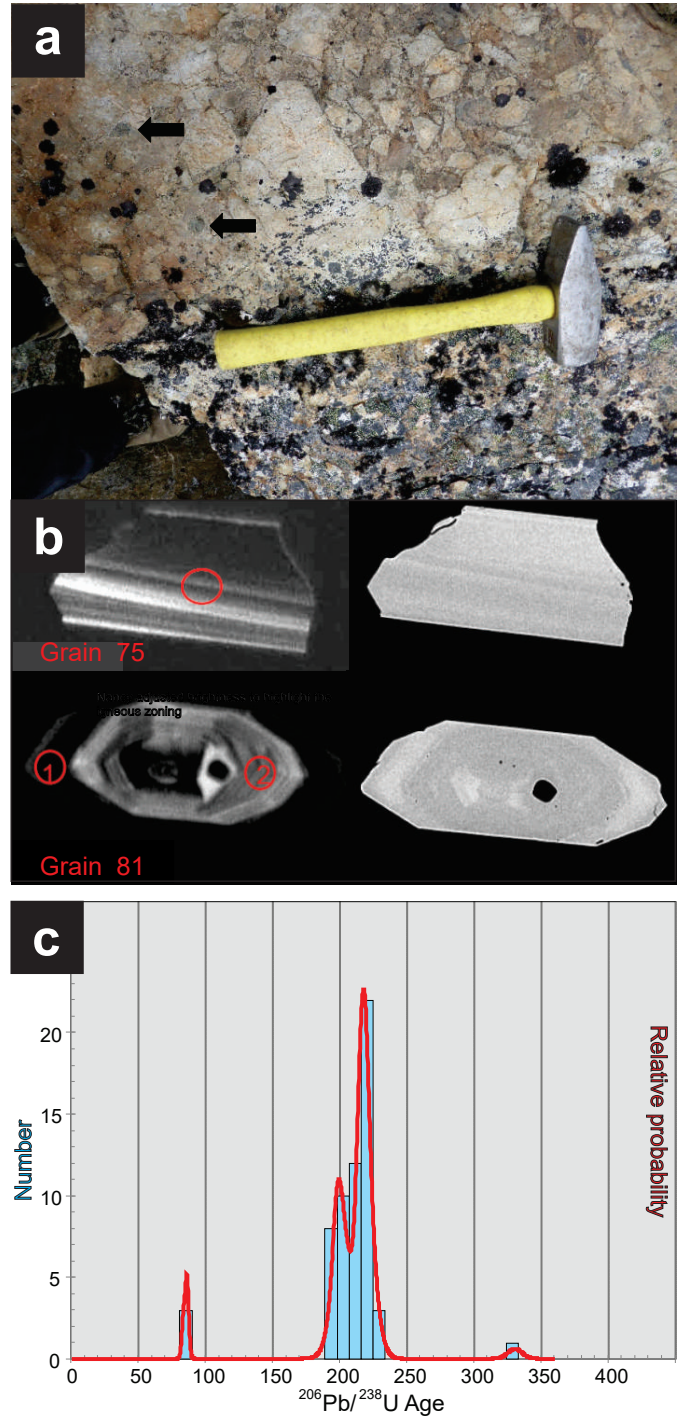


Fig. 18. a) Reworked felsic volcanic breccia at Sunday Peak sampled for age determination. Dark green clasts above the end of the hammer handle may be derived from the adjacent mantle tectonite. A dikelet containing fragments of felsic volcanic rock as well as serpentinized mantle peridotite cuts mantle tectonite is pictured in the inset of Fig. 7a. **b)** Cathodoluminescent and reflected light images of young zircons analyzed by SHRIMP. Grain 81 is especially informative, it has an 86.5 Ma rim (1) and a 216 Ma core (2). **c)** Zircon age distribution plot with a sub-population of 19 zircons that yields an age of 111 ±1Ma (see Mihalynuk et al., 2018).

weighted average age is 85 Ma, (Fig. 18c). Grain 81 (Fig. 18b) has a high-U 86.5 Ma rim and a 216 Ma core with lower U content. We interpret the youngest zircons to represent the age of syn-volcanic deposition and correlate the unit with strata of the same age (85.0 ± 1.8 Ma) near the base of the Windy-Table suite, as recently shown by Zagorevski et al. (2017).

6.3.3. Detrital zircon LA-ICPMS

The two samples analyzed by LA-ICPMS were collected from: a tuffaceous conglomerate containing chert and rhyolite fragments above the eastern shore of Turtle Lake (Fig. 2; Table 4), and an intermediate tuff along the eastern shore of Tagish Lake at the base of Peninsula Mountain (Table 5).

6.3.3.1. Horsefeed Formation, tuffaceous limestone breccia east of Turtle Lake; sample MTS16-24-13

Green and grey-weathering tuffaceous limestone breccia underlies the slopes east of northern Turtle Lake. Outcrop compositions range from predominantly volcanic to limestone clast-bearing. A sample was collected from a relatively volcanic-rich protolith that contained both aphanitic green and cream-coloured, lapilli-sized volcanic clasts as well as angular limestone and rare chert (Fig. 19a). Of the zircon grains separated, 39 were suitable for LA-ICPMS analysis (Table 4); all were angular fragments with strong growth-zoning (Figs. 19b, c). The zircon fragments returned an age distribution with a peak at ~ 295 Ma (37 grains, Fig. 19d), and a minor ill-defined sub population at ~ 310 Ma (2 grains). Nearly two of three grains (64%) display overlapping $^{206}\text{Pb}/^{238}\text{U}$ ($2\sigma < 5\%$) and $^{207}\text{Pb}/^{235}\text{U}$ ($2\sigma < 10\%$) ages, and $^{207}\text{Pb}/^{206}\text{Pb}$ ages that are geologically meaningful and concordant within error. Five of these grains cluster at ~ 285 Ma, which we interpret as the best estimate of the maximum depositional age.

6.3.3.2. Windy-Table suite volcanic rocks at Peninsula Mountain; sample MMI16-8-1

Volcaniclastic strata crop out on the west side of Peninsula Mountain and are well exposed along the shore of Tutshi Lake. Contacts with Laberge Group wacke and argillite to the south are not exposed, but to the north, a fault zone containing panels of chert and argillite juxtapose the unit with limestone of the Horsefeed Formation. Age relations are ambiguous, but most previous workers considered the Peninsula Mountain volcanic strata to be Triassic. Reasons to doubt the Triassic age assignment arose during the field program: tuffaceous and conglomeratic sections at Peninsula Mountain are lithologically similar to strata of probable Cretaceous age to the north and south in the Turtle Lake map area, and strata of presumed Triassic age a few km outside the southeast corner of the map area, were found to be Cretaceous and correlated with the Windy-Table suite (Zagorevski et al., 2017). To address the uncertainty about the affiliation of volcanic rocks at Peninsula Mountain, we collected a sample of grey-green feldspar-phyroxene-phyric breccia (Fig. 9b) for LA-ICPMS analysis.

Six usable zircons were recovered and analyzed (Table 5);

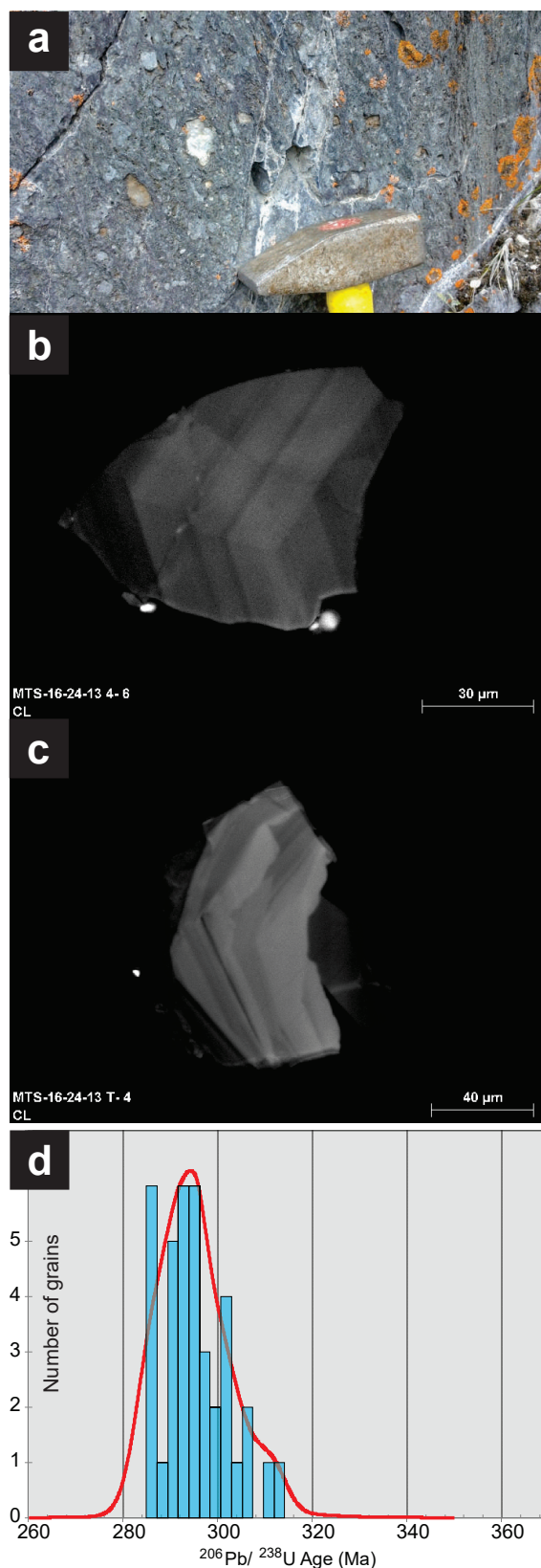


Fig. 19. a) Outcrop of tuffaceous sharpstone conglomerate sampled for age determination. b), c) Cathodoluminescence images of representative, strongly zoned, zircon crystal fragments typical of the unit. d) Zircon age distribution plot shows zircons dated range from Mid Pennsylvanian through Early Permian.

Table 4. U-Pb zircon LA-ICPMS analytical results and computed ages, sample MTS16-24-13 (UTM 543823E, 6635458N).

Sample no.	Isotopic Ratios					Isotopic Ages							
	²⁰⁷ Pb/ ²³⁵ U	2σ (abs)	²⁰⁶ Pb/ ²³⁸ U	2σ (abs)	ρ	²⁰⁷ Pb/ ²⁰⁶ Pb	2σ (abs)	²⁰⁷ Pb/ ²³⁵ U	2σ (Ma)	²⁰⁶ Pb/ ²³⁸ U	2σ (Ma)	²⁰⁷ Pb/ ²⁰⁶ Pb	2σ (Ma)
MTS_16_24_13_1	0.386	0.040	0.0467	0.0015	0.257	0.061	0.006	328	29	294.1	9.4	520	220
MTS_16_24_13_2	0.337	0.043	0.0460	0.0012	0.041	0.054	0.007	291	32	290.1	7.7	250	260
MTS_16_24_13_3	0.345	0.032	0.0465	0.0010	0.067	0.054	0.005	298	24	292.7	5.8	350	210
MTS_16_24_13_4	0.370	0.089	0.0465	0.0029	0.337	0.054	0.012	303	64	293	18	200	420
MTS_16_24_13_5	0.316	0.034	0.0454	0.0010	0.115	0.050	0.005	276	26	286.5	6.3	150	210
MTS_16_24_13_6	0.343	0.024	0.0466	0.0010	0.183	0.053	0.004	298	18	293.7	5.9	300	150
MTS_16_24_13_7	0.333	0.038	0.0462	0.0009	0.159	0.052	0.006	288	29	291.2	5.7	200	240
MTS_16_24_13_8	0.342	0.031	0.0479	0.0016	0.102	0.052	0.005	296	24	301.6	9.7	230	200
MTS_16_24_13_9	0.351	0.029	0.0460	0.0011	0.054	0.055	0.005	303	21	290.1	7	350	170
MTS_16_24_13_10	0.338	0.029	0.0454	0.0011	0.236	0.054	0.005	293	22	286.2	6.5	300	180
MTS_16_24_13_11	0.331	0.030	0.0471	0.0011	0.412	0.051	0.005	288	23	296.6	6.9	200	190
MTS_16_24_13_12	0.345	0.052	0.0484	0.0017	0.109	0.052	0.008	294	39	305	11	160	310
MTS_16_24_13_13	0.330	0.035	0.0479	0.0013	0.167	0.050	0.005	286	27	301.6	7.9	120	210
MTS_16_24_13_14	0.322	0.026	0.0464	0.0015	0.074	0.050	0.004	287	23	292.2	9.5	210	190
MTS_16_24_13_15	0.318	0.036	0.0467	0.0012	0.243	0.049	0.005	277	28	294.4	7.2	90	220
MTS_16_24_13_16	0.290	0.040	0.0479	0.0014	0.104	0.044	0.006	255	31	301.3	8.4	-120	270
MTS_16_24_13_17	0.314	0.018	0.0465	0.0012	0.106	0.048	0.003	276	14	292.9	7.4	100	140
MTS_16_24_13_18	0.333	0.028	0.0452	0.0012	0.327	0.053	0.005	290	21	285.2	7.1	260	190
MTS_16_24_13_19	0.320	0.038	0.0476	0.0012	0.059	0.049	0.006	278	29	300	7.6	120	250
MTS_16_24_13_20	0.331	0.033	0.0481	0.0011	0.025	0.050	0.005	288	25	302.8	6.6	150	210
MTS_16_24_13_21	0.317	0.032	0.0468	0.0014	0.020	0.050	0.005	277	25	295.1	8.7	130	210
MTS_16_24_13_23	0.306	0.031	0.0492	0.0010	0.446	0.046	0.004	268	25	309.5	6.1	-30	190
MTS_16_24_13_24	0.369	0.085	0.0489	0.0039	0.135	0.055	0.013	302	65	307	24	240	490
MTS_16_24_13_25	0.320	0.048	0.0474	0.0017	0.032	0.051	0.008	276	37	299	11	120	310
MTS_16_24_13_26	0.305	0.028	0.0452	0.0010	0.165	0.050	0.005	268	22	285.2	6.1	170	190
MTS_16_24_13_27	0.334	0.027	0.0468	0.0010	0.058	0.053	0.004	291	20	294.5	6	290	170
MTS_16_24_13_28	0.304	0.044	0.0454	0.0012	0.056	0.050	0.007	264	34	286	7.4	100	290
MTS_16_24_13_29	0.307	0.020	0.0460	0.0008	0.150	0.050	0.004	270	16	289.6	5.2	160	160
MTS_16_24_13_30	0.363	0.027	0.0497	0.0009	0.354	0.054	0.004	313	20	312.4	5.5	320	170
MTS_16_24_13_31	0.343	0.062	0.0479	0.0019	0.059	0.051	0.010	290	47	302	11	70	350
MTS_16_24_13_32	0.329	0.048	0.0462	0.0018	0.013	0.050	0.008	283	36	291	11	90	280
MTS_16_24_13_33	0.353	0.033	0.0453	0.0010	0.240	0.054	0.006	304	25	285.4	6.3	290	210
MTS_16_24_13_34	0.369	0.035	0.0473	0.0012	0.239	0.054	0.006	316	26	297.6	7.1	290	210
MTS_16_24_13_35	0.349	0.025	0.0473	0.0010	0.114	0.051	0.004	302	19	298.2	6.2	190	170
MTS_16_24_13_36	0.344	0.045	0.0457	0.0014	0.030	0.052	0.007	295	34	287.8	8.9	170	260
MTS_16_24_13_37	0.347	0.026	0.0470	0.0006	0.164	0.053	0.004	301	19	295.8	3.5	270	160
MTS_16_24_13_38	0.333	0.039	0.0468	0.0011	0.040	0.051	0.006	288	30	294.5	7	180	240
MTS_16_24_13_39	0.346	0.026	0.0463	0.0008	0.031	0.054	0.004	300	20	292	5	310	160

collectively they define an age of 79.7 ± 1.3 Ma (Fig. 20), consistent with Late Cretaceous, not Triassic deposition.

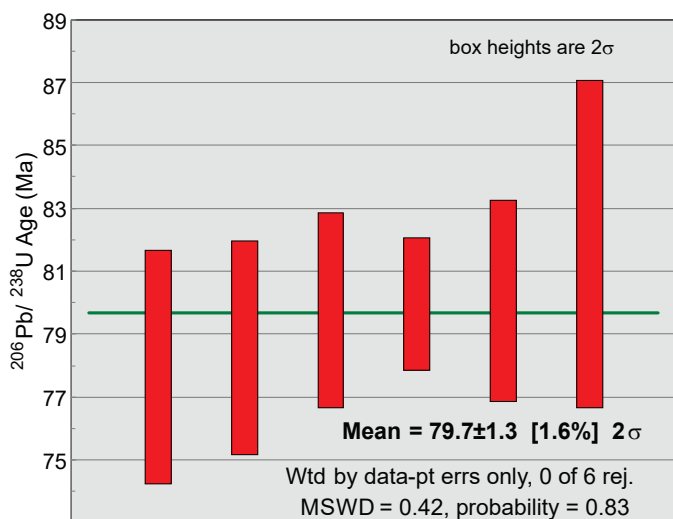


Fig. 20. $^{206}\text{Pb}/^{238}\text{U}$ age determined from regression of ages of six zircons, yields a mean of 79.6 ± 1.3 Ma.

6.3.4. $^{40}\text{Ar}/^{39}\text{Ar}$ results

We collected samples for $^{40}\text{Ar}/^{39}\text{Ar}$ analysis from a late synkinematic phase of the intrusion at Lost Sheep peak and a late quartz diorite phase at Mount Lanning (Fig. 2). We also collected samples from lamprophyre dikes cutting both the intrusion on the northeast flank of Lost Sheep peak, and limestone (part of the swarm above the east shore of Turtle Lake; Fig. 10d). Biotite was separated from all samples. Hornblende from two of these samples was also separated and analyzed to confirm biotite results. For additional quality assurance, duplicate aliquots were run for each mineral and the best behaved release spectrum was selected as the representative cooling age for that sample/mineral. Sample collection locations are plotted on Figure 2 and UTM coordinates are provided in Tables 6, 7 and 8).

6.3.4.1. Synkinematic Lost Sheep peak intrusion; sample MMI16-20-16

The Lost Sheep peak intrusion is a variably foliated, 2.5 km by >9 km, northwest elongated body in the southeast corner of the Turtle Lake map area. It probably averages granodiorite composition, but ranges from gabbro to granitic with mafic phases tending to be the most intensely foliated. Pegmatitic granitic phases are not foliated but come with the variably sheared mafic to intermediate enclaves (Fig. 10c). Fine- to medium-grained hornblende and biotite can comprise more than 30% of the rock and tend to be intimately intergrown, together with titanite (<1% ~4%). We sampled the freshest part of an intermediate, foliated phase of the intrusion, ~400 m from the northeastern contact with the aim of obtaining a post-deformational cooling age.

Separates of both biotite and hornblende were hand-picked. Selected biotite grains yielded a plateau age of 161.61 ± 0.85 Ma,

which considers 100% of ^{39}Ar released (Table 6; Fig. 21). Hornblende separated from this sample returned an age of 166.0 ± 1.1 Ma from 81.7% of ^{39}Ar liberated (see Mihalynuk et al., 2018).

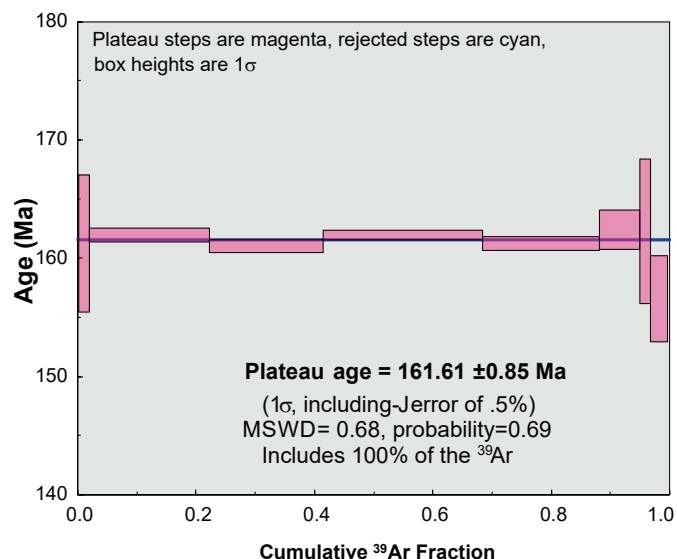


Fig. 21. Synkinematic Lost Sheep peak gabbroic to granitic intrusion biotite step heating spectrum yields a 161.61 ± 0.85 Ma age by considering 100% of ^{39}Ar released.

6.3.4.2. Biotite quartz diorite at Mount Lanning; sample MMI16-29-05

Fresh, unfoliated, medium- to fine-grained, leucocratic, biotite quartz diorite (Fig. 22a) appears to be one of the latest phases of the ~160 km² intrusion that underlies Mount Lanning. It cuts and thermally metamorphoses deformed Laberge Group strata. It is a northwest-trending pluton with an irregular outline, except in the south where it is a southward-tapering, steeply dipping tabular body that terminates near Racine Creek (Fig. 2). It is one of the largest intrusive domains lacking published isotopic age work. A clean separate of vitreous, elastic, black biotite was obtained.

Analysis of two biotite grains yielded statistically identical results of: 56.12 ± 0.29 Ma from 100% of the ^{39}Ar released (Fig. 22b) and 55.99 ± 0.29 Ma from 97.7% of ^{39}Ar released (see Mihalynuk et al., 2018). The fresh mineralogy and field relationships of the quartz diorite at Mount Lanning are consistent with the young, Eocene age.

6.3.4.3. Lamprophyre dikes; samples MMI16-14-9, MTS16-24-23

Lamprophyre dikes have a long-established association with gold mineralization (e.g., Young, 1948; Rock and Groves, 1988), although their role in gold deposit genesis is not without controversy (e.g., Kerrich and Wyman, 1994). In the Atlin gold camp, altered lamprophyre dikes are found with lode gold mineralization at the Yellowjacket deposit, and are intimately associated with precious metal-rich base metal sulphide veins

Table 5. U-Pb zircon LA-ICPMS analytical results and computed ages, sample MMI16-8-1 (UTM 540468N, 6634980N).

Sample no.	Analysis ID	CL image	Isotopic Ratios					Isotopic Ages					
			$^{207}\text{Pb}/^{235}\text{U}$	$^{206}\text{Pb}/^{238}\text{U}$	ρ	$^{207}\text{Pb}/^{206}\text{Pb}$	$^{207}\text{Pb}/^{235}\text{U}$	$^{206}\text{Pb}/^{238}\text{U}$	$^{207}\text{Pb}/^{206}\text{Pb}$	$^{206}\text{Pb}/^{238}\text{U}$	$^{207}\text{Pb}/^{206}\text{Pb}$	2σ (Ma)	
			2σ (abs)	2σ (abs)	2σ (abs)	2σ (abs)	2σ (Ma)	2σ (Ma)	2σ (Ma)	2σ (Ma)	2σ (Ma)		
	MMI_16_8_1_1	MMI 16-8-1 T-3	0.083	0.016	0.0125	0.0005	0.126	79.0	15.0	80.1	3.2	-150	340
	MMI_16_8_1_2	MMI 16-8-1 T-7	0.131	0.028	0.0128	0.0008	0.011	123.0	25.0	81.9	5.2	610	450
	MMI_16_8_1_4	MMI 16-8-1 2-3	0.099	0.011	0.0125	0.0003	0.245	95.0	10.0	80.0	2.1	220	200
	MMI_16_8_1_5	MMI 16-8-1 2-4	0.089	0.016	0.0122	0.0006	0.273	85.0	15.0	78.0	3.7	0	320
	MMI_16_8_1_6	MMI 16-8-1 2-6	0.099	0.017	0.0123	0.0005	0.080	95.0	16.0	78.6	3.4	300	380
	MMI_16_8_1_7	MMI 16-8-1 2-7	0.111	0.018	0.0125	0.0005	0.070	106.0	16.0	79.8	3.1	460	310

Table 6. $^{40}\text{Ar}/^{39}\text{Ar}$ data from biotite and hornblende of the late syn-kinematic phase of the Lost Sheep peak intrusion, sample MMI16-20-16 (UTM 550127E, 6632781N).

Sample no MMI16-20-16	Grain I	Power (%)	Ar40	\pm (1 σ)	Ar39	\pm (1 σ)	Ar38	\pm (1 σ)	Ar37	\pm (1 σ)	Ar36	\pm (1 σ)	Ca/K	\pm (1 σ)	Cl/K	\pm (1 σ)	$^{40}\text{Ar}^{39}/\text{Ar}_{(k)}$	\pm (1 σ)	$^{40}\text{Ar}^{39}$ (%)	Age (Ma)	\pm (1 σ)
			58.837	0.0644	1.6898	0.0615	0.0128	0.0301	0.0521	0.0266	0.0012	0.0007	0.365	0.188	0.014	0.052	34.611	1.286	99.46	161.3	5.7
			647.407	0.1056	18.5084	0.0645	0.2770	0.0300	0.3151	0.0277	0.0126	0.0008	0.202	0.018	0.008	0.005	34.765	0.129	99.45	161.9	0.6
			607.808	0.1107	17.4892	0.0575	0.2423	0.0295	0.1210	0.0271	0.0105	0.0010	0.082	0.018	0.004	0.005	34.557	0.122	99.50	161.0	0.5
			857.842	0.1276	24.5236	0.0625	0.2730	0.0288	0.0871	0.0267	0.0155	0.0009	0.042	0.013	0.003	0.003	34.772	0.097	99.47	162.0	0.4
			629.049	0.1177	18.0925	0.0664	0.2281	0.0301	0.0904	0.0291	0.0083	0.0008	0.059	0.019	0.001	0.005	34.613	0.134	99.62	161.3	0.6
			214.164	0.0797	6.0986	0.0636	0.1586	0.0290	0.0385	0.0267	0.0048	0.0007	0.075	0.052	0.040	0.014	34.864	0.372	99.34	162.4	1.7
			57.189	0.0696	1.6267	0.0631	0.0285	0.0296	0.0669	0.0271	0.0018	0.0007	0.490	0.201	0.015	0.053	34.840	1.379	99.15	162.3	6.1
			91.482	0.0785	2.7001	0.0639	0.0076	0.0291	-0.0197	0.0258	0.0026	0.0007	0.087	0.114	0.044	0.032	33.566	0.811	99.14	156.6	3.6

Sample no MMI16-20-16	Aliquot I	Power (%)	Ar40	\pm (1 σ)	Ar39	\pm (1 σ)	Ar38	\pm (1 σ)	Ar37	\pm (1 σ)	Ar36	\pm (1 σ)	Ca/K	\pm (1 σ)	Cl/K	\pm (1 σ)	$^{40}\text{Ar}^{39}/\text{Ar}_{(k)}$	\pm (1 σ)	$^{40}\text{Ar}^{39}$ (%)	Age (Ma)	\pm (1 σ)
			242.824	0.0921	6.5098	0.0623	0.0778	0.0283	0.6559	0.0258	0.0617	0.0013	1.136	0.046	0.006	0.013	34.537	0.344	92.61	161.2	1.5
			311.163	0.0870	8.4645	0.0630	0.1123	0.0323	3.0659	0.0279	0.0473	0.0014	4.092	0.051	0.000	0.011	35.300	0.275	95.95	164.6	1.2
			284.920	0.0942	7.6289	0.0617	0.1101	0.0304	3.0739	0.0292	0.0387	0.0013	4.556	0.060	0.004	0.012	36.065	0.304	96.47	168.0	1.4
			182.195	0.0857	4.7633	0.0628	0.1316	0.0310	2.0801	0.0295	0.0497	0.0015	4.945	0.098	0.039	0.019	35.404	0.486	92.46	165.0	2.2
			180.015	0.0776	4.9943	0.0614	0.0139	0.0315	2.1422	0.0261	0.0081	0.0010	4.860	0.087	0.028	0.018	35.798	0.452	99.21	166.8	2.0
			94.758	0.0739	2.6890	0.0636	0.0388	0.0302	1.1819	0.0249	0.0019	0.0009	4.984	0.160	0.006	0.033	35.265	0.853	99.96	164.4	3.8
			21.328	0.0665	0.5934	0.0614	0.0377	0.0328	0.3732	0.0243	0.0001	0.0009	7.142	0.884	0.150	0.163	36.238	3.832	100.63	168.7	17.0

* Corrected for blank mass discrimination, and radioactive decay
Sensitivity 6.312E-17 ± 1.047E-18 (mol/fAmp)

Table 7. ⁴⁰Ar/³⁹Ar data from biotite and hornblende of the quartz diorite at Mount Lanning, sample MMI16-29-05 (UTM 533100E, 6635600N).

Sample no MMI16-29-05	Biotite	J		Relative isotopic abundances (fAmps)*											⁴⁰ Ar* (%)	Age (Ma)	± (1σ)		
		2.712E-03	± (1σ) 2.309E-06	Ar40	Ar39	Ar38	Ar37	Ar36	Ca/K	Cl/K	⁴⁰ Ar*/ ³⁹ Ar(k)	± (1σ)	± (1σ)						
Grain 1																			
Power (%)	Ar40	± (1σ)	Ar39	± (1σ)	Ar38	± (1σ)	Ar37	± (1σ)	Ar36	± (1σ)	Ca/K	± (1σ)	Cl/K	± (1σ)	⁴⁰ Ar*/ ³⁹ Ar(k)	± (1σ)	Age (Ma)	± (1σ)	
0.10	117.586	0.0734	3.8713	0.0676	0.1206	0.0299	0.0431	0.0257	0.2620	0.0031	0.123	0.074	0.018	0.022	10.372	0.342	34.17	50.0	1.6
0.60	0.786	0.0624	0.0200	0.0626	0.0737	0.0331	0.0081	0.0294	0.0040	0.0008	4.465	21.496	10.746	34.047	98.406	308.940	250.72	426.8	1193.1
0.90	17.702	0.0664	1.2764	0.0599	0.0627	0.0290	0.0069	0.0264	0.0147	0.0011	0.059	0.230	0.101	0.066	10.454	0.557	75.43	50.4	2.7
1.10	55.914	0.0684	4.0737	0.0661	0.0838	0.0324	0.0635	0.0279	0.0253	0.0012	0.173	0.076	0.021	0.023	11.887	0.214	86.66	57.2	1.0
1.30	119.251	0.0727	9.8662	0.0615	0.1739	0.0295	0.0416	0.0297	0.0162	0.0011	0.046	0.034	0.015	0.009	11.595	0.083	95.99	55.9	0.4
1.50	133.052	0.0786	11.3168	0.0657	0.2333	0.0311	0.0210	0.0263	0.0073	0.0009	0.020	0.026	0.024	0.008	11.559	0.075	98.38	55.7	0.4
2.00	283.948	0.0903	24.0875	0.0639	0.4295	0.0294	0.0724	0.0258	0.0119	0.0010	0.033	0.012	0.016	0.004	11.636	0.039	98.78	56.1	0.2
5.00	2026.80	0.1717	170.6799	0.0840	2.8817	0.0315	1.4313	0.0276	0.1429	0.0019	0.093	0.002	0.013	0.001	11.624	0.022	97.95	56.0	0.1
Grain 2																			
0.50	15.691	0.0626	0.3288	0.0645	0.0058	0.0306	0.0317	0.0263	0.0421	0.0013	1.077	0.920	-0.054	0.272	9.858	2.314	20.68	47.6	11.0
1.00	74.380	0.0739	3.3074	0.0684	0.0511	0.0288	0.0234	0.0290	0.1219	0.0018	0.079	0.098	-0.011	0.025	11.594	0.308	51.59	55.9	1.5
1.30	113.368	0.0748	8.4412	0.0663	0.1535	0.0321	0.0310	0.0287	0.0503	0.0013	0.042	0.038	0.014	0.011	11.660	0.108	86.88	56.2	0.5
1.60	177.728	0.0827	14.8549	0.0627	0.2689	0.0299	0.0283	0.0272	0.0220	0.0010	0.021	0.021	0.016	0.006	11.520	0.058	96.35	55.5	0.3
2.00	229.961	0.0908	19.1745	0.0711	0.3934	0.0319	0.0184	0.0285	0.0236	0.0010	0.010	0.017	0.023	0.005	11.622	0.051	96.97	56.0	0.2
2.50	542.108	0.1076	45.3618	0.0652	0.7643	0.0334	0.0867	0.0270	0.0456	0.0015	0.021	0.007	0.013	0.002	11.647	0.030	97.52	56.1	0.1
3.00	759.736	0.1274	63.8520	0.0762	1.1845	0.0321	0.4518	0.0298	0.0494	0.0016	0.079	0.005	0.018	0.001	11.666	0.027	98.11	56.2	0.1
4.00	650.328	0.1175	54.9349	0.0639	0.9228	0.0291	1.0015	0.0279	0.0302	0.0011	0.204	0.006	0.013	0.002	11.677	0.027	98.70	56.2	0.1
5.00	59.126	0.0716	4.8951	0.0645	0.0860	0.0314	0.2529	0.0257	0.0077	0.0008	0.580	0.060	0.015	0.019	11.630	0.165	96.33	56.0	0.8

* Corrected for blank, mass discrimination, and radioactive decay
Sensitivity 6.312E-17 ± 1.047E-18 (mol/fAmp)

Table 8. $^{40}\text{Ar}/^{39}\text{Ar}$ data from biotite and hornblende of lamprophyre dikes at 'Lost Sheep Peak' (MIMI16-14-9, UTM zone 8, 553871E, 6627723N) and at Turtle Lake (MTS16-24-23, UTM 542755E, 6633812N).

Sample no <i>MIMI16-14-9</i>	Biotite	J		Relative Isotopic abundances (fAmps)*											$^{40}\text{Ar}^*$ (%)	Age (Ma)	\pm (1 σ)
		\pm (1 σ)	2.053E-06	Ar39	Ar38	Ar37	Ar36	Ca/K	Cl/K	$^{40}\text{Ar}^{39}/\text{Ar}_{\text{K}}$	CI/K	\pm (1 σ)	Ca/K	Cl/K			
2.710E-03		0.0839	0.0561	0.0299	0.2457	0.0261	0.0319	0.0011	0.443	0.004	0.014	0.33890	0.309	95.88	158.5	1.4	
1.4581	53.595	0.0726	0.0598	0.0280	0.0606	0.0300	0.0001	0.0007	0.481	0.240	0.056	36.774	1.534	100.09	171.4	6.8	
12.0060	435.049	0.0997	0.0642	0.0287	0.0259	0.0279	0.0028	0.0007	0.025	0.027	0.007	36.144	0.201	99.81	168.6	0.9	
13.6562	491.540	0.1182	0.0688	0.0317	0.0876	0.0261	0.0026	0.0007	0.074	0.022	0.007	35.917	0.189	99.85	167.6	0.8	
7.6261	278.945	0.0861	0.0639	0.1331	0.0298	0.0617	0.0080	0.0007	0.093	0.042	0.011	36.249	0.312	99.16	169.1	1.4	
2.4709	89.137	0.0725	0.0695	-0.0024	0.0292	0.0273	0.0029	0.0007	0.345	0.129	0.035	35.726	1.023	99.09	166.7	4.6	
3.3700	121.342	0.0736	0.0638	0.0729	0.0310	0.0278	0.0020	0.0007	0.471	0.097	0.027	35.829	0.691	99.56	167.2	3.1	
6.5465	227.299	0.0806	0.0653	0.1063	0.0288	0.0281	0.0041	0.0008	0.290	0.050	0.013	34.529	0.353	99.50	161.4	1.6	
2.711E-03		0.1400	0.0658	0.3758	0.4881	0.0262	0.3019	0.0026	0.194	0.010	0.003	34.823	0.103	91.79	162.8	0.5	
0.1880	7.285	0.0592	0.0687	-0.0058	0.0012	0.0270	0.0007	0.0006	0.070	1.638	0.465	37.626	13.951	97.14	175.2	61.9	
2.9123	104.978	0.0636	0.0622	0.0308	0.0291	0.0272	0.0060	0.0008	0.117	0.107	0.029	35.418	0.771	98.32	165.4	3.4	
6.4290	233.016	0.0836	0.0619	0.0356	0.0309	0.0275	0.0112	0.0008	0.157	0.049	0.014	35.712	0.353	98.59	166.7	1.6	
7.2392	263.217	0.0891	0.0642	0.0055	0.0306	0.0910	0.0129	0.0009	0.143	0.045	0.012	35.818	0.327	98.57	167.2	1.5	
5.7801	203.942	0.0787	0.0643	0.0393	0.0305	0.1011	0.0279	0.0101	0.199	0.055	0.015	34.754	0.396	98.56	162.4	1.8	
5.2739	190.516	0.0851	0.0577	0.0954	0.0303	0.0537	0.0089	0.0007	0.116	0.059	0.016	35.608	0.399	98.63	166.3	1.8	
1.7484	63.252	0.0719	0.0625	-0.0165	0.0309	0.0228	0.0025	0.0007	0.148	0.174	0.063	35.731	1.299	98.83	166.8	5.8	
0.6231	22.944	0.0615	0.0593	-0.0471	0.0288	0.0010	0.0008	0.0007	0.020	0.460	0.255	36.417	3.522	98.96	169.9	15.7	

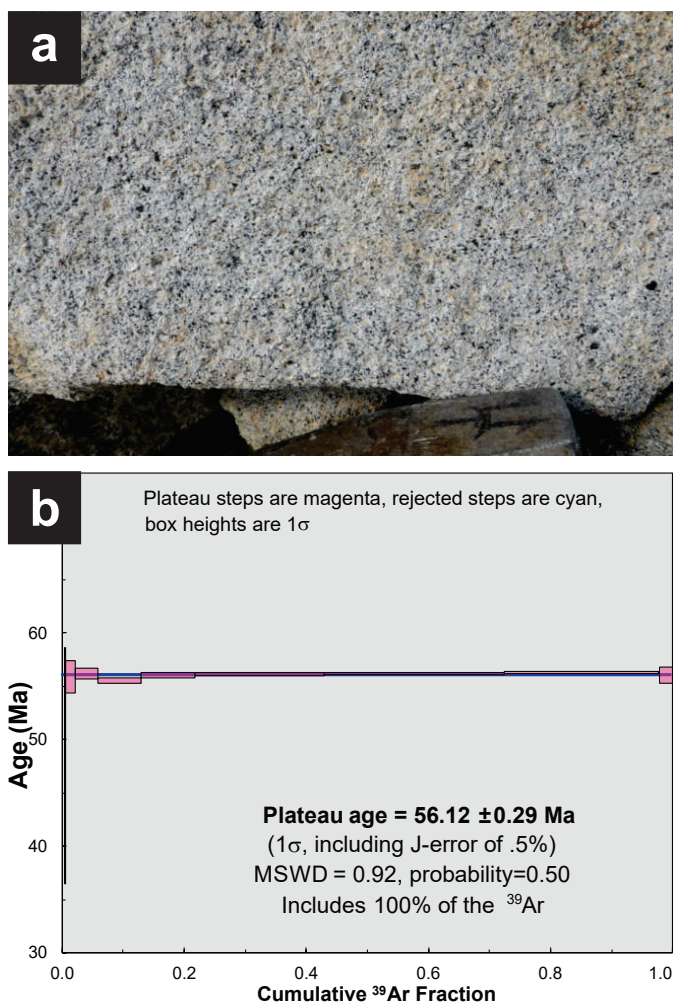


Fig. 22. a) Mount Lanning quartz diorite with fresh biotite collected for a cooling age determination. **b)** Biotite step heating spectrum yields a 56.12 ± 0.29 Ma age by considering 100% of ^{39}Ar released.

at the Atlin Ruffner mine (past producing), where they cut weakly deformed granodiorite of the Fourth of July batholith. Considering such precious metal affiliation, we selected two sites for geochronological investigation: conspicuous southwest-trending lamprophyre dikes that cut the intrusion at Lost Sheep peak (MMI16-14-9), and limestone near Turtle Lake (MTS16-24-23).

On steep faces of Lost Sheep peak lamprophyre dikes are well exposed in fresh landslide scars, but otherwise tend to be weathered slots floored with biotite-rich gruss in the host granodiorite. We sampled the thickest (~15 m) and freshest of the well-exposed biotite-rich dikes (possibly a composite of superimposed dikes) on the northeast flank of Lost Sheep peak. The dike is dark green to black, medium- to coarse-grained and has a knobby weathered appearance due to an abundance of xenoliths, xenocrysts, xenocryst aggregates (Fig. 23a), and calcite filled amygdaloids or ocelli. We picked the freshest and highest purity hornblende and biotite grains to obtain clean separates for $^{40}\text{Ar}/^{39}\text{Ar}$ age determination, but microscopic

intergrowths of the two minerals and pyroxene (Figs. 23b, c) likely escaped detection.

Step heating of the best quality biotite grain produced an age of 168.2 ± 1.0 Ma from 75.8% of ^{39}Ar released. Hornblende analyses returned an age of 174.0 ± 2.7 Ma from 74.5% of ^{39}Ar released (Fig. 23d). the preferred interpreted age for this sample. Results from a second hornblende aliquot were rejected, but integrating all ^{39}Ar from both aliquots yields an age of 171 ± 10 Ma (for hornblende spectra see Mihalynuk et al., 2018).

Extensively diked limestone on the steep slope above eastern Turtle Lake includes fine to medium-grained lamprophyre. Intimate mineral intergrowths precluded isolation of pure mineral separates, but about 10 grains of visually pure biotite were obtained. Even then, the coarsest biotite grains are rutilated (see triangular mesh of dark needles, Fig. 23e). A separate of intergrown hornblende and biotite was also obtained for total fusion analysis, but was not used. The best quality biotite grain yielded a release spectrum from which consideration of 100% of the gas gives an $^{40}\text{Ar}/^{39}\text{Ar}$ age of 163.6 ± 2.2 Ma (Fig. 23f). Removal of the first three steps yields an age of 162.80 ± 0.93 Ma from 53.9% of ^{39}Ar released. Rejection of the first step yields an age of 165.9 ± 1.1 Ma, and is probably closest to the actual crystallization age of the dike.

7. Geochemistry

We analyzed mafic to felsic volcanic and ultramafic mantle units from the Turtle Lake map area in an attempt to elucidate the tectonic and physio-chemical settings in which they formed.

7.1. Methods for major and trace element geochemistry

Samples from the Turtle Lake map sheet were crushed and processed using lithium metaborate/tetraborate fusion and nitric acid dissolution and analyzed for major and trace elements at Activation Laboratories (Ancaster, Ontario) using inductively coupled plasma-optical emission spectrometry (ICP-OES) and inductively coupled plasma-mass spectrometry (ICP-MS; 4Lithores analytical package; Table 9). At a 95% confidence level, the uncertainty in measurement of major elements significantly exceeding their quantification limit (3.33 times the detection limit), is $\leq 4\%$ relative. The uncertainty in P_2O_5 , which is present in low abundances (< 0.75 wt.%), is significantly larger, ranging between 5 and 70% relative at a 95% confidence level.

Most lithophile trace elements in the majority of samples from the Turtle lake map area have concentrations that exceed their quantification limits. The uncertainty in individual measurements, at a 95% confidence level, for transitional metals (e.g., Ni, Cr, V) is $\leq 30\%$. The relative uncertainty in measurement of rare earth elements (REE) at the 95% confidence interval is typically $< 15\%$ for most samples presented in Table 9. The relative uncertainty in measurement of high field strength elements (HFSE) at a 95% confidence interval is generally $< 30\%$.

The results of instrumental neutron activation analysis

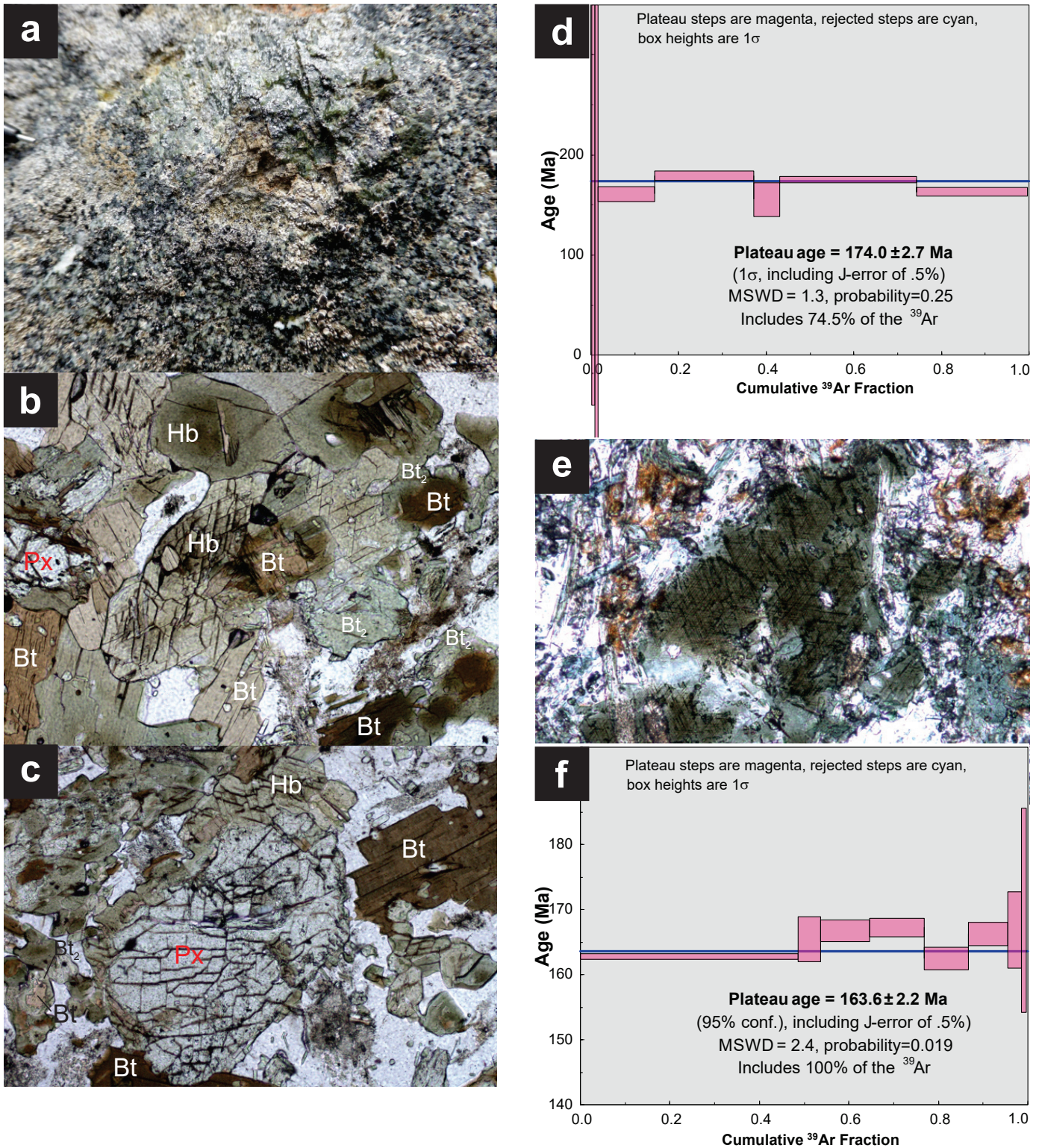


Fig. 23. **a)** Medium-grained lamprophyre from near middle of ~15 m thick dike at northeast flank of Lost Sheep peak contains aggregates up to ~4 cm across of bright green crystals, probably chrome diopside. **b)** Pleochroic green clinopyroxene (diopsidic? augite, Px) is mantled by pleochroic green to brown hornblende (Hb) with fine domains of dark brown to orange-brown biotite (phlogopitic?, Bt) and green pleochroic biotite (Bt₂). Hornblende and biotite have partly altered to chlorite (Chl). **c)** Pleochroic green-brown hornblende (Hb) mantles pyroxene (Px) and is in textural equilibrium with pleochroic brown to orange-tan biotite (Bt) and replaced by pleochroic green biotite (Bt₂). **d)** ³⁹Ar step heating spectrum from a select hornblende grain yielded an age of 174.0 ± 2.7 Ma from 74.5% of ³⁹Ar released. **e)** Photomicrograph showing rutilated, pleochroic green biotite in a lamprophyre dike east of Turtle Lake. **f)** ³⁹Ar step heating spectrum from a select biotite grain yielded an age of 163.6 ± 2.2 Ma from 100% of ³⁹Ar released.

Table 9. Major and trace element composition of samples from the Turtle Lake map sheet (NTS 104M/16).

Sample Suite	MMI16-8-3 IAT	DMI16-9-2A IAT	DMI16-9-2B IAT	DMI16-9-4A IAT	DMI16-16-4A IAT	DMI16-16-6A IAT	MMI16-8-1 Windy-Table
Lithology	basalt	basalt	basalt	basalt	basalt	basalt	lapilli tuff
Easting	540290	539942	539942	549775	549362	549834	540468
Northing	6635377	6637146	6637146	6637335	6625441	6625399	6634980
Major elements (wt.%)							
SiO ₂	48.98	49.48	47.93	50.49	49.27	48.33	53.95
Al ₂ O ₃	15.08	13.28	13.01	14.39	13.8	14.81	20.18
Fe ₂ O ₃ (T)	10.93	10.07	11.11	10.17	10.98	8.67	7.15
MnO	0.12	0.135	0.173	0.172	0.184	0.172	0.16
MgO	5.89	7.88	7.54	7.99	8.68	5.12	2.33
CaO	6.51	7.1	6.47	6.32	9.31	16.68	6.28
Na ₂ O	3.86	2.23	3.05	4.51	3.31	1.05	3.08
K ₂ O	0.17	0.18	0.15	0.05	0.21	0.08	2.80
TiO ₂	1.36	1.08	1.33	1.35	1.23	0.99	0.67
P ₂ O ₅	0.10	0.11	0.11	0.14	0.12	0.09	0.21
LOI	7.29	8.59	9.00	4.13	3.45	3.62	2.46
Total	100.30	100.10	99.88	99.72	100.50	99.61	99.28
Trace elements (ppm)							
Sc	39	34	40	37	40	33	11
Be	< 1	< 1	< 1	< 1	< 1	< 1	2
V	286	288	339	346	313	252	91
Cr	270	210	250	200	280	190	60
Co	38	32	38	36	40	30	10
Ni	90	70	90	70	140	70	< 20
Cu	70	60	70	70	40	50	10
Zn	70	80	80	90	70	60	120
Ga	16	15	15	16	14	20	22
Ge	1.4	1	1.5	0.9	1.1	2.3	1.5
As	7	< 5	< 5	< 5	< 5	< 5	< 5
Rb	7	4	4	< 1	3	1	99
Sr	192	121	160	59	132	32	558
Y	27.7	25	31	31.6	26	23.2	26.3
Zr	76	68	89	80	80	59	181
Nb	1.5	1	0.9	1.1	1.3	1.2	11.5
Mo	< 2	< 2	< 2	< 2	< 2	< 2	< 2
Ag	< 0.5	< 0.5	< 0.5	< 0.5	< 0.5	< 0.5	0.6
In	< 0.1	< 0.1	< 0.1	< 0.1	< 0.1	< 0.1	< 0.1
Sn	< 1	< 1	< 1	< 1	1	1	< 1
Sb	0.8	< 0.2	0.3	0.3	< 0.2	< 0.2	1.6
Cs	3.7	3.7	3.2	1.2	0.2	0.1	12.7
Ba	145	128	188	23	52	11	1715
La	3.55	2.38	2.61	3.22	3.00	2.55	27.4
Ce	10.5	7.4	8.61	9.81	8.93	7.71	50.2
Pr	1.7	1.29	1.49	1.65	1.44	1.23	5.55
Nd	8.86	6.85	7.94	8.95	7.62	6.63	21.3
Sm	3.12	2.68	3.18	3.11	2.67	2.34	4.4
Eu	1.16	0.968	1.13	1.04	1.06	0.842	1.37
Gd	4.20	3.50	4.49	4.49	3.75	3.32	4.13
Tb	0.77	0.66	0.82	0.83	0.68	0.60	0.67
Dy	4.89	4.45	5.39	5.31	4.51	3.82	4.04
Ho	1.02	0.92	1.13	1.09	0.96	0.83	0.81
Er	3.05	2.70	3.35	3.10	2.74	2.48	2.44
Tm	0.452	0.401	0.503	0.475	0.399	0.36	0.368
Yb	3.03	2.71	3.19	3.16	2.69	2.3	2.51
Lu	0.436	0.408	0.502	0.516	0.43	0.36	0.377
Hf	1.9	1.6	2.2	2.0	1.8	1.5	4
Ta	0.08	0.07	0.06	0.08	0.1	0.07	0.41
W	0.7	< 0.5	< 0.5	< 0.5	< 0.5	< 0.5	0.9
Tl	0.06	< 0.05	< 0.05	< 0.05	< 0.05	< 0.05	0.58
Pb	< 5	< 5	< 5	< 5	< 5	< 5	9
Bi	< 0.1	< 0.1	< 0.1	< 0.1	< 0.1	< 0.1	< 0.1
Th	0.24	0.21	0.15	0.21	0.31	0.23	8.59
U	0.12	0.21	0.08	0.26	0.10	0.11	6.98

Table 9. Continued.

Sample Suite	MMI16-23-6 Horsefeed	MMI16-23-8 Horsefeed	DMI16-5-4A Horsefeed	JBA16-5-6 Horsefeed	MMI16-14-9	MTS16-24-12	DMI16-4-3A
Lithology	E-MORB	E-MORB	E-MORB	E-MORB	lamprophyre	lamprophyre	CAB dike
Easting	548161	547679	546083	546059	553871	543783	538671
Northing	6647699	6647539	6650302	6650173	6627723	6635617	6632389
Major elements (wt.%)							
SiO ₂	45.84	38.34	47.26	48.76	51.52	41.52	50.96
Al ₂ O ₃	13.52	10.59	12.86	14.84	11.92	10.80	13.7
Fe ₂ O ₃ (T)	11.71	10.99	14.65	12.07	7.17	8.75	8.51
MnO	0.17	0.12	0.21	0.20	0.13	0.14	0.15
MgO	7.17	6.89	6.25	6.85	12.50	10.85	7.76
CaO	12.99	15.14	9.31	9.25	7.83	10.30	9.13
Na ₂ O	2.11	0.12	1.23	2.83	3.53	2.23	2.09
K ₂ O	0.55	2.05	0.18	0.16	2.45	2.76	3.44
TiO ₂	1.05	0.80	2.15	1.59	0.96	1.31	0.95
P ₂ O ₅	0.08	0.09	0.25	0.15	0.53	0.74	0.52
LOI	3.94	15.73	5.63	3.26	1.42	9.24	2.98
Total	99.12	100.90	99.97	99.94	99.95	98.65	100.2
Trace elements (ppm)							
Sc	43	24	47	43	18	25	26
Be	< 1	< 1	< 1	< 1	3	2	2
V	275	127	380	332	140	205	210
Cr	280	230	100	210	870	650	390
Co	58	44	47	45	40	43	31
Ni	130	160	70	90	330	260	100
Cu	20	80	210	140	20	80	40
Zn	90	70	90	90	90	80	80
Ga	16	10	20	18	16	15	15
Ge	2.1	1	1.9	2.1	1.2	1.1	1.3
As	7	< 5	< 5	< 5	< 5	< 5	< 5
Rb	7	28	4	3	97	115	79
Sr	468	176	171	215	891	690	769
Y	19.8	13.2	44	28.6	18.2	24.8	27.2
Zr	40	43	124	89	187	177	147
Nb	3.8	3.9	5.3	5.7	25.2	17.3	5.7
Mo	< 2	< 2	< 2	< 2	2	3	3
Ag	< 0.5	< 0.5	< 0.5	< 0.5	0.6	0.5	< 0.5
In	< 0.1	< 0.1	< 0.1	< 0.1	< 0.1	< 0.1	< 0.1
Sn	< 1	< 1	1	< 1	< 1	1	< 1
Sb	0.7	0.4	0.4	1.5	< 0.2	1.3	0.4
Cs	0.2	0.9	0.2	0.1	9.8	9.7	3
Ba	38	79	79	226	2591	2470	1611
La	3.36	2.62	9.22	7.11	73.8	52.7	28.7
Ce	8.66	6.23	23.6	17.7	130	106	59.4
Pr	1.3	0.92	3.47	2.47	13.9	12.8	7.36
Nd	6.5	4.28	16.9	11.8	50.9	51	31.5
Sm	2.21	1.49	5.36	3.53	8.72	10.1	7.4
Eu	0.953	0.362	1.91	1.27	2.36	2.79	2.11
Gd	3.01	2.01	6.88	4.53	6.11	7.93	7.05
Tb	0.54	0.36	1.21	0.82	0.77	1.03	1.03
Dy	3.72	2.32	7.82	5.29	3.83	5.26	5.27
Ho	0.76	0.5	1.55	1.05	0.64	0.9	0.99
Er	2.2	1.52	4.32	3	1.69	2.36	2.55
Tm	0.321	0.238	0.618	0.426	0.227	0.307	0.335
Yb	2.06	1.63	3.91	2.92	1.33	1.9	2.14
Lu	0.317	0.286	0.566	0.441	0.202	0.28	0.329
Hf	1.0	1.0	3.2	2.1	3.8	3.9	3.1
Ta	0.21	0.22	0.34	0.37	1.31	0.92	0.35
W	< 0.5	0.8	6	< 0.5	0.6	0.7	< 0.5
Tl	< 0.05	< 0.05	0.06	< 0.05	0.75	0.73	0.67
Pb	< 5	< 5	< 5	< 5	6	7	8
Bi	< 0.1	< 0.1	< 0.1	< 0.1	< 0.1	< 0.1	< 0.1
Th	0.28	0.21	0.63	0.52	23.9	9.03	5.2
U	0.45	0.64	0.3	0.16	6.87	3.09	2.97

Table 9. Continued.

Sample Suite	<u>DMI16-14-9A</u>	<u>DMI16-21-7A</u>	<u>MMI16-6-2</u>	<u>MMI16-18-1</u> Eocene	<u>DMI16-29-20A</u> Eocene intrusion	<u>DMI16-24-14A</u> Eocene intrusion	<u>DMI16-27-8A</u> Eocene Intrusion
Lithology	CAB dike	CAB dike	QFP dike	quartz diorite	diorite	diorite	quartz diorite
Easting	554057	532804	547085	549939	514894	542848	542089
Northing	6626649	6623895	6652002	6674246	6637897	6633199	6634018
Major elements (wt.%)							
SiO ₂	53.33	51.19	65.57	65.47	49.58	55.90	66.81
Al ₂ O ₃	13.46	16.27	17.04	15.93	19.41	18.80	15.08
Fe ₂ O ₃ (T)	7.23	7.22	1.61	4.46	10.59	8.09	4.11
MnO	0.13	0.12	0.03	0.10	0.14	0.18	0.08
MgO	10.8	6.38	0.86	1.36	3.92	2.69	1.36
CaO	7.5	6.07	3.88	3.05	10.56	6.89	3.01
Na ₂ O	3.26	4.02	3.67	3.57	2.99	4.00	4.07
K ₂ O	1.57	3.24	2.43	4.17	0.68	1.68	3.75
TiO ₂	0.80	1.19	0.21	0.63	1.37	1.20	0.51
P ₂ O ₅	0.20	0.43	0.05	0.15	0.33	0.43	0.20
LOI	1.97	3.72	4.69	1.48	0.70	0.71	1.00
Total	100.3	99.85	100.10	100.40	100.30	100.60	99.97
Trace elements (ppm)							
Sc	24	23	4	9	25	17	6
Be	1	1	< 1	2	< 1	1	2
V	159	179	27	64	328	155	49
Cr	630	220	50	110	< 20	< 20	30
Co	35	24	3	7	25	10	7
Ni	240	90	< 20	< 20	< 20	< 20	< 20
Cu	< 10	40	< 10	< 10	20	< 10	10
Zn	60	60	< 30	90	100	100	50
Ga	15	15	16	17	19	18	17
Ge	1.1	1.1	0.8	1.3	1.1	1.2	1.1
As	< 5	< 5	< 5	< 5	< 5	< 5	< 5
Rb	35	82	74	149	14	34	109
Sr	400	747	450	350	772	749	378
Y	17.4	16.8	4	26.1	16.2	27.6	20.2
Zr	118	113	65	193	42	141	232
Nb	7.9	14.5	1.7	10.3	3.1	8.3	12.9
Mo	< 2	< 2	< 2	< 2	< 2	2	3
Ag	< 0.5	< 0.5	< 0.5	0.6	< 0.5	< 0.5	0.7
In	< 0.1	< 0.1	< 0.1	< 0.1	< 0.1	< 0.1	< 0.1
Sn	1	< 1	< 1	3	< 1	1	1
Sb	< 0.2	0.6	0.2	0.5	0.5	0.5	0.5
Cs	3.4	2.2	4.3	7.3	0.4	1.4	1.6
Ba	1006	3175	4129	1647	640	1516	1962
La	16.9	21.1	8.89	38.1	12.5	23.5	37.3
Ce	34.8	42.5	15.4	69.6	26.3	48.4	68.5
Pr	4.25	5.2	1.65	7.71	3.35	6.07	7.3
Nd	17.5	21.8	6.01	28	14.2	25.5	25.9
Sm	3.79	4.6	1.08	5.63	3.62	5.92	4.99
Eu	1.13	1.5	0.474	1.04	1.31	1.73	1.1
Gd	3.56	4.14	0.93	4.89	3.54	5.44	4.03
Tb	0.57	0.56	0.14	0.79	0.54	0.83	0.6
Dy	3.26	3.03	0.74	4.44	3.2	4.95	3.38
Ho	0.62	0.57	0.14	0.88	0.61	0.98	0.68
Er	1.79	1.63	0.38	2.53	1.7	2.79	2.01
Tm	0.265	0.225	0.052	0.394	0.232	0.398	0.313
Yb	1.71	1.44	0.33	2.64	1.47	2.47	2.2
Lu	0.258	0.223	0.055	0.402	0.215	0.392	0.335
Hf	2.5	2.3	1.5	4.8	1.1	2.5	4.7
Ta	0.52	0.92	0.13	1.11	0.22	0.47	1.06
W	< 0.5	< 0.5	< 0.5	1.8	< 0.5	3.8	0.7
Tl	0.37	0.53	0.54	1.4	0.07	0.25	0.59
Pb	< 5	5	< 5	35	< 5	8	14
Bi	0.3	< 0.1	< 0.1	< 0.1	< 0.1	0.1	< 0.1
Th	3.65	4.47	2.15	22.1	2.03	3.99	13.1
U	1.14	1.56	1.31	6.96	0.67	1.03	4.31

Table 9. Continued.

Sample Suite	<u>DMI16-16-6B</u> Eocene Intrusion	<u>DMI16-13-1A</u> L. Cretaceous	<u>DMI16-21-12A</u> L. Cretaceous	<u>DMI16-29-13A</u> L. Cretaceous	<u>DMI16-29-18A</u> L. Cretaceous	<u>DMI16-29-3A</u> L. Cretaceous	<u>DMI16-29-6A</u> L. Cretaceous
Lithology	quartz diorite	quartz diorite	quartz diorite	granodiorite	granodiorite	granodiorite	granodiorite
Easting	549834	528839	540468	529087	528466	528206	528349
Northing	6625399	6626085	6634980	6639906	6640410	6634793	6635781
Major elements (wt.%)							
SiO ₂	63.88	66.34	66.04	73.93	74.26	71.65	71.29
Al ₂ O ₃	15.91	14.56	15.47	13.33	13.26	14.36	14.28
Fe ₂ O ₃ (T)	4.58	3.7	3.92	2.18	2.16	2.27	2.58
MnO	0.09	0.07	0.08	0.06	0.05	0.06	0.06
MgO	2.02	1.64	2.17	0.27	0.22	0.7	0.7
CaO	3.78	3.31	2.69	1.09	0.94	1.56	1.61
Na ₂ O	3.99	3.72	3.79	4.04	3.92	3.96	3.99
K ₂ O	4.07	3.97	3.98	4.23	4.18	4.24	4.31
TiO ₂	0.63	0.46	0.48	0.17	0.15	0.24	0.29
P ₂ O ₅	0.21	0.21	0.17	0.05	0.03	0.09	0.11
LOI	0.88	1.18	1.46	0.37	0.57	0.61	0.74
Total	100.00	99.16	100.30	99.74	99.74	99.75	99.96
Trace elements (ppm)							
Sc	9	7	6	2	2	3	4
Be	2	2	2	3	4	3	2
V	73	61	55	13	9	24	32
Cr	70	40	80	< 20	< 20	30	30
Co	10	8	8	1	1	3	4
Ni	40	< 20	50	< 20	< 20	< 20	< 20
Cu	< 10	20	< 10	< 10	< 10	< 10	< 10
Zn	60	60	50	40	40	< 30	< 30
Ga	15	16	16	17	17	14	15
Ge	1.1	1.2	1.1	1.5	1.5	1.3	1.3
As	< 5	< 5	< 5	< 5	< 5	< 5	< 5
Rb	149	138	139	129	140	138	133
Sr	480	397	409	127	111	246	325
Y	18	16.5	15.9	23.1	28.3	12.9	12.2
Zr	221	212	227	192	164	160	211
Nb	13.4	10.9	10.4	13	10.3	7.4	7.3
Mo	< 2	< 2	3	< 2	< 2	< 2	< 2
Ag	0.7	0.7	0.7	0.7	< 0.5	< 0.5	0.6
In	< 0.1	< 0.1	< 0.1	< 0.1	< 0.1	< 0.1	< 0.1
Sn	1	2	2	1	2	1	1
Sb	< 0.2	0.3	< 0.2	< 0.2	< 0.2	< 0.2	0.4
Cs	4.7	4.5	2.7	2.3	3.2	2.9	2.6
Ba	2057	1734	1660	843	673	1231	1498
La	38	40.7	30.3	36.8	32.2	29.4	29.6
Ce	66.6	71.5	54.2	67.2	61	48.9	49
Pr	7.06	7.36	5.89	6.95	6.65	5	4.89
Nd	24.4	25.2	21.1	23.5	23.5	17.1	16.3
Sm	4.44	4.54	3.86	4.42	5.1	3.11	2.95
Eu	1.21	1.07	0.935	0.371	0.351	0.581	0.639
Gd	3.77	3.55	3.28	3.63	4.41	2.29	2.23
Tb	0.56	0.5	0.51	0.6	0.77	0.36	0.37
Dy	3.26	2.8	2.68	3.61	4.72	2.11	2.22
Ho	0.61	0.56	0.52	0.75	0.94	0.42	0.41
Er	1.75	1.6	1.58	2.45	2.97	1.21	1.13
Tm	0.257	0.246	0.237	0.387	0.449	0.199	0.168
Yb	1.75	1.64	1.61	2.73	3.16	1.36	1.16
Lu	0.299	0.277	0.257	0.44	0.521	0.233	0.194
Hf	5.2	4.5	4.6	5.2	4.1	3.2	4.1
Ta	1.18	0.98	0.99	1.34	1.13	0.84	0.71
W	2.7	1	27.6	< 0.5	< 0.5	< 0.5	1.1
Tl	0.92	0.81	0.72	0.61	0.68	0.73	0.73
Pb	19	20	19	14	11	17	15
Bi	< 0.1	0.1	0.1	< 0.1	< 0.1	0.1	0.1
Th	18.6	19.1	16.7	20.1	21.2	13.3	11.8
U	3.64	6.91	7.20	6.57	6.59	5.18	4.39

(INAA) and sodium peroxide assays, also performed by Activation Laboratories, are presented in Table 9.

7.2. Geochemistry results

Thirty-one samples of igneous rocks typically encountered in the Turtle Lake map area were analyzed. Based on their petrographic and geochemical character they have been grouped into the following principal suites: island arc tholeiite (6), enriched mid-ocean ridge basalt (E-MORB; 4), calc-alkaline basaltic to andesitic rocks (4), lamprophyre (2), and intermediate to felsic rocks (15).

7.2.1. Basaltic to intermediate volcanic rocks

Six samples of pervasively altered augite and plagioclase-phyric basalt and basaltic fragmental rock assigned to the island arc tholeiite suite (Fig. 24) and collected from the eastern shore of Tagish Lake, south of Peninsula Mountain, and the southeastern corner of the study area near Sunday Peak (Fig. 2), have moderate to high LOI (3.5-9.0 wt.%), relatively uniform SiO_2 (51-55 wt.%; reported on anhydrous, LOI-free basis) and Al_2O_3 (14.4-16.4 wt.%), and variable MgO (5.4-9.0 wt.%) concentrations. On a Primitive Mantle (PM; Palme and O'Neill, 2003)-normalized extended trace element diagram (Fig. 25a), these samples have relatively unfractionated rare earth element (REE) profiles, with slight depletion in the most incompatible light REE (LREE). Notably, these samples have pronounced relative depletions in the high-field strength elements (HFSE) Nb and Ta, diagnostic of an island arc tholeiitic (IAT) magmatic affinity. Furthermore, the trace element compositions of the IAT suite overlap the compositions of IAT reported by English et al. (2010) from the Nakina area of the Cache Creek terrane (Figs. 25a and 26). A single sample of lapilli tuff with a basaltic

andesite composition (Fig. 24; $\text{SiO}_2=56$ wt.%) also collected for geochronology from the Windy-Table suite has a pronounced calc-alkaline trace element profile characterized by a strong enrichment in LREE relative to the more incompatible heavy REE (HREE).

In contrast to the IAT suite, the amygdaloidal aphanitic basaltic rocks in the Horsefeed Formation (LOI=3-16 wt.%) have lower abundances of SiO_2 (45-51 wt.%), Al_2O_3 (12.6-15.5 wt.%), while having similar MgO concentrations (6.7-8.2 wt.%). Furthermore, they display slight enrichment of LREE relative to HREE and lack the conspicuous depletion in Nb and Ta (Fig. 25b) displayed by the volcanic rocks of the IAT suite. The basaltic rocks of the Horsefeed formation plot in the mantle array of Pearce (2008), and have compositions that are intermediate between N-MORB and E-MORB (Fig. 26). Although the overlap is not complete (Fig. 26), the E-MORB reported here largely overlap the E-MORB of the Nakina area (English et al., 2010).

Three weakly altered dikes sampled from Mount Clive, Lost Sheep peak, and the western shore of Tagish Lake have basaltic compositions (LOI=2-4 wt.%; $\text{SiO}_2=53-55$ wt.%; $\text{Al}_2\text{O}_3=14.2-17.1$ wt.%, MgO=6.7-11.1 wt.%; Fig. 24), but display variable mineralogy ranging from augite+biotite-phyric to hornblende+plagioclase-phyric. Field relationships, and relatively fresh mineralogy suggest that these dikes are Late Cretaceous or younger. These dikes have similar trace element patterns, characterized by strong enrichment in LREE and depletion of HREE relative to N-MORB, and pronounced depletion in Nb, Ta and Ti (Fig. 25c).

7.2.2. Lamprophyre

Two lamprophyre samples have variable LOI (1-9 wt.%), but relatively uniform SiO_2 (46.9-52.7 wt.%), Al_2O_3 (12 wt.%), and MgO (12.3-12.8 wt.%) concentrations. The combined $\text{Na}_2\text{O}+\text{K}_2\text{O}$ concentration (>5.5 wt.%) is high, but consistent with the sample's biotite-rich alkaline affinity. The two samples have sub-parallel trace element profiles (Fig. 25c), characterized by strongly fractionated, LREE-enriched patterns, and marked Nb-Ta-Ti negative anomalies, which are typical of calc-alkaline lamprophyres (Rock, 1991). The lamprophyres also display strong enrichments in LILE (80-500 x PM, matching the LILE contents of the intermediate-felsic rocks analyzed as part of this study).

7.2.3. Intermediate and felsic samples

Fifteen samples of intermediate- SiO_2 to felsic compositions were analyzed. All samples display pronounced, PM-normalized enrichments of LREE relative to HREE, and strong relative depletions in Nb, Ta, and Ti. In addition, most intermediate to felsic samples show enrichments in Zr-Hf relative to the similarly incompatible REE. Although most samples display significant overlap, some systematic differences between suites may be diagnostic. First, rocks assigned to the Fourth of July suite are the most alkaline, and thereby have the highest abundances of Hf, Zr, and LREE and lowest abundances of

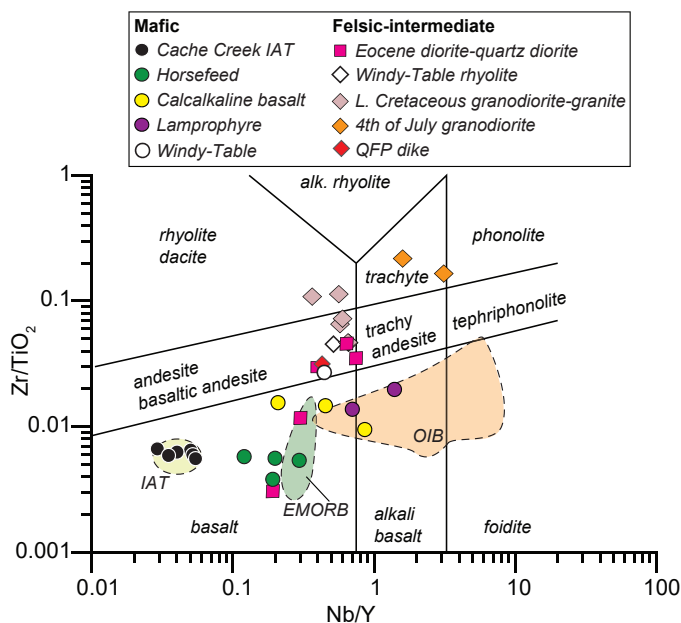


Fig. 24. Rock analyses presented in this report plotted on the modified Zr/TiO_2 vs. Nb/Y classification diagram (Pearce, 1996).

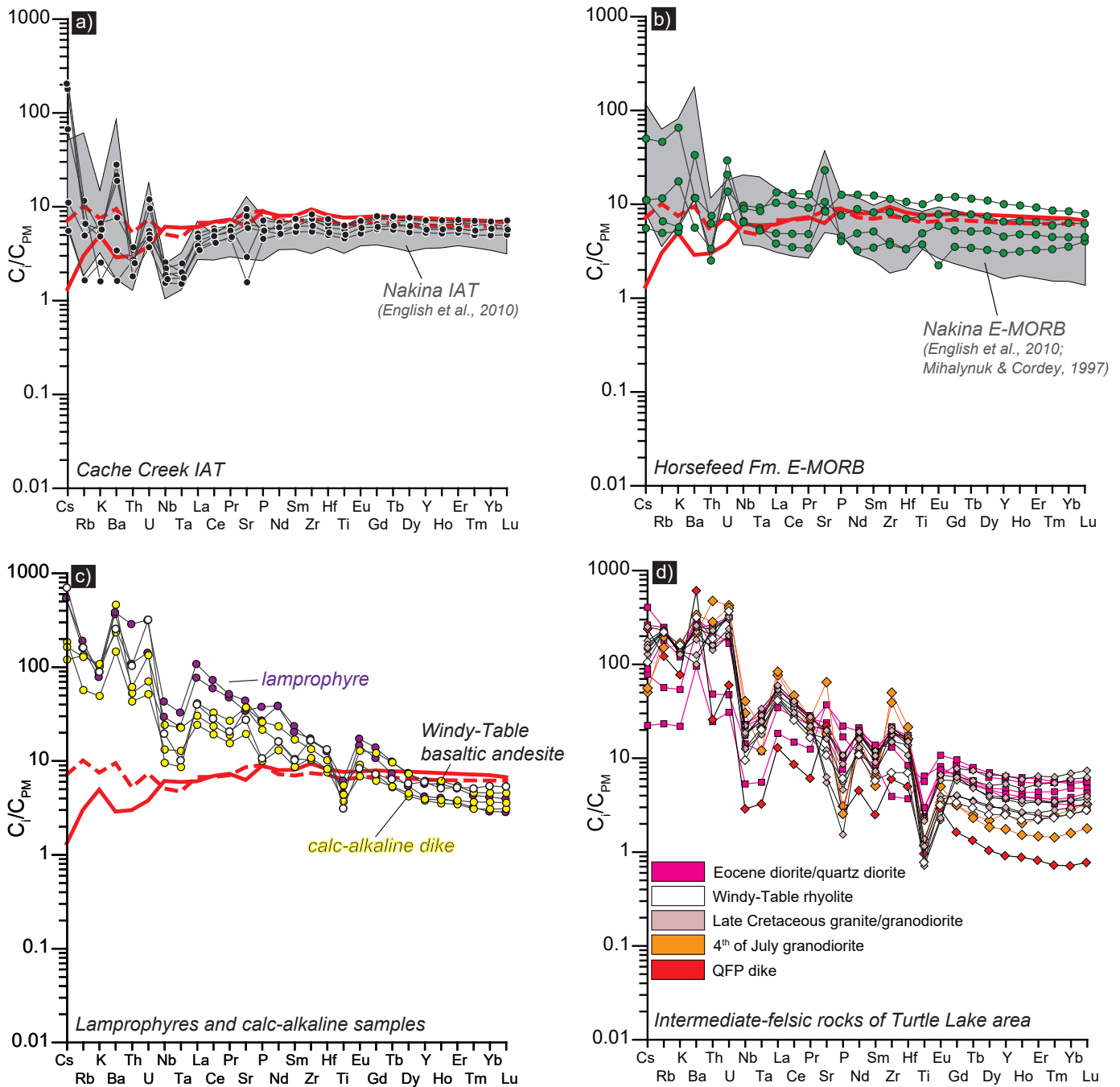


Fig. 25. Primitive mantle-normalized (Palme and O'Neill, 2003) trace element profiles for mafic (a-c) and intermediate to felsic (d) rocks of the Turtle Lake map area. Average compositions (Gale et al., 2013) of normal-MORB (N-MORB) and back-arc basin basalt (BABB) are shown for reference.

HREE. In addition, samples of the Fourth of July suite display U-shaped HREE profiles. Second, Late Cretaceous plutonic rocks ($\text{SiO}_2=67-75$ wt.% and $\text{Al}_2\text{O}_3=13.4-15.7$ wt.%) are typically quartz dioritic to granodioritic in composition and are distinguished from the dioritic to quartz dioritic Eocene plutonic rocks ($\text{SiO}_2=50-68$ wt.% and $\text{Al}_2\text{O}_3=15.3-19.7$ wt.%) by higher SiO_2 and lower Al_2O_3 concentrations.

8. Discussion

Based on macrofossil evidence, the extensive Horsefeed Formation carbonate was deposited in the Late Carboniferous to Early Permian in a tectonic setting that was stable throughout the time span (Monger, 1975). Volcanic rocks interbedded with the Horsefeed Formation are uncommon, but where present, they display within-plate geochemical characteristics and are probably the relicts of ocean islands or plateaux, the

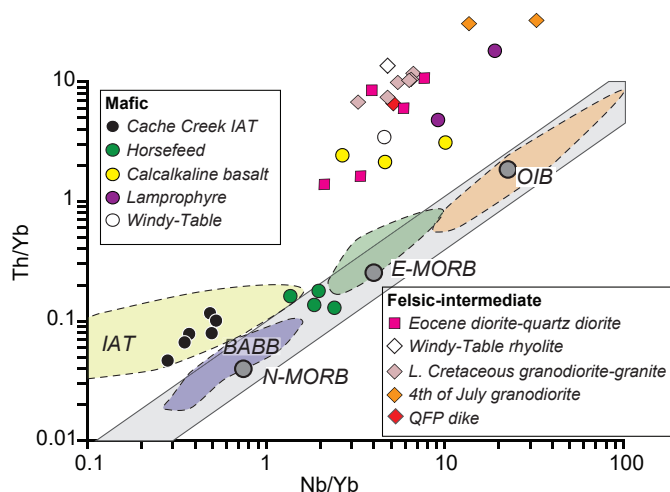


Fig. 26. Th/Yb vs. Nb/Yb diagram (after Pearce, 2008) showing the compositions of the rocks analyzed as part of this study and compared to the composition of oceanic basalts, which plot in the MORB-OIB array (grey band). Fields of IAT, BABB, E-MORB, and OIB are based on the classification of Cache Creek basalts of English et al. (2010).

massive bases of which were subducted (English et al., 2010; Zagorevski et al., 2016). Tuffaceous layers in the Horsefeed Formation point to explosive volcanism during deposition of the carbonate platform. Near Mount Cloutier these tuffs are of EMORB composition. We attempted to date one of the tuff layers using conodonts, but were unsuccessful. However, the polymictic sharpstone conglomerate that we sampled at Turtle Lake contained detrital zircons spanning Middle Pennsylvanian through Early Permian (~25 m.y.). This is the same time span as the most widespread fossil ages obtained from the Horsefeed Formation of the Turtle Lake area (Monger, 1975), and suggests that these fossil-bearing carbonate environments were dependant on volcanic substrates. But is plateau magmatism over a 25 m.y. time span reasonable? Was Horsefeed Formation deposited instead atop an age-progressive chain of islands like Hawaii?

Isolated within-plate volcanic islands, or even those forming seamount chains over hotspots such as the Hawaii-Emperor chain, are prone to submergence at rates faster than carbonate deposition (Detrick and Crough, 1978; Moore and Fornari, 1984) and are unlikely to provide a regionally extensive substrate with sufficient longevity to explain the Horsefeed Formation. Plateaus, such as the Ontong-Java and Kurguelen, the largest plateaus on earth, are tens of thousands of km² in extent, and are long-lived. For example, Ontong-Java plateau formed during at least two separate magmatic pulses, ~121 Ma and ~90 Ma (Tejada et al., 1996), separated by a 30 m.y. magmatic hiatus. Kurguelen formed semicontinuously since ~119 Ma (Duncan, 2002) with present day volcanic activity in the central plateau region. Plateaus such as these could provide a stable long-lasting substrate for thick, regional limestone deposition over 25 m.y. with synchronous within-plate magmatic additions during the carbonate bank deposition.

However, Kurguelen is at least partly underlain by rifted continental crust (we see no evidence in detrital zircons of continental crust) and Ontong-Java is currently too deep to form a substrate for carbonate banks. Part of the difficulty in identifying an analogue for Horsefeed Formation substrate is that thick sections of plateau crust are lacking in northwest British Columbia, and are inferred to have been subducted. Based on existing evidence, the Horsefeed Formation was deposited in an environment isolated from arc volcanic rocks and it was adjacent to basins where chert accumulated.

Ophiolitic magmatic and mantle rocks of the Cache Creek terrane have supra-subduction zone geochemical affinities (English et al., 2010; Zagorevski et al., 2016; McGoldrick et al., 2017), and mostly Late Permian to Early Triassic isotopic ages (Gordey et al., 1998; Mihalynuk et al., 2003; Zagorevski, 2016). Thus, Horsefeed Formation limestone and intercalated within-plate basalts are both geochemically and temporally unrelated to the ophiolitic sections. Although the Kedahda Formation in the Turtle Lake area lacks fossil ages, most stratigraphic evidence points to Kedahda chert as synchronous with, and overlying, the Horsefeed Formation limestones. Deposition of limestone breccia atop soft sediment-deformed chert, and injection of breccia dikes into ribbon chert (Fig. 5b) suggests that the two depositional environments coexisted in close proximity, perhaps where limestone debris flowed into an adjacent pelagic basin.

Jurassic fold and thrust deformation is regionally recognized in areas adjacent to the Turtle Lake mapsheet (e.g., Mihalynuk et al., 1999), farther southeast (see Mihalynuk et al., 2004; English, 2004; Mihalynuk et al., 2017) and in Yukon (e.g., Monger, 1975 and Colpron et al., 2015 and references therein). This deformation is not readily recognizable in the massive Horsefeed Formation limestone of the Turtle Lake area, where marker beds outlining folds and thrusts are lacking, and such structures are not shown on existing maps (Monger, 1975, p. 27). Alternatively, these limestones may have developed a thick(er)-skinned thrust belt where strain was localized into very few thrusts. This appears to be the case to the northwest, in the Windy Arm area (Monger, 1975), where large homoclinal areas are preserved in the limestones; whereas on-strike cherts are intensely folded and imbricated (Gordey, 1991).

Fold and thrust deformation is regionally constrained to have finished by ca. 172 Ma, the age of the Fourth of July plutonic suite, which cuts across and thermally metamorphosed deformed strata. Cooling ages from Fourth of July batholith and related intrusions record the combined effects of conductive and convective cooling of the batholith and satellite intrusions, and tectonic and erosional exhumation. Lamprophyre dikes cutting the undeformed margin of the Lost Sheep peak intrusion yield biotite ages of 168.2 ± 1.0 Ma and a hornblende cooling age of 174.0 ± 2.7 Ma from 74.5% of ³⁹Ar released. Integration of all ³⁹Ar released yields an age of 171 ± 10 Ma. These cooling ages are consistent with those from the Fourth of July batholith nearby (Mihalynuk et al., 2004 and references therein), and the intrusion is probably a satellite of the main batholith. Other

plutons of the Fourth of July suite (part of the regional Three Sisters suite, Woodsworth et al., 1992) cut the outboard edge of the Cache Creek terrane, and yield crystallization ages of ~174-172 Ma (summarized in Mihalynuk et al., 2004). Lamprophyre dikes that cut the Fourth of July batholith have been considered a late stage intrusive phase of the batholith emplacement (Aitken, 1959; Mihalynuk et al., 1999; Ash, 1994). Back-veining of the 174.0 ± 2.7 Ma lamprophyre dike that cuts Lost Sheep Peak intrusion provides consistent textural and geochronologic evidence of this late-stage magmatic relationship.

Hornblende and biotite cooling ages from the synkinematic Lost Sheep peak intrusion record a difference of between 3 and 6 m.y. (inside and outside limits of error). If the age data are reliable, they may be interpreted as recording the rate of cooling from hornblende 166.0 ± 1.1 Ma to biotite 161.61 ± 0.85 Ma closure temperatures (~600 to ~310°C, Harrison and Fitzgerald, 1986; Harrison et al., 1985; or differing by ~300°C, Dodson, 1973; Baxter, 2010) of ~70° to 30°C/m.y., at the limits of error.

Lamprophyre cooling ages that we report are consistent with dikes east and west of Atlin Lake dated by Harris et al. (2003) as 165.3 ± 1.6 Ma and 161.8 ± 1.6 Ma (biotite, each a combination of 2 aliquots). Regionally, these dikes have been mapped from east of Atlin Lake to the east shore of Tagish Lake. On the west shore of Tagish Lake, only a single lamprophyre dike has been mapped by us, and none have been noted farther west. It appears that the zone of diking dies out across Tagish Lake, or the zone was cut off by faulting. It is also possible that our observations are incomplete. For example, a lamprophyre dike was reported at Mt. Clive by Cairnes (1913); although, that dike is presumably part of different suite, of Cretaceous or younger, as Cretaceous granodiorite underlies Mt. Clive. Dike orientation is a field criterion that may help to distinguishing different lamprophyre suites; however, it is not without ambiguity. Dated Middle Jurassic lamprophyre dikes trend northwest-southeast, but south and northeast trends are also recorded.

From east of Atlin Lake to Turtle Lake, the Fourth of July batholith, its outliers, and related lamprophyre dikes, provide constraints on post ~170 Ma crustal displacements implying that lateral transport within the zone of intrusions, if present, has been insufficient to totally truncate lamprophyre dikes. Further investigation of the lamprophyre dikes is warranted because they are a rare example of a potential east-west tie line in the Cordillera, plus they contain abundant crustal xenoliths and are therefore good probes into the crustal composition at their time of emplacement (a record that we did not exploit).

Trans-crustal faulting has resulted in juxtaposition of Cache Creek terrane mantle and upper crustal rocks as well as supracrustal Laberge Group and Windy-Table suite strata. Middle Triassic chert is interbedded with wacke (north of Graham Inlet) and is juxtaposed with pillow basalt, slivers of gabbro, and serpentinized mantle tectonite. Similarly, panels of volcanic rocks at Peninsula Mountain are separated from the Horsefeed Formation by thin domains (less than ~200 m thick) of structurally-disrupted ribbon chert, in places

admixed with blocks of many different lithologies, including serpentinite (Fig. 12e). No relicts of blueschist or other high P/T metamorphic facies have been discovered along this boundary thus far. It is interpreted as demarking the outboard margin of the Cache Creek terrane.

Detrital zircons separated from reworked rhyolite breccia at Sunday Peak are as young as 85 Ma and are correlated with the Windy-Table suite. Some of the zircons have Late Triassic (216 Ma) cores (Figs. 18b, c). Late Triassic was a common magmatic age during construction of the Stikine arc (Stuhini or Lewes River groups), and may indicate that by Late Cretaceous the basement through which the source volcanic rocks erupted, was predominantly Stuhini Group. Alternatively, the Laberge Group, which contains abundant Late Triassic zircons (e.g., Colpron et al., 2015) and immediately underlies parts of the rhyolite breccia, may have been sampled by the Windy-Table suite magmas.

Prior to the new ~80 Ma U-Pb age determination reported here, volcanic rocks at Peninsula Mountain were correlated with volcanic strata that grade into Triassic Kedahda Formation ribbon chert and Laberge-like wacke near Graham Creek, ~20 km south-southeast of Sunday Peak. Such observations were consistent with interpretations of earlier workers (e.g., Bultman, 1979) who considered the Peninsula Mountain suite as basement of the Whitehorse Trough, mainly based on regional southwest dips that project beneath the Laberge Group. Reassignment of 'Middle to Late(?) Triassic Peninsula Mountain volcanic suite' rocks (Mihalynuk and Smith, 1992b) to Windy-Table suite, was required for rocks 7 km east-southeast of Sunday Peak, to explain a new ~85 Ma U-Pb age on rhyolite layers (Zagorevski et al., 2017) originally thought to be deposited with Kedahda Formation chert. The same inconsistency arises from our new ~80 Ma date from 'Peninsula Mountain suite' volcanic rocks in the Turtle Lake area, suggesting that the correlation error is pervasive, and as a consequence, we reassign all 'Peninsula Mountain suite' rocks to Windy-Table suite (largely consistent with original mapping by Monger, 1975). It is possible that not all of the volcanic rocks at Peninsula Mountain belong to the Windy-Table suite as indicated, for example, by island arc tholeiite compositions that are indistinguishable from the most widespread basalts of the Cache Creek terrane, but more detailed mapping and sampling for age determinations will be required to determine if this is so. In support of our reassignment is the absence of notable Middle Jurassic (see above) lamprophyre dikes within the volcanic rocks at Peninsula Mountain, in stark contrast to the eastern side of Turtle Lake where the dike swarm is well developed.

Evidence for Cretaceous extension is accumulating in the Turtle Lake area. Extensional fabrics that have top-to-the-southeast sense of offset are consistent with the orientation of syn-deformational dike swarms in the thermal metamorphic halo of the Racine pluton (Fig. 12f). An extensional fault is inferred to approximately trace the southeast flank of Sunday Peak, explaining at least 500 m of down-to-the-southeast

vertical offset of Windy-Table volcanic strata from near the peak (Fig. 2), to near the valley floor to the south. An extensional fault crossing Turtle Lake may explain along-strike termination of limestone bodies on either side of the lake (Figs. 2, 13). Projection of this inferred fault to the northeast links the steep face of the southwest carbonate ridge of Stovel Peak, at least partly paralleled by an exposed dip slope fault (Fig. 12a). Verification of these inferred faults will require more detailed, focused mapping but such verification is important because it carries broad tectonic significance. For example, the interpretation of paleomagnetic data by Harris et al. (2003) is predicated on the absence of such faults. These authors used geobarometry to show that the northern Fourth of July batholith has been exhumed by nearly 12 km, while the southern part has been exhumed by ~6 to 8 km. They then ascribed the differential uplift to regional tilting and used that tilt to 'correct' paleomagnetic inclination measurements by ~9°. However, such exhumation is also consistent with the south-side-down extensional faulting that we tentatively propose, which would result in northward tilting of block faults and a paleo-inclination 'correction' of the opposite sense (Fig. 27).

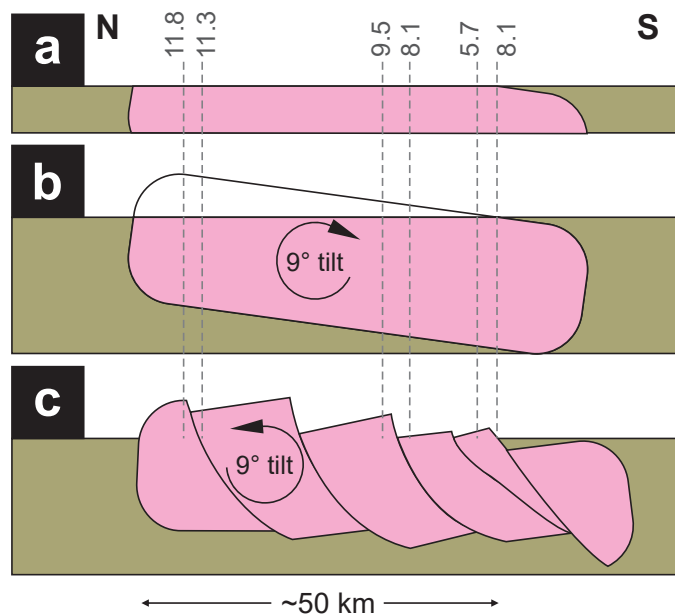


Fig. 27. A cross-section cartoon showing two mechanisms that explain Al in hornblende geobarometric results for the present-day Fourth of July batholith. Values are estimates of intrusion depth in kilometres (Harris et al., 2003). **a)** Distribution of sites in Fourth of July batholith where geobarometric values were obtained. **b)** Bulk 9° southward crustal tilting preferred by Harris et al. to explain geobarometric data, and **c)** Northward rotation of blocks between south-side-down extensional faults that are indicated, but not yet fully demonstrated, by our mapping. Note the opposite effects of (b) versus (c) on a hypothetical paleomagnetic inclination correction.

8.1. Updated geologic history and regional implications

Our work in the Turtle Lake map area helps to further define the Cache Creek and Stikine terranes, refine their geological histories, and interactions between them. Thick accumulations

of Horsefeed Formation limestone (1.5 km) indicate deposition across thousands of km² from Carboniferous to Permian (Monger, 1975). A stable, long-lived plateau substrate is probable, based on a transitional N-MORB to E-MORB geochemical signature of associated basaltic rocks in the Turtle Lake area and elsewhere (English et al., 2010), and isotopic evidence for magmatic additions to this plateau over 25 m.y., approximately coextensive with regionally developed platform limestone deposition in the Turtle Lake area. In contrast, ultramafic and oceanic crustal rocks of northern Cache Creek terrane are everywhere dated as Middle Permian (e.g., Mihalynuk et al., 2003, 2004; Zagorevski et al., 2016) to Early Triassic (Gordey et al., 1998). Ophiolitic rocks at Turtle Lake are correlated with undated mantle-gabbro-basalt along strike to the southeast, at Graham Creek. There the pillow basalt section is overlain by Middle to Late Triassic chert and wacke grading upwards into probable Laberge Group (Mihalynuk et al., 1999). Wacke overlapping both arc ophiolitic and Horsefeed carbonate rocks may provide a loose link between these domains, which formed in disparate tectonic environments. Wacke that we map as part of the Laberge Group in the Turtle Lake area, links the Graham Creek suite, now more firmly affiliated with Cache Creek ophiolites on the basis of similar geochemistry, but is the wacke succession on Cache Creek substrate really part of the Laberge Group? Recent detrital zircon evidence from the Whitehorse trough (west of Cache Creek terrane) and from strata overlying the Cache Creek terrane shows equivalent age distributions, strongly supporting a link by latest Triassic (Colpron et al., 2015). If so, what happened to the basement atop which the Horsefeed Formation was deposited? Only outcrop-sized relicts of it remain, and we infer, as others have (e.g., English et al., 2010), that this crust has been lost to subduction. Timing of this subduction is between the age of the youngest Horsefeed Formation, latest Early Permian, and the age of overlap demonstrated by detrital zircons, latest Triassic. Amalgamation of the Cache Creek terrane was probably multi-staged, as has been suggested by other workers (e.g., Logan and Mihalynuk, 2014), and consumption of the ocean plate carrying the Cache Creek ocean arc and the Horsefeed Formation, delivered the buoyant arc/plateau crust to the Stikine-Quesnel arc around 210 Ma, resulting in collision, angular unconformity, subduction termination, arc disruption, and a pulse of alkalic magmatism including rich Cu-Au-Ag porphyry deposit formation (Mihalynuk et al., 1994; Logan and Mihalynuk, 2014; Mihalynuk et al., 2016). Pre- and post-collisional subduction is recorded by blueschist and eclogite cooling ages ~221 and 224 Ma in the Stuart Lake area (Ghent et al., 1993) and by the youngest blueschists, ~174 Ma in the Dease Lake area (Mihalynuk et al., 2004).

Partial subduction of thick Horsefeed Formation carbonate rocks may have led to efficient transfer of Cu and other chalcophile elements from the mantle wedge (e.g., Canil and Fellows, 2017). In northernmost British Columbia, where the Horsefeed Formation is extensive, Late Triassic copper porphyry deposits are not known. However, until we can

establish the amount of transcurrent motion on the Nahlin, Silver Salmon and related faults, we cannot fully evaluate this apparent spatial relationship.

Final subduction termination is recorded by emplacement and cooling of the youngest blueschists, with the resultant fold and thrust belt cut by ~172 Ma late syn- and post-kinematic Fourth of July batholith and subsequent lamprophyre dikes, which had mostly cooled to biotite closure temperatures by ~162 Ma, at a rate of between 30°-70°C/m.y.

Between ~165-125 Ma, only rare magmatism is recorded; we have found only a single 145 Ma granitic dike in the Turtle Lake area. This North American-wide magmatic lull has been recognized for decades (e.g., Armstrong, 1974, 1988, 155-125 Ma) and has recently been correlated with relict subducted lithosphere at mid-mantle depths, which accumulated in massive high velocity slabs. Location and geometry of these slabs support subduction of oceanic crust attached to the leading edge of North America, westward beneath the intra-oceanic Insular Superterrane (Sigloch and Mihalynuk, 2013; Sigloch and Mihalynuk, 2017).

By 125 Ma, oceanic lithosphere was again forced to subduct beneath the western North American margin (newly defined by addition of the Insular Superterrane). Arc magmatism may have resumed west of the Turtle Lake area, as recorded by a volcanic succession north of Tutshi Lake (Mihalynuk et al., 2003; Zagorevski et al., 2017), and at ~110 Ma, magmatic contributions are recorded in clastic matrix of karst deposits in the Horsefeed Formation. However, it was not until ~85 Ma that widespread volcanism in the Turtle Lake area outpaced erosion, with deposition and preservation of the Windy-Table suite and correlatives extending in an orogen-parallel belt for hundreds of kilometres (Zagorevski et al., 2017).

Cutting the ~85 Ma basal volcanic conglomerate of the Windy-Table suite is a high-angle transcurrent fault marking the leading edge of the Cache Creek terrane. Known as the Silver Salmon fault (Mihalynuk et al., 2017), the amount of offset across it has yet to be constrained. An array of mainly south-side-down extensional faults, some with individual offsets of more than 500 m, also cut the Windy-Table suite, and may be kinematically linked to the Silver Salmon fault. These extensional faults have yet to be evaluated for their potential to focus hydrothermal fluids and mineralization.

By Early Eocene (~56 Ma) the final magmatic epoch recorded in the Turtle Lake area commenced. Sloko Group volcanism recorded south of the Turtle Lake area is represented in the uplifted study area by small zoned plutons and stocks. Sunday Peak intrusion is one such example. It cut and thermally metamorphosed the crustal-scale Silver Salmon fault. These Eocene magmatic centres can be economically important, as demonstrated by rich epithermal gold mineralization at the Engineer Mine, which is genetically and temporally related to Eocene magmatic rocks and is hosted by Laberge Group strata, structurally prepared adjacent to the crustal-scale Llewellyn fault (Mihalynuk et al., 1999; Millonig et al., 2017; Ootes et al., 2017, 2018). Our new dating of intrusions at Sunday Peak

and Mount Lanning, both formerly considered Cretaceous, both hosted by Laberge Group, and both adjacent crustal-scale faults, reveals the same combination of key geologic elements as at the Engineer Mine, ~30 km to the south. To our knowledge, however, neither the Sunday Peak nor the Mount Lanning area have received modern mineral exploration attention.

9. Summary

Our regional geological mapping, geochronologic and geochemical results help to further refine the geological evolution of the Turtle Lake area. Key new observations and data sets include the following.

- New conodont ages of early (Bashkirian) and middle-upper (Moscovian-Gzhelian) parts of the Late Carboniferous (Pennsylvanian), and the last stage of the Early Permian (Kungurian) are consistent with previous fossil age determinations from the >1.5 km thick limestones of the Horsefeed Formation.
- A new detrital zircon age from Horsefeed Formation tuffaceous limestone breccia echoes the ~25 m.y. biochronological age range, suggesting continuous additions to the volcanic substrate, possibly an oceanic plateau, as is also suggested by their transitional N-MORB to E-MORB composition.
- Soft sediment intermingling of carbonate breccia and pelagic strata suggest proximity of, and connections between, the two depositional environments.
- New geochemical data support correlation of arc tholeiite basalt and harzburgite at Sunday Peak with ophiolitic rocks of the Cache Creek terrane.
- Thick sections of Laberge Group wacke mapped either side of the ophiolitic belt extending both north and south of Sunday Peak suggest an unconformable relationship, later modified by high-angle faulting.
- Regional folds and thrusts affecting Cache Creek terrane and Laberge Group are cut by the Lost Sheep peak intrusion, formerly considered Cretaceous, but now constrained by a crosscutting lamprophyre dikes to Middle Jurassic, part of the regional Three Sisters plutonic suite.
- Lamprophyre dikes that cut granitic phases of the Lost Sheep Peak intrusion are locally back-veined by the granite indicating a comagmatic, but not necessarily co-genetic relationship.
- Calc-alkalic lamprophyre dikes cut the Lost Sheep peak intrusion and surrounding Horsefeed Formation and have cooling ages of 168.2 ± 1.0 to 174.0 ± 2.7 Ma.
- Strong fabric development in early phases of the Lost Sheep peak intrusion indicate that it was late syn- to post-kinematic.
- Cooling of the Lost Sheep peak intrusion through the argon diffusion in hornblende and biotite closure temperature occurred between ~166-162 Ma; a cooling rate of ~70° to 30°C/m.y. is implied.

- In the Turtle Lake area, dated magmatic rocks that fall within the Late Jurassic to Early Cretaceous North American magmatic lull are limited to a single 145.75 ± 0.11 Ma granitic dike.
- Cretaceous magmatism may have resumed by ~ 125 Ma in the Boundary Ranges to the west, but earliest records in the Turtle Lake area are a unimodal population of ~ 110 Ma detrital zircons from a karst deposit in Horsefeed limestone.
- A belt of Late Cretaceous volcanic rocks correlated with the Windy-Table suite is now dated at three sites as ~ 86.5 Ma, 80.63 ± 0.07 Ma and 79.7 ± 1.3 Ma.
- The crustal-scale, high-angle, Silver Salmon fault affects rocks at the base of the Windy-Table suite, constraining youngest motion to less than ~ 86.5 Ma.
- Motion on the Silver Salmon fault may be kinematically linked with an as yet inadequately mapped set of east- to northeast-trending extensional faults displaying mainly south-side-down offsets, locally at least 500 m.
- The Silver Salmon fault is cut by the youngest recognized magmatic unit in the map area, a suite of quartz diorite stocks dated as 56.01 ± 0.04 Ma and 56.12 ± 0.29 Ma, coeval with magmatic rocks at the Engineer mine.

Acknowledgments

James Balchin, Siobhan McGoldrick, and Chris Lawley provided key assistance in field data collection. Norm Graham and Paula Vera of Discovery Helicopters safely and efficiently conveyed crews and gear. This report was reviewed and improved by Jim Monger.

References cited

- Aitken, J.D., 1959. Atlin map-area, British Columbia. Geological Survey of Canada, Memoir 307, 89 p.
- Armstrong, R.L., 1974. Magmatism, orogenic timing, and orogenic diachronism in the Cordillera from Mexico to Canada. *Nature*, 247, 348-351.
- Armstrong, R.L., 1988. Mesozoic and early Cenozoic magmatic evolution of the Canadian Cordillera. *Geological Society of America Special Papers*, 218, pp. 55-92.
- Ash, C.H., 1994. Origin and tectonic setting of ophiolitic ultramafic and related rocks in the Atlin area, northwestern British Columbia. British Columbia Ministry of Energy, Mines and Petroleum Resources, British Columbia Geological Survey, Bulletin 94, 140 p.
- Baxter, E.F., 2010. Diffusion of Noble Gases in Minerals. *Reviews in Mineralogy and Geochemistry*, 72, 509-557.
- Best, M.G., Christiansen, E.H., Deino, A.L., Grommé, C.S., Tingey, D.G., 1995. Correlation and emplacement of a large, zoned, discontinuously exposed ash flow sheet; the $^{40}\text{Ar}/^{39}\text{Ar}$ chronology, paleomagnetism, and petrology of the Pahrnagat Formation, Nevada. *Journal of Geophysical Research*, 100, 24593-24609.
- Bloodgood, A., Rees, C.J., and Lefebvre, D.V., 1989. Geology of the Atlin area (NTS 104N/11W, 12E). British Columbia Ministry of Energy, Mines and Petroleum Resources, British Columbia Geological Survey, Open File 1989-15.
- Boleneus, D.E., Raines, G.L., Causey, J.D., Bookstrom, A.A., Frost, T.P., and Hyndman, P.C., 2001. Assessment method for epithermal gold deposits in northeast Washington State using weights-of-evidence GIS modeling. US Geological Survey, Open File 01-501, 52 p.
- Boulanger, O., and Kiss, F., 2017. Aeromagnetic survey of the Llewellyn area, NTS 104-M/9,10,15,16 and parts of 104-M/11,14, British Columbia. British Columbia Ministry of Energy and Mines, British Columbia Geological Survey, Geoscience Map 2017-4.
- Breitsprecher, K., and Mortensen, J.K., 2004. BCAGE 2004A-1-a database of isotopic age determinations for rock units from British Columbia. British Columbia Ministry of Energy and Mines, British Columbia Geological Survey, Open File 2004-03 (Release 2.0), 7766 records, 9.3 Mb.
- Bultman, R.B., 1979. Geology and tectonic history of the Whitehorse Trough west of Atlin, British Columbia. Unpublished Ph.D. thesis, Yale University, 284 p.
- Cairnes, D.D., 1913. Portions of Atlin District, British Columbia: with special reference to lode mining. Geological Survey of Canada Memoir 37, 129 p.
- Canil, D., and Fellows, S.A., 2017. Sulphide-sulphate stability and melting in subducted sediment and its role in arc mantle redox and chalcophile cycling in space and time. *Earth and Planetary Science Letters*, 470, 73-86.
- Canil, D., Mihalynuk, M., MacKenzie, J.M., Johnston, S.T. and Grant, B., 2005. Diamond in the Atlin Nakina region, British Columbia: insights from heavy minerals in stream sediments. *Canadian Journal of Earth Sciences*, 42, 2161-2171.
- Christie, R.L., 1957. Bennett, British Columbia. Geological Survey of Canada, Map 19-1957.
- Colpron, M., Crowley, J.L., Gehrels, G., Long, D.G., Murphy, D.C., Beranek, L., and Bickerton, L., 2015. Birth of the northern Cordilleran orogen, as recorded by detrital zircons in Jurassic synorogenic strata and regional exhumation in Yukon. *Lithosphere*, 7, 541-562.
- Colpron, M., and Nelson, J.L., 2011. A digital atlas of terranes for the Northern Cordillera. British Columbia Ministry of Energy and Mines, British Columbia Geological Survey, GeoFile 2011-11.
- Cordey, F., Gordey, S.P., and Orchard, M.J., 1991. New biostratigraphic data for the northern Cache Creek Terrane, Teslin map area, southern Yukon. In: *Current Research; Part E*, Geological Survey of Canada Paper 1991-1, pp. 67-76.
- Crowley, J.L., Schoene, B., and Bowering, S.A., 2007. U-Pb dating of zircon in the Bishop Tuff at the millennial scale. *Geology*, 35, 1123-1126.
- Dazé, A., Lee, J.K., and Villeneuve, M., 2003. An intercalibration study of the Fish Canyon sanidine and biotite $^{40}\text{Ar}/^{39}\text{Ar}$ standards and some comments on the age of the Fish Canyon Tuff. *Chemical Geology*, 199, 111-127.
- Detrick, R.S., and Crough, S.T., 1978. Island subsidence, hot spots, and lithospheric thinning. *Journal of Geophysical Research: Solid Earth*, 83, 1236-1244.
- Dickie, J.R., and Hein, F.J., 1995. Conglomeratic fan deltas and submarine fans of the Jurassic Laberge Group, Whitehorse Trough, Yukon Territory, Canada; fore-arc sedimentation and unroofing of a volcanic island arc complex. In: Chough, S.K., and Orton, G.J., (Eds.), *Fan deltas: Depositional styles and controls*. Special Volume, *Sedimentary Geology*, 98, 263-292.
- Dodson, M.H., 1973. Closure temperature in cooling geochronological and petrological systems. *Contributions to Mineralogy and Petrology*, 40, 259-274.
- Duncan, R.A., 2002. A time frame for construction of the Kerguelen Plateau and Broken Ridge. *Journal of Petrology*, 43, 1109-1119.
- English, J.M., 2004. Convergent margin tectonics in the North American Cordillera: implications for continental growth and orogeny. Unpublished Ph.D. thesis, University of Victoria, Victoria, 191 p. Available from <http://dspace.library.uvic.ca/handle/1828/391> accessed November, 2015.
- English, J.M., Mihalynuk, M.G., and Johnston, S.T., 2010.

- Geochemistry of the northern Cache Creek terrane and implications for accretionary processes in the Canadian Cordillera. *Canadian Journal of Earth Sciences*, 47, 13-34.
- Friedman, R.M., Mihalynuk, M.G., Diakow, L.J., and Gabites, J.E., 2016. Southern Nicola Arc Project 2015: Geochronologic data constraining Nicola arc history along a transect near 50°N. British Columbia Ministry of Energy and Mines, British Columbia Geological Survey GeoFile 2016-3.
- Gale, A., Dalton, C.A., Langmuir, C.H., Su, Y., and Schilling, J.-G., 2003. The mean composition of ocean ridge basalts. *Geochemistry, Geophysics, Geosystems*, 14, 489-518.
- Ghent, E.D., Stout, M.Z., and Erdmer, P., 1993. Pressure-temperature evolution of lawsonite-bearing eclogites, Pinchi Lake, British Columbia. *Journal of Metamorphic Geology*, 11, 279-290.
- Golding, M.L., and Orchard, M.J., 2017. Magnigondolella, a new conodont genus from the Triassic of North America. *Journal of Paleontology*, 1-14. NO Volume, on-line only at present Published online: 23 November 2017 <https://doi.org/10.1017/jpa.2017.123>.
- Gordey, S.P., 1991. Teslin map area, a new geological mapping project in southern Yukon. In: *Current Research, Part A*, Geological Survey of Canada Paper 91-1A, pp. 171-178.
- Gordey, S.P., McNicoll, V.J., and Mortensen, J.K., 1998. New U-Pb ages from the Teslin area, southern Yukon, and their bearing on terrane evolution in the northern Cordillera. In: *Geological Survey of Canada, Current Research-Radiogenic age and isotopic studies, Report 11*, pp. 129-148.
- Gwillim, J.C., 1901. Atlin mining district. *Geological Survey of Canada Annual Report 1899, Volume 12*, 48 p.
- Harris, M.J., Symons, D.T., Blackburn, W.H., Hart, C.J., and Villeneuve, M., 2003. Travels of the Cache Creek Terrane: a paleomagnetic, geobarometric and ⁴⁰Ar/³⁹Ar study of the Jurassic Fourth of July Batholith, Canadian Cordillera. *Tectonophysics*, 362, 137-159.
- Harris, R.W., and Hollingsworth, R.V., 1933. New Pennsylvanian conodonts from Oklahoma. *American Journal of Science*, 25, 193-204.
- Harrison, T.M., and Fitzgerald, J.D., 1986. Exsolution in hornblende and its consequences for ⁴⁰Ar/³⁹Ar age spectra and closure temperature. *Geochimica et Cosmochimica Acta*, 50, 247-253.
- Harrison, T.M., Duncan, I., and McDougall, I., 1985. Diffusion of ⁴⁰Ar in biotite: temperature, pressure and compositional effects. *Geochimica et Cosmochimica Acta*, 49, 2461-2468.
- Hart, C.J.R., 1997. A transect across northern Stikinia: Geology of the northern Whitehorse map area, southern Yukon Territory (105D/13-16). *Exploration and Geological Services Division, Yukon Region, Indian and Northern Affairs Canada, Bulletin*, 8, 112 p.
- Hart, C.J.R., Dickie, J.R., Ghosh, D.K., and Armstrong, R.L., 1995. Provenance constraints for Whitehorse Trough conglomerate; U-Pb zircon dates and initial Sr ratios of granitic clasts in Jurassic Laberge Group, Yukon Territory. In: *Jurassic magmatism and tectonics of the North American Cordillera*. Geological Society of America, Special Paper 299, pp. 47-63.
- Jaffey, A.H., Flynn, K.F., Glendenin, L.E., Bentley, W.C., and Essling, A.M., 1971. Precision measurement of half-lives and specific activities of ²³⁵U and ²³⁸U. *Physics Review*, C4, 1889-1906.
- Jeppsson, L., Anehus, R., and Fredholm, D., 1999. The optimal acetate buffered acetic acid technique for extracting phosphatic fossils. *Journal of Paleontology*, 73, 964-972.
- Johannson, G.G., Smith, P.L., and Gordey, S.P., 1997. Early Jurassic evolution of the northern Stikinian arc; evidence from the Laberge Group, northwestern British Columbia. *Canadian Journal of Earth Sciences*, 34, 1030-1057.
- Kerrick, R., and Wyman, D.A., 1994. The mesothermal gold-lamprophyre association: significance for an accretionary geodynamic setting, supercontinent cycles, and metallogenic processes. *Mineralogy and Petrology*, 51, 147-172.
- Kuiper, K.F., Deino, A., Hilgen, F.J., Krijgsman, W., Renne, P.R., and Wijbrans, J.R., 2008. Synchronizing rock clocks of Earth history. *Science*, 320, 500-504.
- Lane, H.R., 1967. Uppermost Mississippian and Lower Pennsylvanian conodonts from the type Morrowan region, Arkansas. *Journal of Paleontology*, 41, 920-942.
- Logan, J.M., and Mihalynuk, M.G., 2014. Tectonic controls on early Mesozoic paired alkaline porphyry deposit belts (Cu-Au ±Ag-Pt-Pd-Mo) within the Canadian Cordillera. *Economic Geology*, 109, 827-858.
- Lowey, G.W., 2003. Preliminary lithostratigraphy of the Laberge Group (Jurassic), south-central Yukon: Implications concerning the petroleum potential of the Whitehorse Trough. *Yukon Exploration and Geology*, 129-142.
- Lowey, G.W., 2004. Sedimentology, stratigraphy and source rock potential of the Richthofen formation (Jurassic), northern Whitehorse Trough, Yukon. In: *Yukon Exploration and Geology*, Yukon Geological Survey, 177-191.
- Mattinson, J.M., 2005. Zircon U-Pb chemical abrasion (CA-TIMS) method: combined annealing and multi-step partial dissolution analysis for improved precision and accuracy of zircon ages. *Chemical Geology*, 220, 47-66.
- McGoldrick, S., Zagorevski, A., and Canil, D., 2017. Geochemistry of volcanic and plutonic rocks from the Nahlin ophiolite with implications for a Permo-Triassic arc in the Cache Creek terrane, northwestern British Columbia. *Canadian Journal of Earth Sciences*, 1-14. doi: 10.1139/cjes-2017-0069.
- Mihalynuk, M.G., and Cordey, F., 1997. Potential for Kutcho Creek volcanogenic massive sulphide mineralization in the northern Cache Creek terrane: a progress report. In: *Geological Fieldwork 1996*, British Columbia Ministry of Energy, Mines and Petroleum Resources, British Columbia Geological Survey Paper 1997-1, pp.157-170.
- Mihalynuk, M.G., and Mountjoy, K.J., 1990. Geology of the Tagish Lake area (104M/ 8, 9E). In: *Geological Fieldwork, 1989*, British Columbia Ministry of Energy, Mines and Petroleum Resources British Columbia Geological Survey Paper 1991-1, pp. 181-196.
- Mihalynuk, M.G., and Rouse, J.N., 1988. Preliminary geology of the Tutshi Lake area, northwestern British Columbia (104M/15). In: *Geological Fieldwork 1987*, British Columbia Ministry of Energy and Mines, British Columbia Geological Survey, Paper 1988-1, pp. 217-231.
- Mihalynuk, M.G., and Smith, M.T., 1992a. Geology and geochemistry of the Atlin (west) map area (104N/12W). *British Columbia Ministry of Energy, Mines and Petroleum Resources, British Columbia Geological Survey, Open File 1992-08*.
- Mihalynuk, M.G., and Smith, M.T., 1992b. Highlights of 1991 mapping in the Atlin-West Map area (104N/ 12). In: *Geological Fieldwork 1991*, British Columbia Ministry of Energy, Mines and Petroleum Resources, British Columbia Geological Survey, Paper 1992-1, pp. 221-227.
- Mihalynuk, M.G., Bellefontaine, K.A., Brown, D.A., Logan, J.M., Nelson, J.L., Legun, A.S., and Diakow, L.J., 1996. Geological compilation, northwest British Columbia (NTS 94E, L, M; 104F, G, H, I, J, K, L, M, N, O, P; 114J, O, P). *British Columbia Ministry of Energy and Mines, British Columbia Geological Survey Open File 1996-11*.
- Mihalynuk, M.G., Diakow, L.J., Friedman, R.M., and Logan, J.M., 2016. Chronology of southern Nicola arc stratigraphy and deformation. In: *Geological Fieldwork 2015*, British Columbia Ministry of Energy and Mines, British Columbia Geological Survey Paper 2016-1, pp. 31-64.
- Mihalynuk, M.G., P. Erdmer, Ghent, E.D., Cordey, F., Archibald, D.A., Friedman, R.M., and Johannson, G.G., 2004. Coherent French Range blueschist: Subduction to exhumation in < 2.5 m.y.? *Geological Society of America Bulletin*, 116, 910-922.
- Mihalynuk, M.G., Friedman, R.M., Joyce, N., Camacho, A.,

- and Zagorevski, A., 2018. Geochronologic data from samples collected in the Turtle Lake area, NTS 104M/16, northwest British Columbia. British Columbia Ministry of Energy, Mines and Petroleum Resources, British Columbia Geological Survey GeoFile in press.
- Mihalynuk, M.G., Johnston, S.T., English, J.M., Cordey, F., Villeneuve, M.J., Rui, L., and Orchard, M.J., 2003. Atlin TGI Part II: Regional geology and mineralization of the Nakina area (NTS 104N/2W and 3). In: Geological Fieldwork, British Columbia Ministry of Energy and Mines, British Columbia Geological Survey Paper 2003-1, pp. 9-37.
- Mihalynuk, M.G., Mountjoy, K.J., McMillan, W.J., Ash, C.H., and Hammack, J.L., 1991. Highlights of 1990 fieldwork in the Atlin area. In: Geological Fieldwork 1990, British Columbia Ministry of Energy, Mines and Petroleum Resources, British Columbia Geological Survey, Paper 1991-1, pp. 145-152.
- Mihalynuk, M.G., Mountjoy, K.J., Smith, M.T., Currie, L.D., Gabites, J.E., Tipper, H.W., Orchard, M.J., Poulton, T.P., and Cordey, F., 1999. Geology and mineral resources of the Tagish Lake area (NTS 104M/ 8,9,10E, 15 and 104N/ 12W), northwestern British Columbia. British Columbia Ministry of Energy and Mines, British Columbia Geological Survey, Bulletin 105, 202 p.
- Mihalynuk, M.G., Nelson, J., and Diakow, L.J., 1994. Cache Creek Terrane entrapment: oroclinal paradox within the Canadian Cordillera. *Tectonics*, 13, 575-595.
- Mihalynuk, M.G., Zagorevski, A., English, J.M., Orchard, M.J., Bidgood, A., K., Joyce, N., and Friedman, R.M., 2017. Geology of the Sinwa Creek area, northwest BC (104K/14). In: Geological Fieldwork 2016, British Columbia Ministry of Energy and Mines, British Columbia Geological Survey Paper 2017-1, pp. 153-178.
- Millonig, L.J., Beinlich, A., Raudsepp, M., Devine, F., Archibald, D.A., Linnen, R.L., and Groat, L.A., 2017. The Engineer Mine, British Columbia: An example of epithermal Au-Ag mineralization with mixed alkaline and subalkaline characteristics. *Ore Geology Reviews*, 83, 235-257.
- Monger, J., 1975. Upper Paleozoic rocks of the Atlin Terrane, northwestern British Columbia and south-central Yukon. Geological Survey of Canada, Paper 74-47, 63 p.
- Moore, J., and Fornari, D., 1984. Drowned reefs as indicators of the rate of subsidence of the Island of Hawaii. *Journal of Geology*, 92, 752-759.
- Ootes, L., Elliott, J.M., and Rowins, S.M., 2017. Testing the relationship between the Llewellyn fault, gold mineralization, and Eocene volcanism in northwest British Columbia: A preliminary report. In: Geological Fieldwork 2016, British Columbia Ministry of Energy and Mines, British Columbia Geological Survey Paper 2017-1, pp. 49-59.
- Ootes, L., Castonguay, S., Friedman, R., Devine, F., and Simmonds, R., 2018. Testing the relationship between the Llewellyn fault, Tally-Ho shear zone, and gold mineralization in northwest British Columbia. In: Geological Fieldwork 2017, British Columbia Ministry of Energy, Mines and Petroleum Resources, British Columbia Geological Survey Paper 2018-1, pp. 67-81.
- Palme, H., and O'Neill, H.St.C., 2003. Cosmochemical estimates of mantle composition. In: Holland, H.D., Turekian, K.K., Davis, A.M., (Eds.), *Treatise on Geochemistry*, vol. 2. Elsevier, Amsterdam, The Netherlands, pp. 1-38.
- Pearce, J.A., 1996. A users guide to basalt discrimination diagrams. In: Wyman D.A., (Ed.), *Trace element geochemistry of volcanic rocks: Applications for Massive Sulphide Exploration*. Geological Association of Canada, Short Course Notes, 12, pp. 79-113.
- Pearce, J.A., 2008. Geochemical fingerprinting of oceanic basalts with applications to ophiolite classification and the search for Archean oceanic crust. *Lithos*, 100, 14-48.
- Renne, P.R., and Norman, E.B., 2001. Determination of the half-life of ^{40}Ar by mass spectrometry. *Physical Review C*, 63, 047302.
- Renne, P.R., Cassata, W.S., and Morgan, L.E., 2009. The isotopic composition of atmospheric argon and $^{40}\text{Ar}/^{39}\text{Ar}$ geochronology: time for a change?. *Quaternary Geochronology*, 4, 288-298.
- Renne P.R., Swisher C.C., Deino A.L., Karner D.B., Owens T.L., and DePaolo D.J., 1998. Intercalibration of standards, absolute ages and uncertainties in $^{40}\text{Ar}/^{39}\text{Ar}$ dating. *Chemical Geology*, 145, 117-152.
- Rock, N.M.S., 1991. *Lamprophyres*, Springer, Boston, 285 p.
- Rock, N.M., and Groves, D.I., 1988. Do lamprophyres carry gold as well as diamonds? *Nature*, 332, 253-255.
- Roddick, J.C., 1983. High precision intercalibration of ^{40}Ar - ^{39}Ar standards. *Geochimica Cosmochimica Acta*, 47, 887-898.
- Ross, J., 2017. Pychron documentation. New Mexico Institute of Mining and Technology, 115 p. <<https://media.readthedocs.org/pdf/pychron/latest/pychron.pdf>> Last accessed January 11, 2018.
- Schmitz, M.D., and Schoene, B., 2007. Derivation of isotope ratios, errors, and error correlations for U-Pb geochronology using ^{205}Pb - ^{235}U (^{233}U)-spiked isotope dilution thermal ionization mass spectrometric data. *Geochemistry, Geophysics, Geosystems*, 8, Q08006 doi:10.1029/2006GC001492.
- Scoates, J.S., and Friedman, R.M., 2008. Precise age of the plantiferous Merensky Reef, Bushveld Complex, South Africa, by the U-Pb ID-TIMS chemical abrasion technique. *Economic Geology*, 103, 465-471.
- Sigloch, K., and Mihalynuk, M.G., 2013. Intra-oceanic subduction shaped the assembly of Cordilleran North America. *Nature*, 496, 50-56.
- Sigloch, K., and Mihalynuk, M.G., 2017. Mantle and geological evidence for a Late Jurassic-Cretaceous suture spanning North America. *Geological Society of America Bulletin*, 129, 1489-1520.
- Souther, J.G., 1971. Geology and mineral deposits of Tulsequah map-area, British Columbia. Geological Survey of Canada, Memoir 362, 84 p.
- Spell, T.L., and McDougall, I., 2003. Characterization and calibration of $^{40}\text{Ar}/^{39}\text{Ar}$ dating standards. *Chemical Geology*, 198, 189-211.
- Steiger R.H., and Jäger E., 1977. Subcommission on geochronology: convention on the use of decay constants in geo- and cosmochronology. *Earth and Planetary Science Letters*, 36, 359-362.
- Stern, R., 1997. The GSC Sensitive High Resolution Ion Microprobe (SHRIMP): Analytical techniques of zircon U-Th-Pb age determinations and performance evaluation. In: *Radiogenic Age and Isotopic Studies*, Report 10, Geological Survey of Canada, Current Research 1997-F, pp. 1-31.
- Stern, R.A., and Amelin, Y., 2003. Assessment of errors in SIMS zircon U-Pb geochronology using a natural zircon standard and NIST SRM 610 glass. *Chemical Geology*, 197, 111-142.
- Stone, J., 1987. Review of investigative techniques used in the study of conodonts. In: *Conodonts: Investigative Techniques and Applications*, British Micropalaeontological Society Series, pp. 17-34.
- Tejada, M.L.G., Mahoney, J.J., Duncan, R.A., and Hawkins, M.P., 1996. Age and geochemistry of basement and alkalic rocks of Malaita and Santa Isabel, Solomon Islands, southern margin of Ontong Java Plateau. *Journal of Petrology*, 37, 361-394.
- Tempelmann-Kluit, D.J., 1978. Reconnaissance geology, Laberge map-area, Yukon. In: *Current Research, Part A*, Geological Survey of Canada, Paper 78-1A, pp. 61-66.
- Tempelmann-Kluit, D.J., 1984. Geology, Laberge (105E) Carmacks (115I), Geological Survey of Canada, Open File 1101.
- Thorstad, L.E., and Gabrielse, H., 1986. The Upper Triassic Kutcho Formation, Cassiar Mountains, north-central British Columbia. Geological Survey of Canada, Paper 86-16, 53 p.
- Watson, K.D., and Mathews, W.H., 1944. The Tuya-Teslin area, northern British Columbia. British Columbia Department of Mines, Bulletin 19, 52 p.
- Wheeler, J.O., 1961. Whitehorse map-area, Yukon Territory, 105D. Geological Survey of Canada, Memoir 312, 156 p.

- Wheeler, J.O., Brookfield, A.J., Gabrielse, H., Monger, J.W.H., Tipper, H.W., and Woodsworth, G.J., 1988. Terrane map of the Canadian Cordillera. Geological Survey of Canada, Map 1712A.
- Woodsworth, G.J., Anderson, R.G., Armstrong, R.L., Struik, L.C., and van der Heyden, P., 1992. Plutonic regimes. In: *Geology of the Cordilleran Orogen in Canada, Geology of North America, Volume G-2*, pp. 493-531.
- Young, J.W., 1948. The relationship between lamprophyre dykes and ore deposits with special reference to British Columbia. Unpublished M.A.Sc. thesis, The University of British Columbia, 184 p.
- Youngquist, W., Hawley, R.W., and Miller, A.K., 1951. Phosphoria conodonts from southeastern Idaho. *Journal of Paleontology*, 25, pp. 356-364.
- Zagorevski, A., Mihalynuk, M.G., Joyce, N., and Anderson, R.G., 2017. Late Cretaceous magmatism in the Atlin-Tagish area, northern British Columbia (104M, 104N). In: *Geological Fieldwork 2016*, British Columbia Ministry of Energy and Mines, British Columbia Geological Survey Paper 2017-1, pp. 133-152.
- Zagorevski, A., Mihalynuk, M.G., McGoldrick, S., Bedard, J.H., Golding, M., Joyce, N., Canil, D., Corriveau, A.-S., Bogatu, A., Lawley, C., and Tremblay, A., 2016. Geological framework of ancient oceanic crust in northwestern British Columbia and southwestern Yukon GEM 2 Cordillera, Geological Survey of Canada, Open File 8140, 15 p.